ตัวเร่งปฏิกิริยาเหล็กคอปเปอร์/ซิลิกาที่เตรียมโดยวิธีออโตคอมบัสชันสำหรับการสังเคราะห์ฟิสเชอร์-ทรอปช์

ร้อยตำรวจตรีหญิงสุธาสินี เพ็งนรพัฒน์

จุฬาลงกรณ์มหาวิทยาลัย
CHULALONGKORN UNIVERSITY

บทคัดย่อและแฟ้มข้อมูลฉบับเต็มของวิทยานิพนธ์ตั้งแต่ปีการศึกษา 2554 ที่ให้บริการในคลังปัญญาจุฬาฯ (CUIR)
เป็นแฟ้มข้อมูลของนิสิตเจ้าของวิทยานิพนธ์ ที่ส่งผ่านทางบัณฑิตวิทยาลัย
The abstract and full text of theses from the academic year 2011 in Chulalongkorn University Intellectual Repository (CUIR)
are the thesis authors' files submitted through the University Graduate School.

วิทยานิพนธ์นี้เป็นส่วนหนึ่งของการศึกษาตามหลักสูตรปริญญาวิทยาศาสตรดุษฎีบัณฑิต
สาขาวิชาปิโตรเคมี
คณะวิทยาศาสตร์ จุฬาลงกรณ์มหาวิทยาลัย
ปีการศึกษา 2560

ลิขสิทธิ์ของจุฬาลงกรณ์มหาวิทยาลัย

$FeCu/SiO_2$ CATALYSTS PREPARED BY AUTOCOMBUSTION METHOD FOR FISCHER-TROPSCH SYNTHESIS

Police Second Lieutenant Suthasinee Pengnarapat

จุฬาลงกรณ์มหาวิทยาลัย
CHULALONGKORN UNIVERSITY

A Dissertation Submitted in Partial Fulfillment of the Requirements
for the Degree of Doctor of Philosophy Program in Petrochemistry
Faculty of Science
Chulalongkorn University
Academic Year 2017

Copyright of Chulalongkorn University

Thesis Title	$FeCu/SiO_2$ CATALYSTS PREPARED BY AUTOCOMBUSTION METHOD FOR FISCHER-TROPSCH SYNTHESIS
By	Police Second Lieutenant Suthasinee Pengnarapat
Field of Study	Petrochemistry
Thesis Advisor	Professor Tharapong Vitidsant, Ph.D.
Thesis Co-Advisor	Professor Noritatsu Tsubaki, Ph.D.

Accepted by the Faculty of Science, Chulalongkorn University in Partial Fulfillment of the Requirements for the Doctoral Degree

.....Dean of the Faculty of Science

(Associate Professor Polkit Sangvanich, Ph.D.)

THESIS COMMITTEE

.....Chairman

(Assistant Professor Warinthorn Chavasiri, Ph.D.)

.....Thesis Advisor

(Professor Tharapong Vitidsant, Ph.D.)

.....Thesis Co-Advisor

(Professor Noritatsu Tsubaki, Ph.D.)

.....Examiner

(Associate Professor Nuanphun Chantarasiri, Ph.D.)

.....Examiner

(Associate Professor Prasert Reubroycharoen, Ph.D.)

.....External Examiner

(Kitima Pinkaew, Ph.D.)

จุฬาลงกรณ์มหาวิทยาลัย
Chulalongkorn University

สุธาสินี เพ็งนรพัฒน์ : ตัวเร่งปฏิกิริยาเหล็กคอปเปอร์/ซิลิกาที่เตรียมโดยวิธีออโตคอมบัสชันสำหรับการสังเคราะห์ฟิสเชอร์-ทรอปช์ ($FeCu/SiO_2$ CATALYSTS PREPARED BY AUTOCOMBUSTION METHOD FOR FISCHER-TROPSCH SYNTHESIS) อ.ที่ปรึกษาวิทยานิพนธ์หลัก: ศ. ธราพงษ์ วิทิตศานต์ดร., อ.ที่ปรึกษาวิทยานิพนธ์ร่วม: ศ. โนริทัทซึ ซึบากิดร., 105 หน้า.

งานวิจัยนี้ศึกษาตัวเร่งปฏิกิริยาเหล็กซึ่งใช้ซิลิกาเป็นตัวรองรับ โดยวิธีออโตคอมบัสชันเพื่อสำหรับการสังเคราะห์ฟิสเชอร์-ทรอปช์ โดยตรงไม่ต้องผ่านขั้นตอนการรีดักชันและศึกษาผลกระทบอัตราส่วนโดยโมลของกรดซิตริกต่อไนเตรตไอรอน ชนิดของกรดและตัวรองรับซิลิกาต่อประสิทธิภาพของตัวเร่งปฏิกิริยา พบว่าอัตราส่วนโดยโมลของกรดซิตริกต่อไนเตรตไอรอนมีอิทธิพลสำคัญต่อการเกิดไอรอนเฟสที่มีความว่องไวในการเข้าทำปฏิกิริยาและความสามารถในการทำปฏิกิริยาการสังเคราะห์ฟิสเชอร์-ทรอปช์ นอกจากนี้เมื่ออัตราส่วนโดยโมลของกรดซิตริกต่อไนเตรตไอรอนเพิ่มขึ้นเท่ากับ 0.1 มีผลทำให้ค่าการเปลี่ยนของคาร์บอนมอนอกไซด์เพิ่มขึ้นเป็น 86.5% และลดลงอย่างมีนัยสำคัญเมื่ออัตราส่วนโดยโมลของกรดซิตริกต่อไนเตรตไอรอนเพิ่มขึ้น ในขณะที่ปริมาณกรดซิตริกที่มากเกินไปส่งผลให้มีคาร์บอนหลงเหลือบนพื้นผิวตัวเร่งปฏิกิริยาและลดความสามารถในการทำปฏิกิริยาการสังเคราะห์ฟิสเชอร์-ทรอปช์ พบว่าอัตราส่วนโดยโมลของกรดซิตริกต่อไนเตรตไอรอนที่เหมาะสมที่สุด ส่งผลให้ประสิทธิภาพค่าการเปลี่ยนของคาร์บอนมอนอกไซด์ที่สูงสุด เมื่อเปรียบเทียบตัวเร่งปฏิกิริยาที่เตรียมโดยวิธีออโตคอมบัสชันอื่นๆ เช่นเดียวกับตัวเร่งปฏิกิริยาอ้างอิงที่เตรียมด้วยวิธีการเคลือบฝังซึ่งตามด้วยขั้นตอนการรีดักชัน ในงานวิจัยนี้สนใจว่าตัวเร่งปฏิกิริยาเหล็กในการสังเคราะห์ฟิสเชอร์-ทรอปช์ ต้องการช่วงเวลาการเหนี่ยวนำเริ่มต้นของกระบวนการสังเคราะห์ฟิสเชอร์-ทรอปช์ ถึงแม้ว่าหลังจากผ่านขั้นตอนการรีดักชันก็ตาม เนื่องด้วยโลหะไอรอนต้องการช่วงเวลาการเหนี่ยวนำในการเปลี่ยนแปลงเฟสเป็นไอรอนเฟสที่มีความว่องไวในการเข้าทำปฏิกิริยา แต่พบว่าถึงแม้ว่าไม่ต้องผ่านขั้นตอนการรีดักชันไอรอนเฟสที่มีความว่องไวในการเข้าทำปฏิกิริยาสามารถเกิดขึ้นได้โดยตรงด้วยวิธีออโตคอมบัสชันและไม่ต้องการช่วงเวลาการเหนี่ยวนำเริ่มต้นในระหว่างการสังเคราะห์ฟิสเชอร์-ทรอปช์ ตัวเร่งปฏิกิริยาซึ่งเตรียมจากการใช้กรดซิตริกและตัวรองรับคิว 50 ให้ค่าการเปลี่ยนของคาร์บอนมอนอกไซด์สูงที่สุดเมื่อเปรียบเทียบกับชนิดอื่นๆ ดังนั้นผลการศึกษาวิธีออโตคอมบัสชันมีประโยชน์เพื่อสำหรับสังเคราะห์ตัวเร่งปฏิกิริยาที่มีประสิทธิภาพสูงโดยไม่ต้องผ่านขั้นตอนการรีดักชันเมื่อนำไปใช้ในการสังเคราะห์ฟิสเชอร์-ทรอปช์

สาขาวิชา ปิโตรเคมี	ลายมือชื่อนิสิต .....
ปีการศึกษา 2560	ลายมือชื่อ อ.ที่ปรึกษาหลัก .....
	ลายมือชื่อ อ.ที่ปรึกษาร่วม .....

จุฬาลงกรณ์มหาวิทยาลัย
Chulalongkorn University

5672853823 : MAJOR PETROCHEMISTRY
KEYWORDS: FISCHER-TROPSCH SYNTHESIS / AUTOCOMBUSTION / IRON CATALYSTS / SILICA / IRON CARBIDE

SUTHASINEE PENGNARAPAT: $FeCu/SiO_2$ CATALYSTS PREPARED BY AUTOCOMBUSTION METHOD FOR FISCHER-TROPSCH SYNTHESIS. ADVISOR: PROF. THARAPONG VITIDSANT, Ph.D., CO-ADVISOR: PROF. NORITATSU TSUBAKI, Ph.D., 105 pp.

The purpose of this study was to prepare iron-based catalysts supported on silica by autocombustion method for directly using for Fischer-Tropsch synthesis (FTS) without a reduction step. The effect of different citric acid (CA):iron nitrate (N) molar ratios (CA:N), acid types and SiO_2 supports on the FTS performance of catalysts were investigated. The CA:N had an important influence on the formation of iron active phases (Fe_xC) and FTS activity. Increasing the CA:N molar ratios up to 0.1 increased CO conversion of catalyst to 86.5%, which was then decreased markedly at higher CA:N molar ratios. An excess of CA resulted in carbon residues covering the catalyst surface and declined FTS activity. The optimal catalyst (CA:N molar ratio = 0.1) achieved the highest CO conversion when compared with other autocombustion catalysts as well as reference catalyst prepared by impregnation method, followed by a reduction step. More interestingly, iron-based FTS catalysts need induction duration at the initial stage of FTS reaction even after reduction, because metallic iron species need time to be transformed to Fe_xC. But here, even if without reduction, Fe_xC was formed directly by autocombustion and induction period was eliminated during FTS reaction. The catalyst prepared using CA and Q-50 type of SiO_2 gave a maximum CO conversion when compared with other catalysts. The autocombustion method had the advantage to synthesize more efficient catalysts without a reduction step for FTS.

จุฬาลงกรณ์มหาวิทยาลัย
Chulalongkorn University

Field of Study: Petrochemistry
Academic Year: 2017

Student's Signature .....
Advisor's Signature .....
Co-Advisor's Signature .....

ACKNOWLEDGEMENTS

I would never have been able to finish my dissertation without the guidance of my committee members, help from friends, and support from my family.

I would like to express my deepest gratitude to my advisor, Prof. Tharapong Vitidsant, for his excellent guidance, caring, patience, and guiding my research for the past several years. I would like to thank my co-advisor, Prof. Noritatsu Tsubaki, and Prof. Yoshiharu Yoneyama who let me experience the research of Fischer-Tropsch synthesis at Toyama University, Japan, patiently corrected my writing and financially supported my research. I would also like to thank Asst. Prof. Warinthorn Chavasiri, Assoc. Prof. Nuanphun Chantarasiri, Assoc. Prof. Prasert Reubroycharoen and Dr. Kitima Pinkaew, who was willing to participate in my final defense committee at the last moment.

I would like to acknowledge the Overseas Academic Presentation Scholarship for Graduate Students, Graduate School, Chulalongkorn University.

I would like to thank every laboratory worker of Prof. Tharapong, Prof. Tsubaki and Assoc. Prof. Prasert for helping and teaching me how to use laboratory equipments. My research would not have been possible without their helps.

I would also like to thank my parents. They were always supporting me and encouraging me with their best wishes.

จุฬาลงกรณ์มหาวิทยาลัย
CHULALONGKORN UNIVERSITY

CONTENTS

Page

THAI ABSTRACT iv

ENGLISH ABSTRACT v

ACKNOWLEDGEMENTS vi

CONTENTS vii

LIST OF TABLES xi

LIST OF FIGURES xii

LIST OF ABBREVIATION xv

CHAPTER I GENERAL BACKGROUND 1

1.1 Introduction 1

1.2 Scope of this work 3

1.3 Objectives 4

CHAPTER II THEORY AND LITERATURE REVIEWS 5

2.1 Fischer-Tropsch Synthesis (FTS) 5

2.1.1 Introduction 5

2.1.2 Feedstocks 5

2.1.2.1 Syngas composition 6

2.1.2.2 Process of syngas 8

2.1.3 Products 10

2.1.4 Mechanism 11

2.1.4.1 Surface carbide mechanism 11

2.1.4.2 Surface enol mechanism 12

2.1.4.3 CO insertion mechanism 13

จุฬาลงกรณ์มหาวิทยาลัย
Chulalongkorn University

Page

2.2 Catalysts of Fischer-Tropsch synthesis (FTS) 14
2.2.1 Key factors 14
2.2.2 FTS catalysts 15
2.2.3 Co and Fe Catalysts 16
2.2.4 Comparison between Co and Fe Catalysts 17
2.3 Fe catalysts 18
2.3.1 Introduction 18
2.3.2 Fe active phase 19
2.3.3 Promoters 21
2.3.4 Supports 22
2.4 Reactors for Fischer-Tropsch synthesis (FTS) 24
2.4.1 Fixed bed reactors 24
2.4.2 Slurry bed reactors 25
2.4.3 Fluidized bed reactors 26
2.5 Methods for Fischer-Tropsch synthesis (FTS) 27
2.5.1 Impregnation method 27
2.5.2 Autocombustion method 28
2.5.2.1 Introduction 28
2.5.2.2 Properties of reductants 29
2.5.2.3 Literature reviews 30
CHAPTER III EXPERIMENTAL 36
3.1 Materials and reagents 36
3.2 Catalyst Preparation 37

จุฬาลงกรณ์มหาวิทยาลัย
Chulalongkorn University

Page

3.2.1 Synthesis of CA: N molar ratios by autocombustion method 37

3.2.2 Synthesis of catalysts by impregnation method 38

3.2.3 Synthesis of acid types by autocombustion method 39

3.2.4 Synthesis of different SiO_2 supports by autocombustion method 39

3.3 Catalyst characterization 39

3.3.1 Nitrogen (N_2) physisorption 39

3.3.2 Scanning electron microscopy (SEM) 40

3.3.3 Energy-diffusive X-ray analysis (EDX) 41

3.3.4 X-ray diffraction (XRD) 41

3.3.5 Hydrogen-temperature programmed reduction (H_2-TPR) 42

3.3.6 X-ray photoelectron spectroscopy (XPS) 43

3.3.7 Thermogravimetric and differential thermal analyses (TG-DTA) 43

3.3.8 Transmission electron microscopy (TEM) 44

3.4 Catalytic activity test 45

CHAPTER IV RESULTS AND DISCUSSION 47

4.1 Characterization of catalysts with different CA:N molar ratios 47

4.1.1 Textural characteristic of catalysts 47

4.1.2 Morphology and element composition of the catalysts 49

4.1.3 Phase structure of the catalysts 50

4.1.3.1 XRD for calcined catalysts before FTS 50

4.1.3.2 XRD for used catalysts after FTS 52

4.1.4 Reduction behavior of catalysts 53

4.1.5 Phase structure of the catalysts in the surface region 54

จุฬาลงกรณ์มหาวิทยาลัย
Chulalongkorn University

Page

4.1.6 TG-DTA analysis of catalysts 56

4.1.6.1 Combustion process of catalysts 56

4.1.6.2 Level of residual carbon on used catalysts 58

4.1.7 TEM observation of catalyst 59

4.2 FTS activity and selectivity with different CA:N molar ratios 60

4.2.1 CO conversion 60

4.2.2 Products selectivity 63

4.3 FTS activity and selectivity with different acid types 65

4.4 Characterization of catalysts with different SiO_2 supports 66

4.4.1 Textural characteristic of catalysts 66

4.4.2 Phase structure of the catalysts 68

4.4.2.1 XRD for calcined catalysts before FTS 68

4.4.2.2 XRD for used catalysts after FTS 69

4.4.3 TEM observation of catalyst 70

4.5 FTS activity and selectivity with different SiO_2 supports 71

4.5.1 CO conversion 71

4.5.2 Products selectivity 73

CHAPTER V CONCLUSION AND RECOMMENDATION 75

5.1 Conclusion 75

5.2 Suggestion and Recommendation 76

REFERENCES 78

APPENDIX 89

VITA 105

จุฬาลงกรณ์มหาวิทยาลัย
Chulalongkorn University

LIST OF TABLES

Table 2.1 Fischer-Tropsch Synthesis (FTS) reactions 6

Table 2.2 Syngas composition from various feedstocks 7

Table 2.3 Properties of the FTS active metal 16

Table 2.4 Comparison of Co and Fe FTS Catalysts 18

Table 2.5 Physical properties of Fe 19

Table 2.6 Physical properties of SiO_2 23

Table 3.1 List of materials and reagents 36

Table 4.1 Physical properties of the SiO_2, Imp and calcined catalysts with different CA:N molar ratios 48

Table 4.2 FTS[a] performance of Imp and calcined catalysts with different CA:N molar ratios 61

Table 4.3 FTS[a] performance of calcined catalysts with different acid types 65

Table 4.4 Physical properties of SiO_2 and calcined catalysts with different SiO_2 supports 67

Table 4.5 FTS[a] performance of calcined catalysts with different SiO_2 supports 72

CHULALONGKORN UNIVERSITY

LIST OF FIGURES

Figure 2.1 Fischer-Tropsch Synthesis (FTS) plants operation [11]..... 8

Figure 2.2 Stages production process of syngas from biomass gasification [12]..... 9

Figure 2.3 Three main strategies of gasification for syngas from biomass [13]..... 10

Figure 2.4 Product distribution of the chain growth probability [8]..... 11

Figure 2.5 Surface carbide mechanism [18]..... 12

Figure 2.6 Surface enol mechanism [18]..... 13

Figure 2.7 CO insertion mechanism [18]..... 14

Figure 2.8 Three main parts of the catalysts [27]..... 15

Figure 2.9 Transformation for Fe phase during pretreatment and FTS [37]..... 20

Figure 2.10 Carburization behaviors of reduced iron phases [40]..... 21

Figure 2.11 Fixed bed reactors [50]..... 24

Figure 2.12 Slurry bed reactors [50]..... 25

Figure 2.13 Fluidized bed reactors [50]..... 26

Figure 2.14 Experimental set up for impregnation method [33]..... 28

Figure 2.15 Structures of (a) citric acid, (b) oxalic acid and (c) formic acid [61]..... 30

Figure 3.1 Schematic of catalyst preparation by autocombustion method..... 37

Figure 3.2 Calcination Instrument..... 38

Figure 3.3 Brunauer-Emmett-Teller (BET), NOVA 2200e..... 40

Figure 3.4 Scanning electron microscopy (SEM), JEOL JSM-6360..... 40

จุฬาลงกรณ์มหาวิทยาลัย
Chulalongkorn University

Figure 3.5 X-ray diffraction (XRD), Rigaku RINT 2200 41

Figure 3.6 Hydrogen-temperature programmed reduction (H_2-TPR)..... 42

Figure 3.7 Schematic of temperature programmed TPR 42

Figure 3.8 X-ray photoelectron spectroscopy (XPS), Thermo Scientific..... 43

Figure 3.9 Thermogravimetric and differential thermal analyses (TG-DTA)..... 44

Figure 3.10 Transmission electron microscopy (TEM), Philips Tecnai..... 45

Figure 3.11 Process Flow Diagram for Fischer-Tropsch synthesis (FTS)..... 46

Figure 3.12 The FTS unit for fixed bed reactor 46

Figure 4.1 SEM micrograph of (a) Imp, (b) 0.05CA, (c) 0.1CA, (d) 0.2CA and (e) 0.3CA 49

Figure 4.2 XRD patterns of Imp and calcined catalysts with different CA:N molar ratios before FTS; (◆) SiO_2; (■) Fe_2O_3; (●) Fe_3O_4 and (▲) Fe_xC 51

Figure 4.3 XRD patterns of used catalysts after FTS with Imp and different CA:N molar ratios; (◆) SiO_2; (●) Fe_3O_4 and (▲) Fe_xC 53

Figure 4.4 H_2-TPR profile of Imp and catalysts with different CA:N molar ratios.... 54

Figure 4.5 XPS spectra of (a) Imp, (b) 0.05CA, (c) 0.1CA, (d) 0.2CA and (e) 0.3CA... 55

Figure 4.6 TG-DTA curves of calcined catalyst before FTS of (a) 0.05CA, (b) 0.1CA, (c) 0.2CA, (d) 0.3CA and (e) citric acid..... 57

Figure 4.7 TG curves used catalysts after FTS with Imp and different CA:N molar ratios..... 59

จุฬาลงกรณ์มหาวิทยาลัย
CHULALONGKORN UNIVERSITY

Figure 4.8 TEM images of used catalysts after FTS (a) Imp, (b) 0.05CA, (c) 0.1CA, (d) 0.2CA and (e) 0.3CA 60

Figure 4.9 CO conversion vs time on stream with different CA:N molar ratios and impregnation method reaction condition: T=300 °C, P=1.0 MPa and W/F=10 g_{cat}h/mol 62

Figure 4.10 Products selectivity with different CA:N molar ratios and impregnation reaction condition: T=300 °C, P=1.0 MPa and W/F=10 g_{cat}h/mol 64

Figure 4.11 Influence of acid types on CO conversion and products selectivity with reaction condition: T=300 °C, P=1.0 MPa and W/F=10 g_{cat}h/mol 66

Figure 4.12 XRD patterns of calcined catalysts with different SiO_2 supports before FTS; ( ) SiO_2; ( ) Fe_2O_3; ( ) Fe_3O_4 and ( ) Fe_xC 69

Figure 4.13 XRD patterns of used catalysts with different SiO_2 supports after FTS reaction; ( ) SiO_2; ( ) Fe_3O_4 and ( ) Fe_xC 70

Figure 4.14 TEM images of used catalysts after FTS (a) 0.1CA/Q-3, (b) 0.1CA/Q-10 and (c) 0.1CA/Q-50 71

Figure 4.15 Influence of different SiO_2 supports on CO conversion and products selectivity with reaction condition: T=300 °C, P=1.0 MPa and W/F=10 g_{cat}h/mol . 74

จุฬาลงกรณ์มหาวิทยาลัย
CHULALONGKORN UNIVERSITY

LIST OF ABBREVIATION

Fe	Iron
SiO_2	silicon dioxide
wt%	weight percent
°C	degree celsius
nm	nanometer
mL	milliliter
min	minute (s)
g	gram (s)
et al.	and others
h	hour (s)
mol	mole
P	pressure
MPa	megapascal
T	temperature
MW	molecular weight
m^2	square metre
cm^3	cubic centimetre
cat	catalyst
W/F	ratio of weight of catalyst (g) to flow rate of reactant (mol/h)

จุฬาลงกรณ์มหาวิทยาลัย
Chulalongkorn University

CHAPTER I

GENERAL BACKGROUND

1.1 Introduction

Fischer-Tropsch synthesis (FTS) has recently received more attraction because of its highly environmental friendly property. The FTS is a process for the conversion of synthesis gas, a mixture of carbon monoxide (CO) and hydrogen (H_2), into a various range of liquid hydrocarbon fuels and highly valued chemicals. The advantage of hydrocarbons produced from FTS is high-quality free of sulfur and nitrogen. Therefore, FTS hydrocarbons are promising ultra clean hydrocarbon fuels for industry and transportation such as diesel and gasoline [1]. Three metals, ruthenium (Ru), iron (Fe) and cobalt (Co), have been found to be active as FTS catalysts. Nevertheless, Ru catalysts are expensive, making them economically prohibitive for large-scale industry. The cheaper Co and Fe catalysts are employed for industrial FTS. Although Co catalysts produce linear alkanes and have a high activity for hydrogenation, they are more expensive than Fe catalysts. Whereas, Fe catalysts are also active in FTS and can also be used for the processing of alkenes or oxygenates, which are significant chemicals raw materials. Furthermore, Fe catalysts prefer syngas with lower H_2/CO ratios and have a much higher water gas shift reaction (WGS) activity than Co or Ru catalysts. Consequently, these advantages make Fe catalysts quite attractive for coal or biomass

technology [2]. Fe catalysts readily transform to iron carbides (Fe_xC) in the presence of H_2/CO under a typical FTS, which is the principal active phase for hydrocarbon production in FTS. The iron phases are converted from the reduction of hematite phases (Fe_2O_3) to magnetite phases (Fe_3O_4), and then followed by the carburization of Fe metal to Fe_xC [3].

To achieve a high performance, copper (Cu) is frequently added to the Fe to realize a lower reduction temperature and reduce the level of sintering. Furthermore, Fe catalysts need an alkali metal, such as potassium (K), as a chemical promoter to enhance both the FTS and WGS activity and increase the selectivity for the long chain hydrocarbons. Lastly, Fe catalysts are often supported on silica (SiO_2), which provides a large surface area, small crystallites and high attrition resistance of catalyst [4]. Impregnation is a method of metal precursors is deposited on the porous support, followed by a drying, calcination and reduction [5]. The reduction step is the most significant. However, it is of high cost and some metals are difficult to reduce. Therefore, a new Fe catalyst preparation method, without a subsequent reduction process, will be of benefit for FTS.

Autocombustion is another method which uses energy from the exothermic decomposition of a redox mixture of organic acid and metal nitrates [6, 7]. The reducing gases such as H_2 and CO are released from the exothermic decomposition of the organic acid and then reduce the metal ions to active metal. Therefore, this process

can continue without an external energy source. This approach has the advantage of low cost and high energy performance.

1.2 Scope of this work

In this study, Fe-based FTS catalysts supported on SiO_2, containing Cu, K and citric acid (CA), were prepared by autocombustion method for directly using in FTS without a reduction step. The effect of different CA:iron nitrate (N) molar ratios, acid types and SiO_2 supports on the FTS performance of catalysts were investigated. The optimal catalyst was then compared with reference catalyst prepared by impregnation method, followed by a reduction step. The research studies were performed as follows:

1. Synthesis of Fe-based FTS catalysts supported on SiO_2, containing Cu, K and citric acid (CA), were prepared by autocombustion method.
2. Characterization of the Fe-based/SiO_2 catalysts using nitrogen physisorption (BET), scanning electron microscopy (SEM) with energy-diffusive X-ray spectroscopy (EDX), X-ray diffraction (XRD), hydrogen-temperature programmed reduction (H_2-TPR), X-ray photoelectron spectroscopy (XPS), thermogravimetric and differential thermal analyses (TG-DTA) and Transmission electron microscopy (TEM).
3. Study catalytic performance of Fe-based/SiO_2 catalysts for directly using in a fixed-bed reactor for FTS without a reduction step. Investigated parameters are
    - The different CA:iron nitrate (N) molar ratios (0.05, 0.1, 0.2 and 0.3)

จุฬาลงกรณ์มหาวิทยาลัย
CHULALONGKORN UNIVERSITY

- The different acid types (citric acid, oxalic acid and formic acid)
- The different SiO_2 supports (Q-3, Q-10 and Q-50)

1.3 Objectives

1. To prepare Fe-based FTS catalysts supported on SiO_2, containing Cu, K and citric acid (CA).
2. To investigate the effect of different CA:iron nitrate (N) molar ratios, acid types and SiO_2 supports on the FTS performance of catalysts.
3. To compare with reference catalyst prepared by impregnation method, followed by a reduction step.

จุฬาลงกรณ์มหาวิทยาลัย
CHULALONGKORN UNIVERSITY

CHAPTER II

THEORY AND LITERATURE REVIEWS

2.1 Fischer-Tropsch Synthesis (FTS)

2.1.1 Introduction

Fischer-Tropsch Synthesis (FTS) is a heterogeneous catalytic process for the transformation of synthesis gas (syngas, $CO+H_2$) into hydrocarbons. This process was first reported more than eighty years ago by two German chemists, Han Fischer and Franz Tropsch. The FTS process generally includes the following main and side reactions, as in Table 2.1. Both paraffins and olefin reactions are strongly exothermic reaction. In addition to the formation of alkanes and alkenes, which are usually the target products for FTS. Moreover, the water-gas shift (WGS) reaction also occurs over most FTS catalysts [8].

จุฬาลงกรณ์มหาวิทยาลัย
CHULALONGKORN UNIVERSITY

2.1.2 Feedstocks

Synthesis gas (Syngas) can be produced from many non-petroleum resources, such as natural gas, landfill gas, coal and biomass, through steam reforming, partial oxidation or gasification processes. The hydrocarbon products of FTS can be sulfur and nitrogen free high quality fuels such as diesel and gasoline fuels, which have been proven to be more environmentally than the petroleum based fuels. Therefore, they may easily meet the increasingly severe environmental regulations, for example low residual

sulfur content. Furthermore, chemicals such as alkenes or alkene may also be directly produced from syngas if a highly selective FTS catalyst can be developed. Therefore, FTS is an important step for the transformation of non-petroleum resources into super clean fuels or valuable chemicals from syngas [8, 9].

Table 2.1 Fischer-Tropsch Synthesis (FTS) reactions

Reactions	Equations
Main reactions	
1. Paraffins	$(2n+1)H_2 + nCO \longrightarrow C_nH_{(2n+2)} + nH_2O$
2. Olefins	$2nH_2 + nCO \longrightarrow C_nH_{2n} + nH_2O$
3. Water-gas shift (WGS) reaction	$CO + H_2O \longrightarrow CO_2 + H_2$
4. Methane	$3H_2 + CO \longrightarrow CH_4 + H_2O$
Side reactions	
5. Organic oxygenates	$2nH_2 + nCO \longrightarrow C_nH_{(2n+2)}O + (n-1)H_2O$
6. Alcohols	$2nH_2 + nCO \longrightarrow C_nH_{(2n+1)}O + nH_2O$
7. Boudouard reaction	$2CO \longrightarrow C + CO_2$

2.1.2.1 Syngas composition

Table 2.2 shows that syngas compositions from natural gas feedstocks have high H_2/CO ratios and low % CO_2 compared to those of coal, biomass and black oil feedstocks. Biomass gives syngas feeds with low H_2/CO ratio. Thus, syngas feeds from

coal and biomass sources are either H_2-deficient or CO_2 rich and fall short of the stoichiometric ratio required for the most desired reactions. Part of the energy in these fuel feedstocks is used to provide the heat needed in the endothermic steam reforming reactions. It has been estimated that about 20% of carbon in natural gas is completely burned and converted to CO_2 for this purpose. The H_2 content can be enhanced when the feed gas is reconditioned by mixing with feed gas from steam reforming of methane; but when used directly it implies much of the excess carbon in the feed gas must release as CO_2 via WGS. However, CO_2 has low level in terms of environmental impact and it is an important greenhouse gas. It also harmful affects the economy of the reaction and the process economy at large [10, 11].

Table 2.2 Syngas composition from various feedstocks

Feedstocks	Component (Vol %)			
	H_2	CO	CO_2	Others
Natural gas	73.8	15.5	6.6	4.1
Coal	39.1	18.9	29.7	12.3
Biomass	29.9	30.3	28.3	11.5
Black oil	39.2	38.1	19.1	3.6

As a result of these disadvantage, syngas from natural gas feedstocks are often preferred to those from coal and biomass feedstocks. However, fossil reserves are

จุฬาลงกรณ์มหาวิทยาลัย
CHULALONGKORN UNIVERSITY

localized in some regions of the world and some countries may have comparative advantage of one kind of fossil reserve over the other. Moreover for potential energy security and economic reasons, a country may adopt FTS plant on the basis of its fossil deposits. For example, coal based FTS plants have been in operation in South Africa since 1955, and several other FTS plants based on coal, as in Figure 2.1. The CO_2 emissions and the economy of hydrocarbon production via FTS reactions from these plants can be assumed [10].

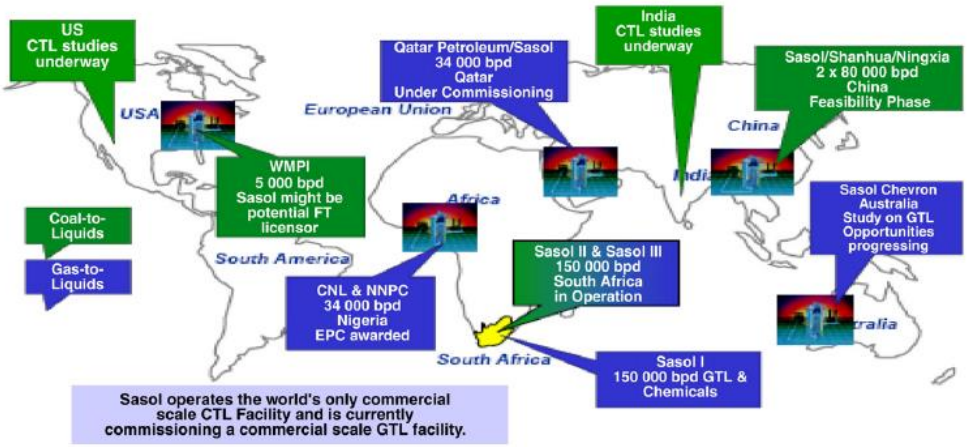

Figure 2.1 Fischer-Tropsch Synthesis (FTS) plants operation [11]

2.1.2.2 Process of syngas

High purity syngas from biomass gasification is currently a complex process involving many stages. Figure 2.2 shows the different stages of a conventional gasification process including pretreatment, gasification, gas purification and gas conditioning. These four main stages are generally processed in individual process units contributing to enlarge both the plant size and the associated investment and energy

costs. A catalytic cracking or reforming, CO_2 elimination, H_2 separation and the elimination of particles and other contaminants are first stage of pretreatment process. The second stage of gasification process, implementation of efficient primary catalysts for direct use in a fluidized bed gasifier is not a novel method in itself, but remains a technically challenging studied strategy [12, 13].

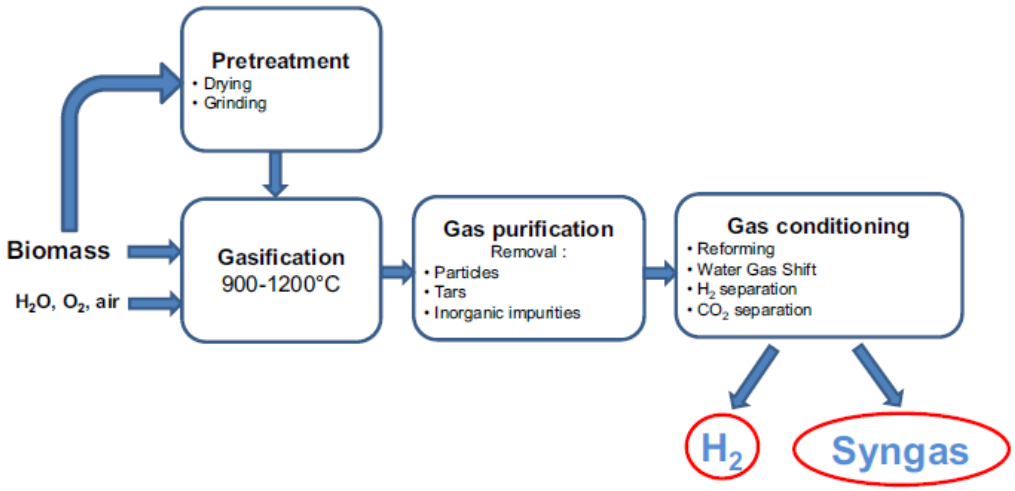

Figure 2.2 Stages production process of syngas from biomass gasification [12]

จุฬาลงกรณ์มหาวิทยาลัย
CHULALONGKORN UNIVERSITY

Multifunctional systems, incorporated into fluidized bed gasifiers can be considered a method and will be showed through a few relevant research in the third stage of gas purification process [12]. The last stage of gas conditioning process will be studied the development of new catalytic integrated gasification concepts recently proposed to achieve high conversion performances while carrying on significant process. Figure 2.3 shows the three main strategies are gasification, gas purification and gas conditioning which addressed in this review towards optimization and process intensification of syngas from biomass gasification [14].

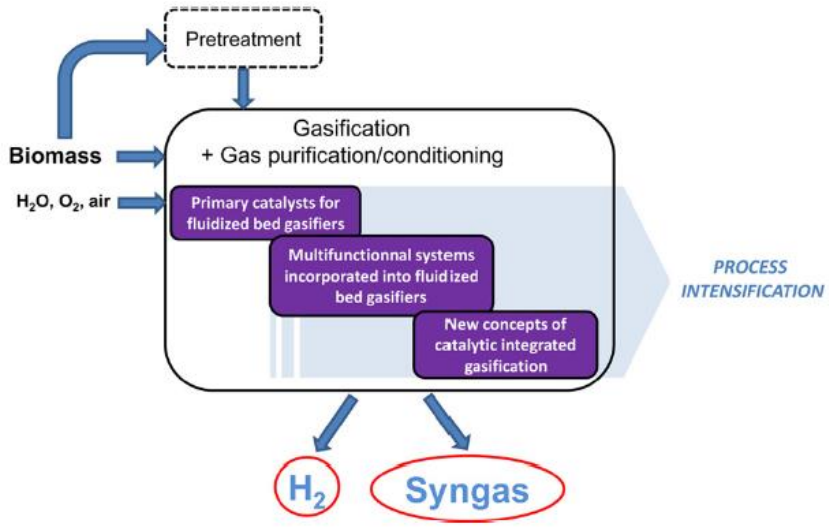

Figure 2.3 Three main strategies of gasification for syngas from biomass [13]

2.1.3 Products

However some challenges still remain, many studies have significantly contributed to the development of efficient FTS catalysts and reaction mechanism. Selectivity control is one of the most important challenges for FTS. As a result of the products of FTS generally follow a statistical hydrocarbon distribution, which is known as the Anderson-Schulz-Flory (ASF) distribution [8]. In the ideal case, when the chain growth probability (α) is expressed by α = Rp/(Rp+Rt), which is determined by the rates of chain growth (Rp) and chain termination (Rt). While the molar fraction (M_n) of a hydrocarbon with a carbon chain length (n) can be expressed by $M_n = (1-\alpha)^{n-1}$. So, the product distribution is determined by chain growth probability, as in Figure 2.4. Such a statistical product distribution is nonselective for a desired range of hydrocarbons. For example, the maximum selectivities to C_5-C_{11} for gasoline fuel and C_{12}-C_{20} diesel fuel are roughly 45% and 30 %, respectively [15-17].

จุฬาลงกรณ์มหาวิทยาลัย
CHULALONGKORN UNIVERSITY

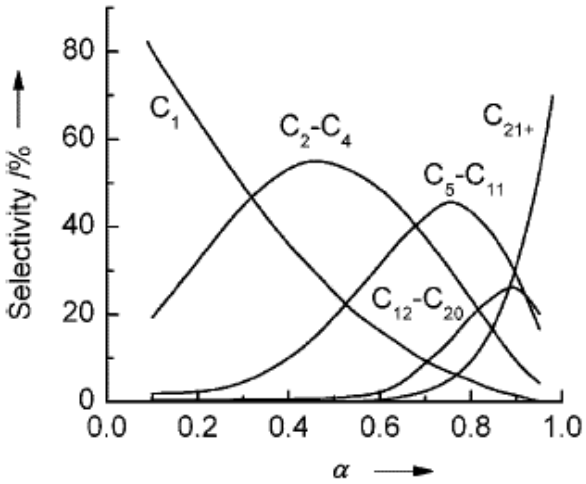

Figure 2.4 Product distribution of the chain growth probability [8]

2.1.4 Mechanism

The FTS reactions mechanism still continue a topic of discussion ever since the first mechanism was proposed in the original paper by Fischer and Tropsch. Many detailed reviews are available on the mechanism and models of hydrocarbon and oxygenate formation in FTS. Because a deeply discussion of the different reaction mechanisms would be further the scope of this review so a short overview of the three main mechanisms have been proposed. In general, all mechanisms assume six elementary reaction steps are reactant adsorption, chain initiation, chain growth, chain termination, product desorption, readsorption and further reaction [18].

2.1.4.1 Surface carbide mechanism

Surface carbide mechanism is the first, oldest and perhaps most accepted mechanism for FTS especially on Fe [18]. It proposed chain growth by CH_2 insertion, as in Figure 2.5. This mechanism assumes dissociative adsorption of CO and H_2,

followed by the formation of CH_2 which can combine and insert in growing chains. Chain termination can occur either by abstraction or addition of H atoms from or to the growing chain. It is remarked that in this mechanism, the CH_2 species should be either fixed to the catalyst surface, which implies the need for them to adsorb in close proximity to react alternatively. It can be assumed that the CH, CH_2 and CH_3 species are more mobile and are able move over the catalyst surface [19-21].

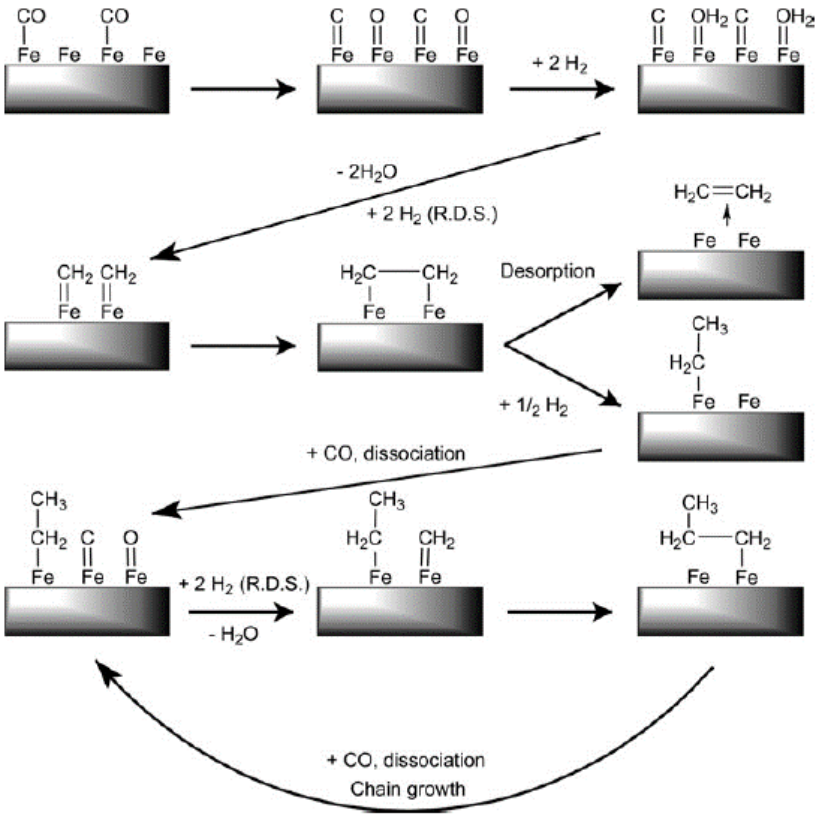

Figure 2.5 Surface carbide mechanism [18]

2.1.4.2 Surface enol mechanism

The second mechanism proposes chain growth through undissociative adsorption of CO [18], as in Figure 2.6. Surface H atoms react with the chemisorbed CO groups to

form enolic groups (HCOH). These enolic groups are presumed to either combine through a surface polymerization condensation reaction with loss of H_2O. Or, an alternative option for this mechanism is the individual hydrogenation of the enolic group, forming H_2O and CH_2 groups which can grow chains as was described in the previous mechanism [22-24].

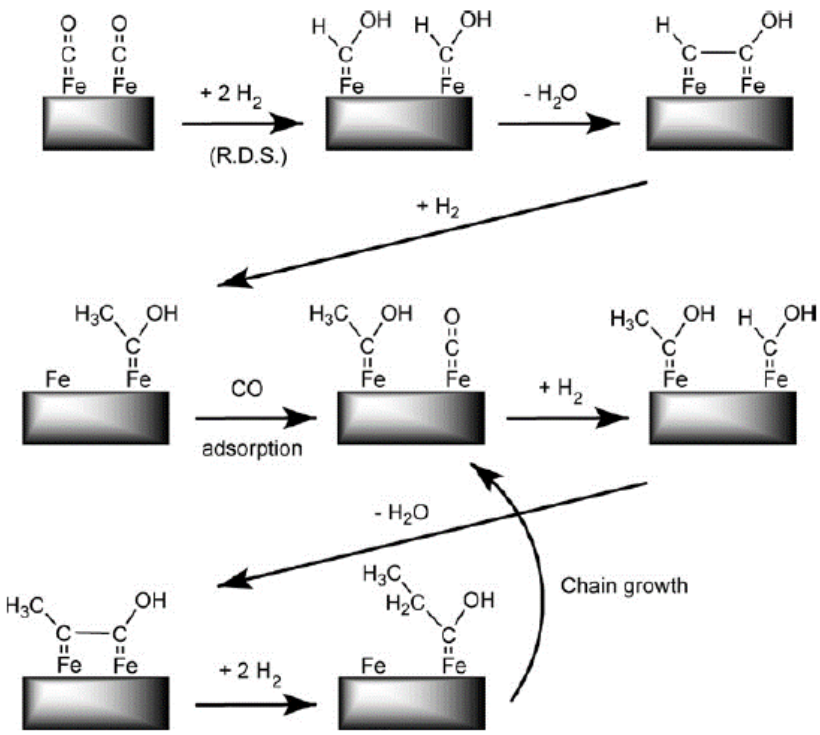

Figure 2.6 Surface enol mechanism [18]

2.1.4.3 CO insertion mechanism

Figure 2.7 shows the third reaction mechanism involves chain growth through insertion of CO molecules in the metal carbon bonds [18]. The reaction mechanism closely resembles well known patterns from coordination and organometallic chemistry. A CO molecule is inserted into the metal H bond in the initiation step. After

this, the formed surface aldehyde species is hydrogenated to CH_3 by nearby chemisorbed H atoms. Subsequently, CO can be inserted into the metal carbon bond and the resulting enol species can be hydrogenated again. Chain growth takes place by repeating this step. Termination can take place by hydrogenation of the growing chain, resulting in a free olefin chain and an adsorbed H atoms, from which another chain can initiate [25, 26].

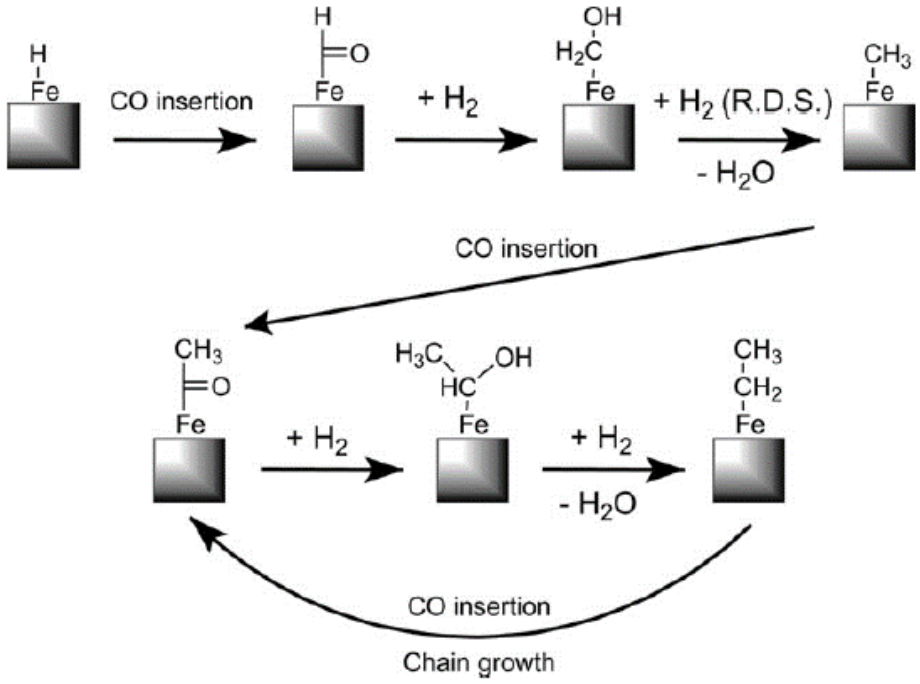

Figure 2.7 CO insertion mechanism [18]

2.2 Catalysts of Fischer-Tropsch synthesis (FTS)

2.2.1 Key factors

Most catalysts have three types of easily differentiate factors which are active component, a support and promoters [27]. Figure 2.8 shows a triangle to present

dependencies between these three factors. Active components are responsible for the principal chemical reaction. Selection of the active component is the first step in catalyst design. All of these investigations have shown that the supports and promoters strongly affect the structure, morphology and surface area and subsequently the catalytic performance of different catalytic systems [28].

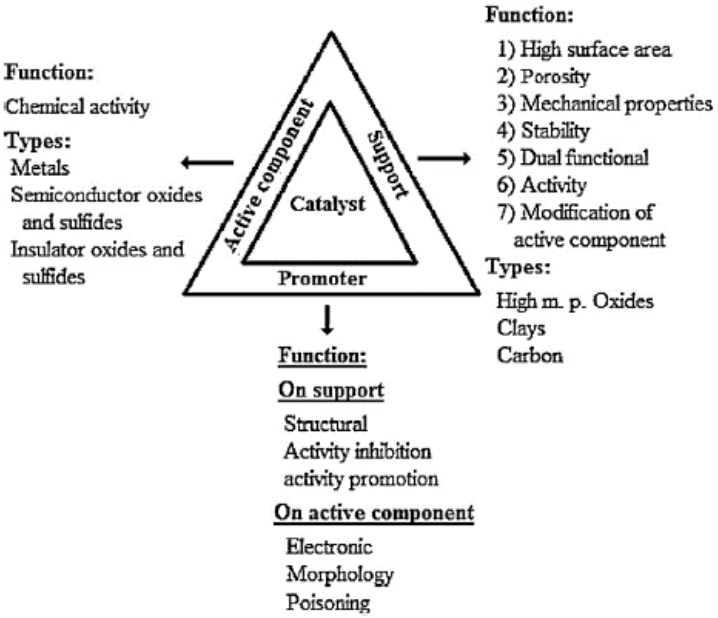

CHULALONGKORN UNIVERSITY

Figure 2.8 Three main parts of the catalysts [27]

2.2.2 FTS catalysts

FTS catalysts are typically based on group VIII metals such as Iron (Fe), Cobalt (Co), Nickel (Ni) and Ruthenium (Ru), with Fe and Co being the most popular. Ru, Fe and Co have been used in this process, but the latter are the most widely studied [29]. Although, Ru shows good catalytic properties, its annual world supply cannot even fulfil the requirements of plant. On another aspect of catalytic active center, Fe, Ni,

and Co are the most active metals for FTS. Vannice et al. [30] showed that the molecular average weight of hydrocarbons produced by FTS decreased in the following sequence: Fe> Co > Rh > Ni > Ir > Pt > Pd [31]. The active metals and their properties as FTS catalysts are presented in Table 2.3. The choice of active metal has important implications on the selectivity and the cost of the FTS catalyst. It is clear that Co and Fe catalyst are commonly used commercially [10].

Table 2.3 Properties of the FTS active metal

Active metal	Price ratio	Properties
Fe	1	Considered suitable for FTS with syngas with low H_2/CO ratio and good water-gas shift (WGS) reaction
Co	230	Considered suitable for FTS with syngas with high H_2/CO ratio and little water-gas shift (WGS) reaction
Ni	250	Considered suitable primarily for methanation
Ru	31,000	Too expensive
Rh	570,000	Too expensive

2.2.3 Co and Fe Catalysts

Under the same experimental conditions, Fe catalysts lead to the formation of light hydrocarbons and small amounts of CH_4 in comparison to Co catalysts. On the other hand, Co catalysts show high catalytic activity and are suitable for the production

of middle distillates and waxes, but they are more expensive [31]. Co and Fe are the metals which were proposed by FTS as the first catalysts for syngas conversion. Both Co and Fe catalysts have been used in the industry for hydrocarbon synthesis. Co catalysts operate at a very narrow range of temperatures and pressures. Increasing temperature of them leads to a spectacular increase in methane selectivity. Fe catalysts have been used in FTS of hydrocarbons from syngas since 1923. Fe catalysts seem to be more appropriate for conversion of biomass derived syngas to hydrocarbons than Co systems because they can operate at lower H_2/CO ratios [32].

2.2.4 Comparison between Co and Fe Catalysts

Co and Fe are the metals which were proposed by FTS as the first catalysts for syngas conversion. Both Co and Fe catalysts have been used in the industry for hydrocarbon synthesis [33]. A comparison of Co and Fe catalysts is shown in Table 2.4. Co catalysts are more expensive, but they are more resistant to deactivation. The productivity at higher conversion is more significant with Co catalysts. Water generated by FTS slows the reaction rate on Fe to a greater extent than on Co catalysts. The water-gas shift (WGS) reaction is more significant on Fe than on Co catalysts. Both Fe and Co catalysts are very sensitive to sulfur, which could readily contaminate them. For Fe catalysts, the syngas should contain less than 0.2 ppm of sulphur but, the amount of sulfur for Co catalyst should be less than 0.1 ppm. Co catalysts on oxide supports are generally more resistant to attrition than Fe catalysts support. Fe catalysts

seem to be more appropriate for conversion of biomass derived syngas to hydrocarbons than Co systems because they can operate at lower H_2/CO ratios [34].

Table 2.4 Comparison of Co and Fe FTS Catalysts

Parameter	Co	Fe
Cost	More expensive	Less expensive
Lifetime	More resistance	Less resistance
Activity	Higher; less significant of H_2O on rate CO conversion	Lower; strong negative of H_2O on rate CO conversion
Water-gas shift	Not very significant	Significant
Maximal sulfur	<0.1 ppm	<0.2 ppm
Attrition resistance	Good	Not very resistant
H_2/CO	2	0.5-2.5

จุฬาลงกรณ์มหาวิทยาลัย
CHULALONGKORN UNIVERSITY

2.3 Fe catalysts

2.3.1 Introduction

Fe is a chemical element with atomic number 26. It is a metal in the first transition series. It is by mass the most common element on Earth, forming much of Earth's outer and inner core. Like the other group VIII, Fe exists in a wide range of oxidation states, -2 to +7, although +2 and +3 are the most common [35], as in Table 2.5. Fe catalysts have been widely investigated recently because of their low cost, high activity, and

capability, and they operate over a wide temperature range to produce diesel fuel in low temperature FTS or gasoline fuel in high temperature FTS.

Table 2.5 Physical properties of Fe

Parameter	Properties
Name	Iron
Symbol	Fe
Electron configuration	$[Ar]3d^6 4s^2$
Atomic number	26
Density, g/cm^3	7.87
Melting point, °C	1538
Boiling point, °C	2862

จุฬาลงกรณ์มหาวิทยาลัย
CHULALONGKORN UNIVERSITY

2.3.2 Fe active phase

Normally, Co, Ni and Ru remain in metallic state under FTS conditions, but the composition of Fe catalysts changes during FTS. Several phases of Fe are known in Fe catalysts subjected to FTS conditions. These include metallic iron (α-Fe), iron oxides (hematite, α-Fe_2O_3; magnetite Fe_3O_4, and Fe_xO), and five different forms of iron carbides [36]. The formation and composition of these iron phases depend on the process

conditions, catalysts activation and deactivation, and catalyst composition. The role of Fe phases in FTS that indicate the iron carbide phases result in high FTS activity whereas the magnetite phase has negligible catalytic activity toward FTS reactions but may be active for WGS reaction. For this reason, the reduction and carburization processes are performed by H_2 and syngas, respectively. Bulk and surface changes in the speciation of iron during the pretreatment of FTS reaction on iron catalysts have been studied and sequential bulk phase modifications during the activation process from Fe_2O_3 to Fe_3O_4 to Fe_xC have been reported [37]. The sequence of transformation for iron phases during the pretreatment and FTS, as in Figure 2.9. It also addresses the changes that occur during the exposure to H_2 and syngas environments.

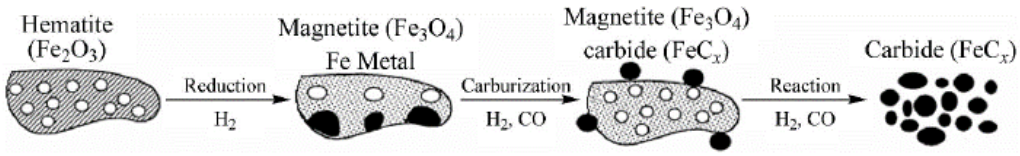

จุฬาลงกรณ์มหาวิทยาลัย

Figure 2.9 Transformation for Fe phase during pretreatment and FTS [37]

CHULALONGKORN UNIVERSITY

Combined with the characterization results in both the bulk and surface regions and a clear scene is obtained on reduction and carburization behaviors of different iron species, as in Figure 2.10. In H_2 the α-Fe_2O_3 in the fresh catalyst is firstly reduced to Fe_3O_4 in both the bulk and surface regions. The formed Fe_3O_4 is reduced continually to FeO in the role of metal support interaction. Then the FeO is reduced to α-Fe which both occurring in the bulk and on the surface layers. The reduced iron phases such as Fe_3O_4, FeO and α-Fe can be converted to iron carbides in CO and/or syngas.

Carburization ability of reduced iron species is following the order α-Fe > FeO > Fe_3O_4 [38, 39]. Because of the strongest carburized ability of α-Fe, iron carbides are formed mainly on Fe_3O_4 sites. As the surface iron phases are converted completely to iron carbides (Fe_xC) and the hydrocarbons species are formed mainly on the catalyst. This suggesting that Fe_xC plays a positive role in providing the FTS active sites [40].

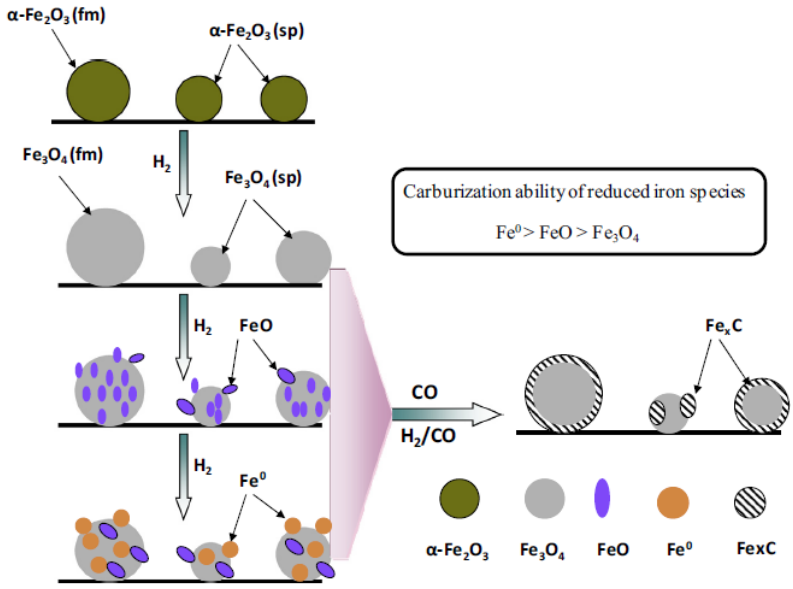

Figure 2.10 Carburization behaviors of reduced iron phases [40]

จุฬาลงกรณ์มหาวิทยาลัย
CHULALONGKORN UNIVERSITY

2.3.3 Promoters

Catalysts for the FTS reaction are mostly based on Fe which is promoted with copper as a reduction promoter, potassium as a chemical promoter and silica (SiO_2) as a support. The influence of Cu and K promoters on the activity of Fe catalysts has been studied extensively [41]. Copper is a chemical element with symbol Cu and atomic number 29. Cu have several functions in Fe catalysts. It functions as a physical promoter by enhancing H_2 adsorption, delaying Fe oxidation and improving Fe oxide

reducibility. Moreover, it functions as chemical promoter through charge transfer from Cu to adsorbed CO, weakening the adsorbed CO bonds and enhancing the dissociative adsorption rates. Cu also enhances the conversion of CO and the selectivity towards hydrocarbons with higher carbon number [42, 43]. Potassium is a chemical element with symbol K and atomic number 19. The K promoter is usually related to the formation of surface oxygen (from K_2O) that improves the polarization within co-adsorbed CO and H_2, favouring the adsorption and dissociation of CO while improving the selectivity towards C_{5+} products. Li et al [44] found that the addition of Cu enhances the rate of Fe_2O_3 reduction to Fe_3O_4 in H_2, and the coexistence of K and Cu provides an easier route for the formation of Fe_3O_4 which is benefit to carbonization under CO conditions [45].

2.3.4 Supports

Several supports for Fe catalysts have been developed and tested to obtain FTS products. SiO_2, alumina, molecular sieves, titania, zirconia, carbon and zeolites have been the most studied supports for FTS catalysts. SiO_2, as a common support used in the catalysts of FTS, presented the characteristics of higher surface area, porosity, stability and weaker metal support interaction than alumina as support [46, 47], as in Table 2.6. While, Fe forms mixed oxides when supported on alumina due to the influence of strong metal support interactions, which are difficult to reduce and to allow the formation of the active Fe carbide. So, using SiO_2 is alternative choice to

supports for Fe FTS catalysts High surface area of SiO_2 also functions is as a support in selected industrial application. It is used for primarily the catalytic oxidation of SO_2 to SO_3 in the production of sulfuric acid. SiO_2 is also used to support chromium oxide in catalysts for polyethylene production [48, 49]. The effect of different SiO_2 supports (pore size) can be investigated from many products such Q-3, Q-10 and Q-50.

Table 2.6 Physical properties of SiO_2

Parameter	**Properties**
Names	Silica
Molecular formula	SiO_2
Molar mass	60.1 g/mol
Appearance	White or colorless solid
Status	Solid at atmosphere
Density	2.6 g/cm^3
Melting point	1610 °C
Boiling point	2230 °C
Solubility	Insoluble in water

จุฬาลงกรณ์มหาวิทยาลัย
CHULALONGKORN UNIVERSITY

2.4 Reactors for Fischer-Tropsch synthesis (FTS)

The clarification of key factors determining the catalytic behaviors, the development of novel catalysts with enhanced catalytic performances and the elucidation of reaction mechanism were the main targets of fundamental research in FTS in the past decade. The reactor types are engineering factors which are the key catalyst factors for FTS.

2.4.1 Fixed bed reactors

The fixed bed reactor type is multi-tubular with the catalyst placed inside the tubes with small diameter and cooling water on the shell side, as in Figure 2.11.

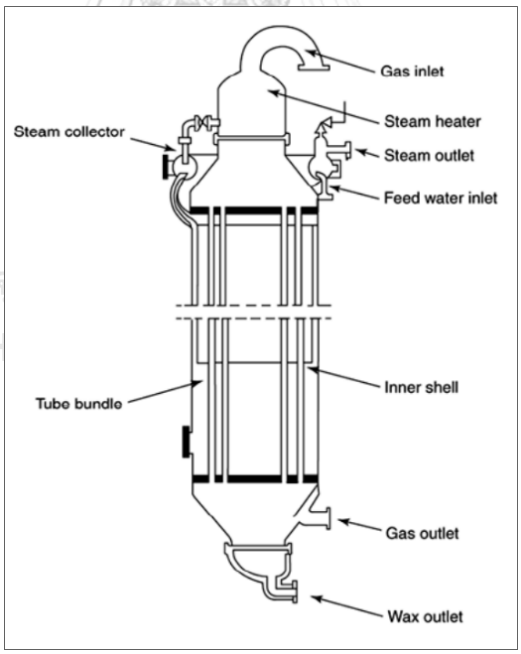

Figure 2.11 Fixed bed reactors [50]

Heavy wax products is produced from the fixed bed reactor. Having a short distance between the catalyst particles and the tube walls and operating at high gas

linear velocities, to ensure turbulent flow, greatly improves the transfer of the heat of reaction from the catalyst particles to the cooling water. The most important advantages, for the fixed bed reactors is easy to operate, that the performance of a large scale commercial reactor can be predicted with relative certainty based on the performance of a pilot unit consisting of a single reactor tube [50, 51].

2.4.2 Slurry bed reactors

The slurry bed reactors type is proceeded by gas that is passed through suspension of small catalyst particles in a liquid with low vapor pressure, as in Figure 2.12.

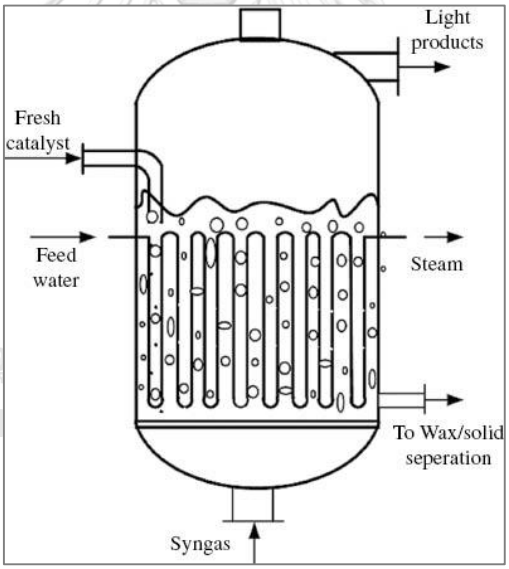

Figure 2.12 Slurry bed reactors [50]

Low temperature FTS operation is used since the liquid wax itself would be the medium in which the finely divided catalyst is suspended. Heavy wax products is produced from the slurry bed reactor. However, a practical and efficient means of separating the product wax from the catalyst is an essential requirement. The serious

issues for slurry bed reactors are back mixing of the gas phase, catalyst attrition and separation from the liquid and wax products [52].

2.4.3 Fluidized bed reactors

For this application fluidized bed reactors type are the units of choice. So, the Fluidized bed reactors of two phase are used to run the FTS process. Due to the high degree of turbulence in fluidized beds they exhibit very high rates of heat exchange. This means they can cope with the large amounts of reaction heat released at high conversion with high feed gas throughputs that can be achieved at high operating temperatures, as in Figure 2.13. However, they all have disadvantages. For instance, fluidized bed reactors require catalysts with good mechanical strength and complicated downstream recovery processes [53].

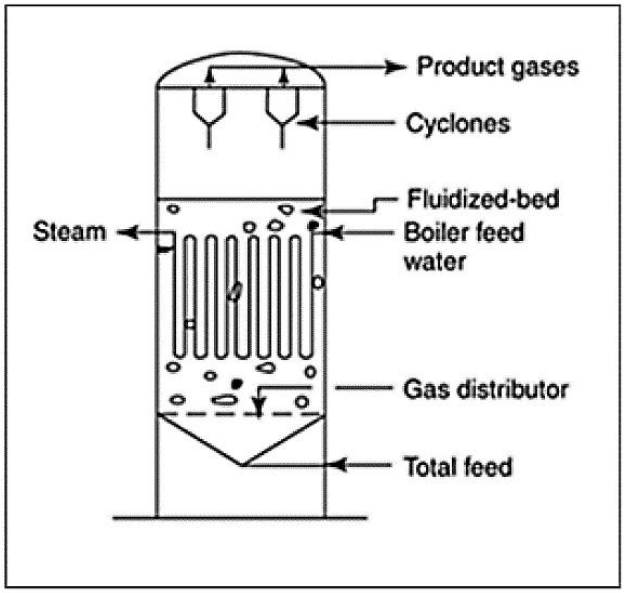

Figure 2.13 Fluidized bed reactors [50]

2.5 Methods for Fischer-Tropsch synthesis (FTS)

Most of Fe catalysts used in FTS were prepared using co-precipitation method. Simultaneously, promoters, such as Cu and K, were added to improve the activity and the selectivity. Compared to the precipitated Fe catalysts, supported Fe catalysts exhibit many advantages, such as improved catalyst stability, decreased deactivation rate, and improved long chain hydrocarbon selectivity. So, supported Fe catalysts which is impregnation method is used for method of FTS [54].

2.5.1 Impregnation method

Impregnation is the most common method to prepare metal supported catalysts. In impregnation method a solution of metal salt, typically metal nitrate, is contacted with a dry porous support. After being contacted, the solution is desired by the capillary forces inside the pores of the support. All pores of the support are filled with the liquid and there is no excess moisture over and above the liquid required to fill the pores [33]. Although at the first sight the practical execution of impregnation is simple, the fundamental phenomena underlying impregnation and drying are extremely complex. Reproducible synthesis of metal catalyst requires careful control of all impregnation parameters for example, temperature and time of support drying, rate of addition of impregnating solution, and temperature and time of drying. An experimental set up used in our laboratory for impregnation method, as in Figure 2.14. The reduction step is the final step in the production of supported metal catalysts.

The purpose of it is to convert oxides and catalyst precursor salts to the metal by treatment in H_2 or other reducing agent such as CO and syngas. The reducing agents should be purified of impurities such as O_2, sulfur, H_2O and hydrocarbons which serve to contaminate the catalyst. Temperature is the most important variable in the reduction step. It needs to be carefully optimized for each supported metal system. For example, there is an optimum temperature for maximizing dispersion and surface area and extent of reduction for a given metal support system [55, 56].

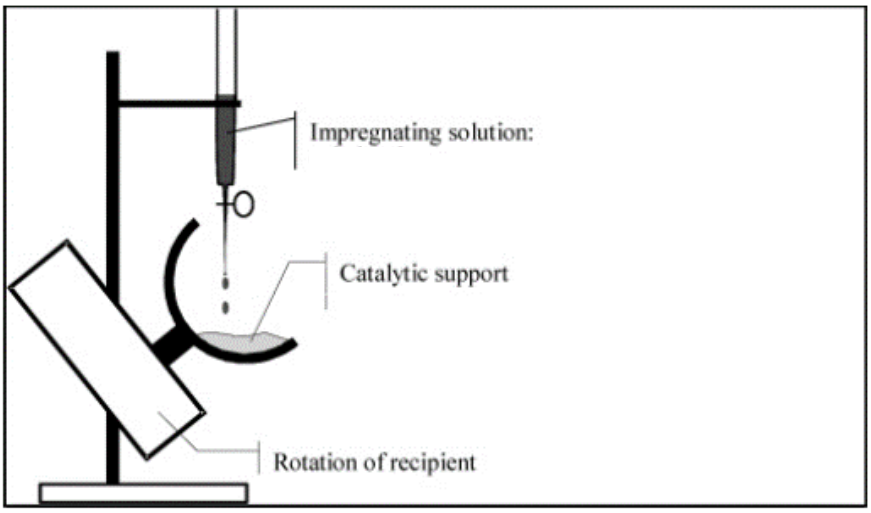

CHULALONGKORN UNIVERSITY

Figure 2.14 Experimental set up for impregnation method [33]

2.5.2 Autocombustion method

2.5.2.1 Introduction

Autocombustion is a method to produce catalysts with high reduction levels. A low temperature is required to start the combustion and then the combustion can continue without external energy supply. It is exothermic decomposition of a redox

mixture of metal salts and reductants [6, 7]. Therefore, the advantages of low cost and high energy efficiency. During the combustion process, the metal can be reduced by the released gases such as H_2, CH_4 and CO from the pyrolysis of the reductant. However, the autocombustion process is very complex and usually occurs violently. It is more difficult to control the reduction level than using H_2 reduction.

2.5.2.2 Properties of reductants

Citric acid is a weak organic tricarboxylic acid having the chemical formula $C_6H_8O_7$, as shown in Figure 2.15. It occurs naturally in citrus fruits. More than a million tons of citric acid are manufactured every year. It is used widely as an acidifier, as a flavoring and chelating agent. Citric acid is an excellent chelating agent, binding metals by making them soluble [57-59]. A chelating agent is a molecule with two or more potential electron pair donor atom that can act as a ligand, which attaches itself to a metal ion. Actually, the formation of a metal chelate is a Lewis acid-base reaction. The chelating agents most commonly used for the preparation of supported catalysts from aqueous solution are citric acid. The Lewis structures of the related anions of citric acid for the formula of the citrate ion is written as trisodium citrate, $C_6H_5O_7^{3-}$.

Oxalic acid is an organic compound with the formula $C_2H_2O_4$ (Figure 2.15). It is a colorless crystalline solid that forms a colorless solution in water, as the simplest dicarboxylic acid. Its acid strength is much greater than that of acetic acid. Oxalic acid

is a reducing agent and its conjugate base, known as oxalate ($C_2O_2^{-4}$), is a chelating agent for metal cations [60].

Formic acid, systematically named methanoic acid, is the simplest carboxylic acid. The chemical formula is HCO_2H (Figure 2.15). It is an important intermediate in chemical synthesis and occurs naturally, most notably in some ants. The anion derived from formic acid were called formates [61].

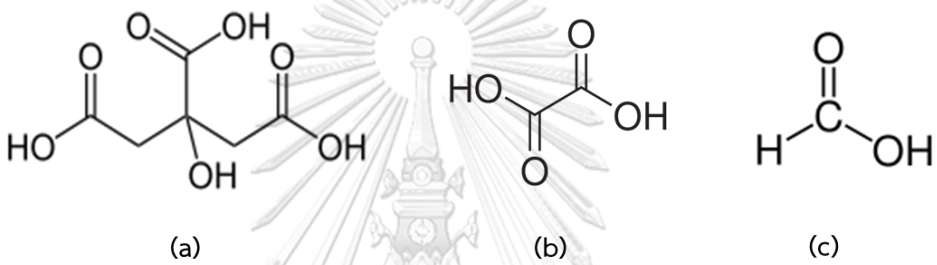

Figure 2.15 Structures of (a) citric acid, (b) oxalic acid and (c) formic acid [61]

2.5.2.3 Literature reviews

Shi et al. [62] investigated Co/SiO_2 catalysts prepared by autocombustion method using nitrate ions, varying levels of citric acid and burning in an argon atmosphere. Increasing the citric acid content in the mixture increased the reduction and dispersion of Co as the Co crystalline size gradually declined. Increasing levels of carbonic residues were found in the catalysts as the citric acid contents increased. Nevertheless, the supported Co catalysts were directly achieved in a slurry phase reactor for FTS without further reduction.

Phienluphon et al. [63] discussed the Ru-Co/SiO_2 catalysts have been synthesized by autocombustion method using citric acid as the reductant and nitrate ions as the oxidant. The addition of a small amount of Ru enhanced the reduction and dispersion of Co. The FTS activity significantly increased from 0.8 to 41.4% due to existing of Ru, so this Ru-Co/SiO_2 catalysts prepared by autocombustion was used successfully in FTS without further reduction.

Li et al. [64] studied homogeneous, crystalline and unagglomerated multicomponent of lithium aluminate using different fuel types by autocombustion method. As citric acid, urea, carbohydrazide, glycine and alanine were used as different fuels. The phase formation of the final products results from the fuel types and the ratio of fuel to nitrates. Furthermore, lithium aluminate from combustion synthesis is more efficient, quick and economic than conventional solid state reaction method.

Chandradass et al. [65] examined synthesis of alumina-zirconia nanopowder by autocombustion method using different fuel types such as, citric acid, acetyl acetone, oxalic acid and urea. The results showed fuel types are significant on phase formation and tetragonal phase. The presence of citric acid was observed that particle size was approximately 60 nm.

Hua et al. [66] obtained a series of Co-Ni alloy powder were prepared by autocombustion method. The results of XRD patterns displayed the mixing of components in the alloys at atomic level. Moreover, TEM images reveal size of the

grain size of the samples is about 10 nm. Thus, the synthesis of Co-Ni alloy powder was effectively prepared by autocombustion method.

Chen et al. [67] applied nanocrystalline ceria based powders which were prepared using autocombustion method with ethylene glycol as a fuel and nitrate ions as the oxidant. Ethylene glycol was successfully used as a fuel in solution combustion synthesis of nanocrystalline ceria based powders for the first time. Moreover, it was not only cheap but also readily available and had a great potential for large scale application in solution combustion synthesis.

Marinšek et al. [68] built mixed oxide powders which were prepared by the citrate (c)/nitrate (n) autocombustion method that can produce final composite without employing any intermediate processes. The c/n initial molar ratio has an important influence on the combustion processing. NiO-YSZ powders e average particle sizes occurred from redox combustion reaction between the c/n molar ratio. Ni particles are randomly distributed inside. Good Ni distribution and appropriate Ni content achieved metallic conduction throughout the composite.

Vajargah et al. [69] exhibited auto catalytic behavior, which can be used to synthesize nanocrystalline yttrium iron garnet powders by a autocombustion method. The influence of metal nitrates to citric acid molar ratio (MN/CA) of the precursor solution on the combustion behavior and crystallite size of synthesized powder. It must be noted that increasing MN/CA value, the combustion rate increases and the

single phase forms at a higher temperature. Besides, the crystallite size of the powders increased with increasing the calcination temperature.

Peng et al. [70] studied nanocrystalline alumina powders were prepared by autocombustion method using glycine as fuel and nitrate as an oxidizer. With decreasing the pH values in the precursor solutions, the obtained materials could be modified from various nanoparticles. The rates of decomposition at different pH values were found to be responsible for the generation of flake or segregated nanoparticles during auto ignition reactions. The specific surface areas of the products ranged from 96 to 39 m^2/g with the pH decreased from 10.5 to 2.5.

Bahadur et al. [71] discovered single barium ferrite nanoparticles which were synthesized with narrow particle size distribution using autocombustion method. In this process, citric acid was used as a fuel and ratios of cation to fuel were maintained variously. A cation to citric acid ratio of 1:2 gives better yield in the formation of crystalline and single particles with a narrow range of size distribution. Most particles are in the range of 80 to 100 nm.

จุฬาลงกรณ์มหาวิทยาลัย
CHULALONGKORN UNIVERSITY

Shi et al. [72] suggested a series of Co/SiO_2 catalysts were prepared by autocombustion method using cobalt nitrates and citric acid, and the precursors were burnt in different calcination atmospheres. The burnt catalyst was first burnt in argon and then oxidized in air (C-argon-air-reduction) had about 10 nm Co_3O_4 crystalline size, much smaller than that which was directly burnt in air has about 15 nm and that prepared by impregnation method (CN-reduction) had about 32 nm. So, the activity of

the C-argon-air-reduction was three fold higher than that of the reference CN-reduction. The autocombustion method succeeded to prepare highly dispersed supported metallic catalysts with smaller particle sizes.

Gegova et al. [73] proposed nanoparticles in the $ZnO-TiO_2$ catalysts which were synthesized by autocombustion method using different precursors. It was found that the nanosized ZnO particles (2-8 nm) in the $ZnO-TiO_2$ system. Also, it was established that the addition of zinc nitrate solution to the titanium ethoxide one, lead to obtaining of more fine particles (2 nm). The obtained powders are with good photocatalytic activity in the UV and VIS range of the spectra.

Xu et al. [74] studied $BaFe_{12}O_{19}$ powders with nanocrystalline sizes were produced by autocombustion method. Fe^{3+} and Ba^{2+}, in a molar ratio of 11.5, were chelated by citric acid ions at different pH. XRD patterns of the powders showed that the well-crystalline powder was produced when pH was 10. It was exhibited that pH in the starting solution had an important influence on magnetic properties.

จุฬาลงกรณ์มหาวิทยาลัย
CHULALONGKORN UNIVERSITY

Yue et al. [75] showed the dried nitrate-citrate gels were prepared autocombustion method. It was indicated that the pH value of the mixed precursor solutions has a significant influence on the morphology of dried gels. With increasing pH value, the combustion rate is increased significantly. The as-burnt powders become uniform in size and the crystallites size is increased from 26 to 48 nm with pH value increasing from 2 to 7.

Shi et al. [76] used autocombustion method to prepare Cu/ZnO and Cu-ZnO/SiO_2 nanostructured metallic catalysts. The XRD patterns showed all the xerogels were turned to nanostructured metallic catalysts directly without further reduction. The activity of nanostructured metallic catalyst was related on Cu surface areas and crystallite sizes. Furthermore, preparation of Cu/ZnO and Cu-ZnO/SiO_2 nanostructured metallic catalysts are cheap raw materials and uncomplicated operation conditions. So, this method opens a new way especially the catalysts which were difficult to be reduced at higher temperature.

จุฬาลงกรณ์มหาวิทยาลัย
CHULALONGKORN UNIVERSITY

CHAPTER III

EXPERIMENTAL

3.1 Materials and reagents

The materials and reagents used in this research were listed in Table 3.1.

Table 3.1 List of materials and reagents

Chemicals	Sources
Iron (III) nitrate nonahydrate ($Fe(NO_3)_3.9H_2O$)	Wako Pure Chemical
Copper (II) nitrate trihydrate ($Cu(NO_3)_2.3H_2O$)	Wako Pure Chemical
Potassium nitrate (KNO_3)	Kanto Chemical
Citric acid ($C_6H_8O_7$)	Sigma-Aldrich
Ammonia solution (28%, A.R. Grade)	Wako Pure Chemical
Silica (Cariact, Q-3, Q-10 and Q-50)	Fuji Silysia Chemical
Oxalic acid ($C_2H_2O_4$)	Wako Pure Chemical
Formic acid (CH_2O_2)	Kanto Chemical
Argon gas (99.99% purity)	Praxair
Carbon monoxide gas/Hydrogen gas (CO/H_2) 1:1	BOC Scientific
Standard gas CO:20%, CH_4:20%, H_2:20% and bal He	BOC Scientific
Nitrogen gas (99.99% purity)	Praxair

จุฬาลงกรณ์มหาวิทยาลัย
CHULALONGKORN UNIVERSITY

3.2 Catalyst Preparation

3.2.1 Synthesis of CA: N molar ratios by autocombustion method

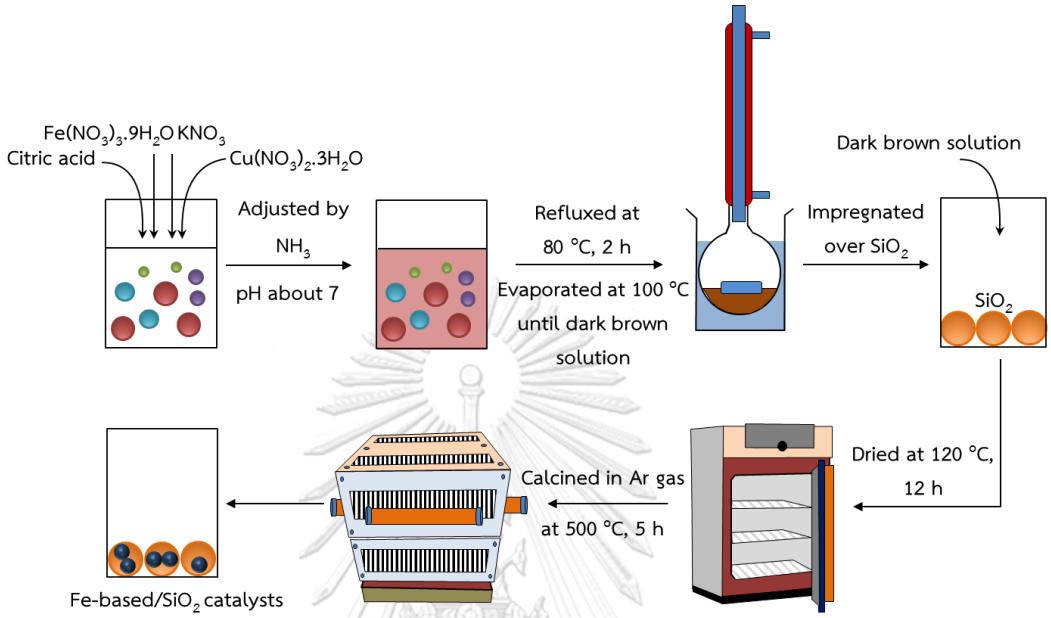

Figure 3.1 Schematic of catalyst preparation by autocombustion method

From Figure 3.1, the Fe-based catalysts supported on SiO_2 (Fuji Silysia Co.Ltd., Q-50), containing Cu and K, were prepared by autocombustion method, using iron (III) nitrate nonahydrate, copper (II) nitrate trihydrate and potassium nitrate at a Fe:Cu:K molar ratio of 200:30:5 and various amounts of citric acid (CA). The respective chemicals were initially dissolved in distillation water to give a CA:iron nitrates (N) molar ratios of 0.05, 0.1, 0.2 and 0.3, with the derived catalysts denoted as 0.05CA, 0.1CA, 0.2CA and 0.3CA, respectively. The solutions were adjusted to pH 7.0 using ammonia solution, refluxed at 80 °C for 2 h and then evaporated at 100 °C until a dark brown solution of 25 mL were obtained. They were next impregnated over the SiO_2 of 5 g at

a 20 wt% Fe metal loading and dried at 120 °C for 12 h. The resulting samples were calcined in argon (Ar) at 500 °C for 5 h with the ramping rate of 1.5 °C/min (Figure 3.2) and then applied directly for FTS without a reduction step.

Figure 3.2 Calcination Instrument

3.2.2 Synthesis of catalysts by impregnation method

For comparison, catalysts were also prepared by the impregnation method as reported elsewhere [77]. The aqueous solution of iron (III) nitrate nonahydrate, copper (II) nitrate trihydrate and potassium nitrate (200:30:5 molar ratio) were mixed with stirring and then impregnated over SiO_2 (Q-50) of 5 g with 20 wt% Fe metal loading. They were next dried at 120 °C for 12 h then calcined at 400 °C in air for 5 h and finally reduced in situ at 300 °C for 10 h in H_2/CO. The obtained catalyst was denoted as Imp.

จุฬาลงกรณ์มหาวิทยาลัย
CHULALONGKORN UNIVERSITY

3.2.3 Synthesis of acid types by autocombustion method

For evaluating the effect of different acid types, similar catalysts were also prepared as above except using formic acid (FA) or oxalic acid (OA) instead of the CA with a FA:N or OA:N molar ratio of 0.1. The derived catalysts denoted as 0.1FA and 0.1OA, respectively.

3.2.4 Synthesis of different SiO_2 supports by autocombustion method

For comparison, the effect of different SiO_2 supports (pore size), the catalysts with the same composition were prepared by using Q-3 and Q-10 (Fuji Silysia Co.Ltd.,) as supports instead of the Q-50 with a CA:N molar ratio of 0.1. The Q-3, Q-10 and Q-50 with the derived catalysts denoted as 0.1CA/Q-3, 0.1CA/Q-10 and 0.1CA/Q-50, respectively.

3.3 Catalyst characterization

จุฬาลงกรณ์มหาวิทยาลัย
CHULALONGKORN UNIVERSITY

3.3.1 Nitrogen (N_2) physisorption

The pore structure of calcined catalyst was characterized by nitrogen (N_2) physisorption using a NOVA 2200e equipment (Figure 3.3). The specific surface area (S_{BET}) was obtained by the Brunauer-Emmett-Teller (BET) method, while total pore volume (V_p) was calculated by the single point method and average pore size (D_p) was obtained by $4V_p/S_{BET}$.

Figure 3.3 Brunauer-Emmett-Teller (BET), NOVA 2200e

3.3.2 Scanning electron microscopy (SEM)

The surface morphology and metal content of calcined catalyst were evaluated using a scanning electron microscopy (SEM), JEOL, JSM-6360 model (Figure 3.4).

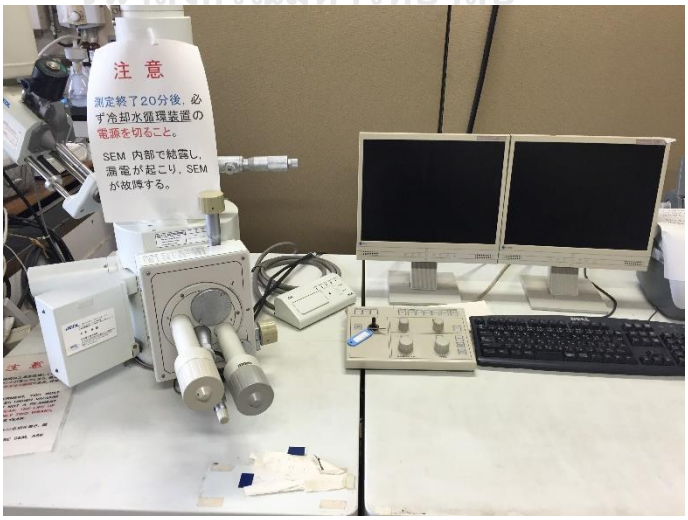

Figure 3.4 Scanning electron microscopy (SEM), JEOL JSM-6360

3.3.3 Energy-diffusive X-ray analysis (EDX)

The determination of the amount of metal in each catalyst was performed using energy dispersive X-ray analysis (EDX) on a Rayny EDX-700 instrument (Figure 3.4).

3.3.4 X-ray diffraction (XRD)

X-ray diffraction (XRD) patterns of calcined and used catalysts were performed using a Rigaku RINT 2200 (Figure 3.5) with a monochromatic Cu-$K\alpha$ radiation source, with the 2θ range from 10–80°. The Scherrer equation, $D = K\lambda/(\beta\cos\theta)$ was used to calculate the average crystalline sizes of calcined and used catalysts.

Figure 3.5 X-ray diffraction (XRD), Rigaku RINT 2200

3.3.5 Hydrogen-temperature programmed reduction (H_2-TPR)

Figure 3.6 Hydrogen-temperature programmed reduction (H_2-TPR)

The hydrogen-temperature programmed reduction (H_2-TPR) was used to measure the reduction behavior of calcined catalyst from BELCAT-B-TT apparatus (Figure 3.6). Initially, about 0.05 g of sample was flowed with Ar at 150 °C for 2 h. The sample was then cooled down to 50 °C for 30 min. Then, gas was changed to H_2 in Ar and temperature increased up to 850 °C at a heating rate of 5 °C/min. The effluent gas was analyzed by a thermal conductivity detector (TCD). The schematic of TPR are showed in Figure 3.7.

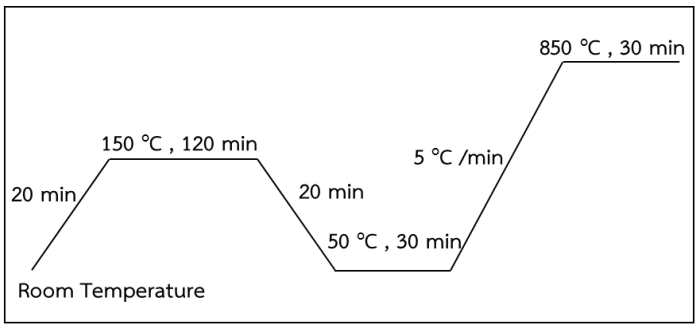

Figure 3.7 Schematic of temperature programmed TPR

3.3.6 X-ray photoelectron spectroscopy (XPS)

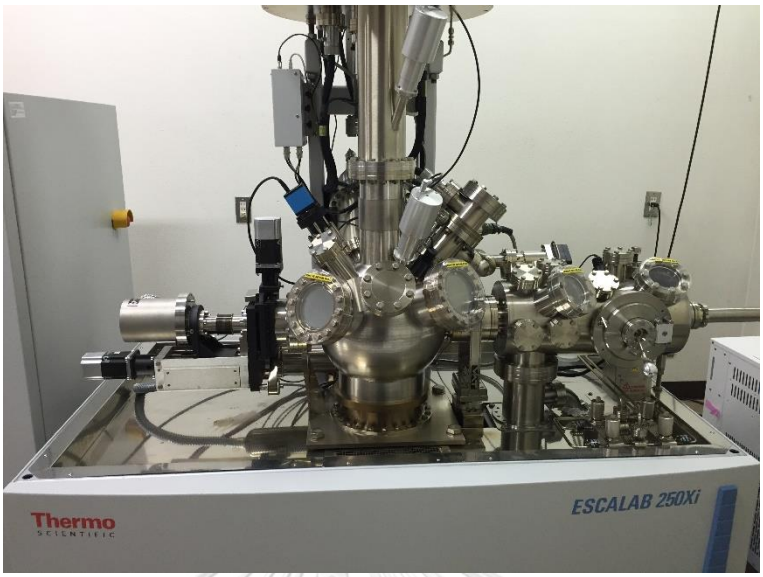

Figure 3.8 X-ray photoelectron spectroscopy (XPS), Thermo Scientific

X-ray photoelectron spectroscopy (XPS) data of calcined catalyst was obtained with a Thermo Scientific ESCALAB 250 spectrometer. The binding energy was calibrated relative to that of adventitious carbon, using the C 1*s* peak at 284.8 eV (Figure 3.8).

3.3.7 Thermogravimetric and differential thermal analyses (TG-DTA)

จุฬาลงกรณ์มหาวิทยาลัย
CHULALONGKORN UNIVERSITY

From Figure 3.9, the autocombustion process of calcined catalyst was evaluated by thermogravimetric and differential thermal analyses (TG-DTA) using a Shimadzu, TG-60 in N_2 atmosphere, while the residue carbon on used catalyst was analysed in the same manner except in an air atmosphere.

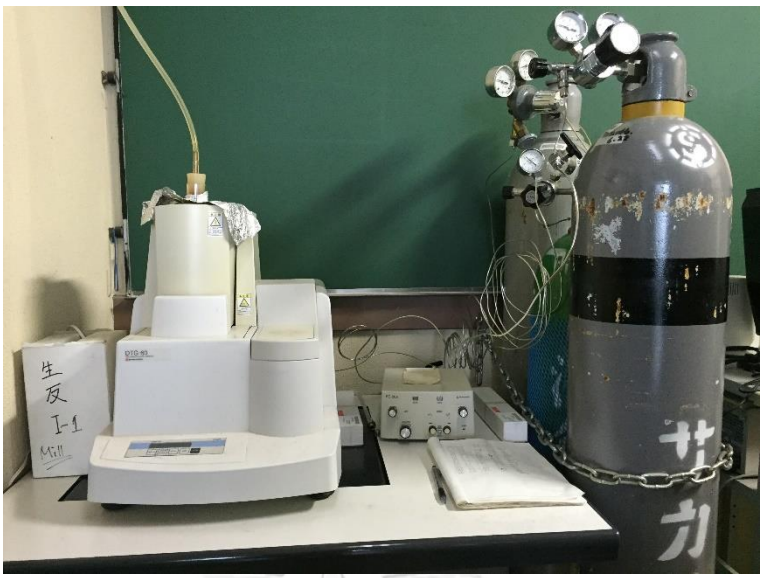

Figure 3.9 Thermogravimetric and differential thermal analyses (TG-DTA)

3.3.8 Transmission electron microscopy (TEM)

Transmission electron microscopy (TEM) images were analyzed by a Philips Tecnai F20 TEM at 200 kV acceleration voltage and field emission source which was equipped with digital STEM. The average crystallite sizes of used catalyst were calculated by the SemAfore program, as in Figure 3.10.

จุฬาลงกรณ์มหาวิทยาลัย
CHULALONGKORN UNIVERSITY

Figure 3.10 Transmission electron microscopy (TEM), Philips Tecnai

3.4 Catalytic activity test

From Figure 3.11, the feed gas for FTS consisted of Ar (3.0%), CO (48.5%) and H_2 (48.5%). Initially, the respective catalyst (0.5 g) was placed in a fixed bed reactor tube and the FTS reaction was performed for 5 h at T=300 °C, P=1.0 MPa and W/F=10 g_{cat}h/mol. The stream was characterized by online gas chromatographs (GC) as follows: a thermal conductivity detector (TCD) was used to analyze the gaseous products (CH_4, CO_2, CO and Ar) and a flame ionization detector (FID) was used to evaluate the light hydrocarbons (C_1- C_5). The liquid products were collected in an ice trap and analyzed by GC-FID. Also, Figure 3.12 showed the Fischer-Tropsch synthesis (FTS) unit for fixed bed reactor.

จุฬาลงกรณ์มหาวิทยาลัย
CHULALONGKORN UNIVERSITY

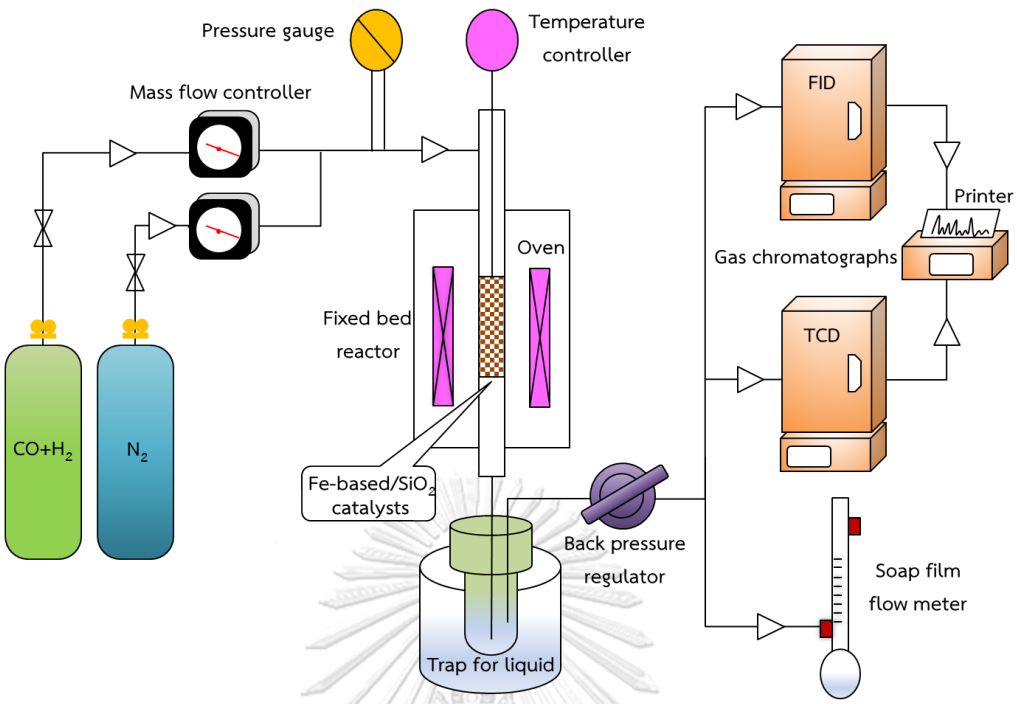

Figure 3.11 Process Flow Diagram for Fischer-Tropsch synthesis (FTS)

Figure 3.12 The FTS unit for fixed bed reactor

CHAPTER IV

RESULTS AND DISCUSSION

4.1 Characterization of catalysts with different CA:N molar ratios

4.1.1 Textural characteristic of catalysts

The physical properties of the SiO_2, Imp catalyst and calcined catalysts with different CA:N molar ratios, as measured by N_2 physisorption, are shown in Table 4.1. The S_{BET} of SiO_2 support (Q-50) was 80 m^2/g, while that for 0.1CA was 92 m^2/g. The increased S_{BET} after autocombustion was mainly due to some iron particles entering into the pores of SiO_2 [78, 79]. Increasing the CA:N molar ratios increased the S_{BET} of calcined catalysts to a maximum at a CA:N molar ratio of 0.1, where more gases were released during the CA decomposition resulting in a more porous structure and higher S_{BET}. However, the S_{BET} markedly decreased with higher CA:N molar ratios of > 0.1, due to the formation of excess carbon residues that coated the surface of catalyst and decreased the S_{BET} [63]. Therefore, the 0.3CA, with the highest CA:N molar ratio, had the lowest S_{BET}, only about 68 m^2/g because the carbon residues were accumulated on catalyst surface, as observed with the EDS analysis in Table 4.1.

The V_p and D_p of 0.1CA were 0.57 cm^3/g and 20.2 nm respectively, significantly lower than those of SiO_2 (V_p of 1.1 cm^3/g and D_p of 48.5 nm). This marked decreasing in the V_p and D_p suggests that the iron particles were loaded into the pores of SiO_2

more than deposited on the outer surface. As expected, it is noted that coexisting SiO_2 helped to protect Fe-based/SiO_2 catalysts matrix during the calcination step, to absorb heat from autocombustion, avoiding structure collapse [80].

Table 4.1 Physical properties of the SiO_2, Imp and calcined catalysts with different CA:N molar ratios

Support/ Catalysts	S_{BET}[a] (m^2/g)	V_p[a] (cm^3/g)	D_p[a] (nm)	d_{XRD}[b] (nm)		Metal contents[e] (wt%)			
				before[c]	used[d]	Fe	Cu	K	C
SiO_2	80	1.10	48.5	-	-	-	-	-	-
Imp	85	0.86	28.4	28.0	10.2	35.5	14.5	1.5	-
0.05CA	85	0.67	18.5	25.8	13.6	37.4	14.5	1.5	3.2
0.1CA	92	0.57	20.2	27.5	14.8	38.2	14.7	1.5	6.3
0.2CA	79	0.72	25.7	28.2	18.6	33.1	14.4	1.4	10.1
0.3CA	68	0.90	30.5	31.2	25.2	31.7	14.3	1.3	15.7

[a] Determined by the N_2 adsorption method; [b] Derived from diffraction line in XRD and calculated the crystalline sizes by the Scherrer formula; [c] Fe_2O_3 at 35.5° and Fe_3O_4 at 35.3° for calcined catalysts before FTS; [d] Fe_xC at around 43° for used catalysts after FTS; [e] Measured by the EDX technique.

จุฬาลงกรณ์มหาวิทยาลัย
CHULALONGKORN UNIVERSITY

4.1.2 Morphology and element composition of the catalysts

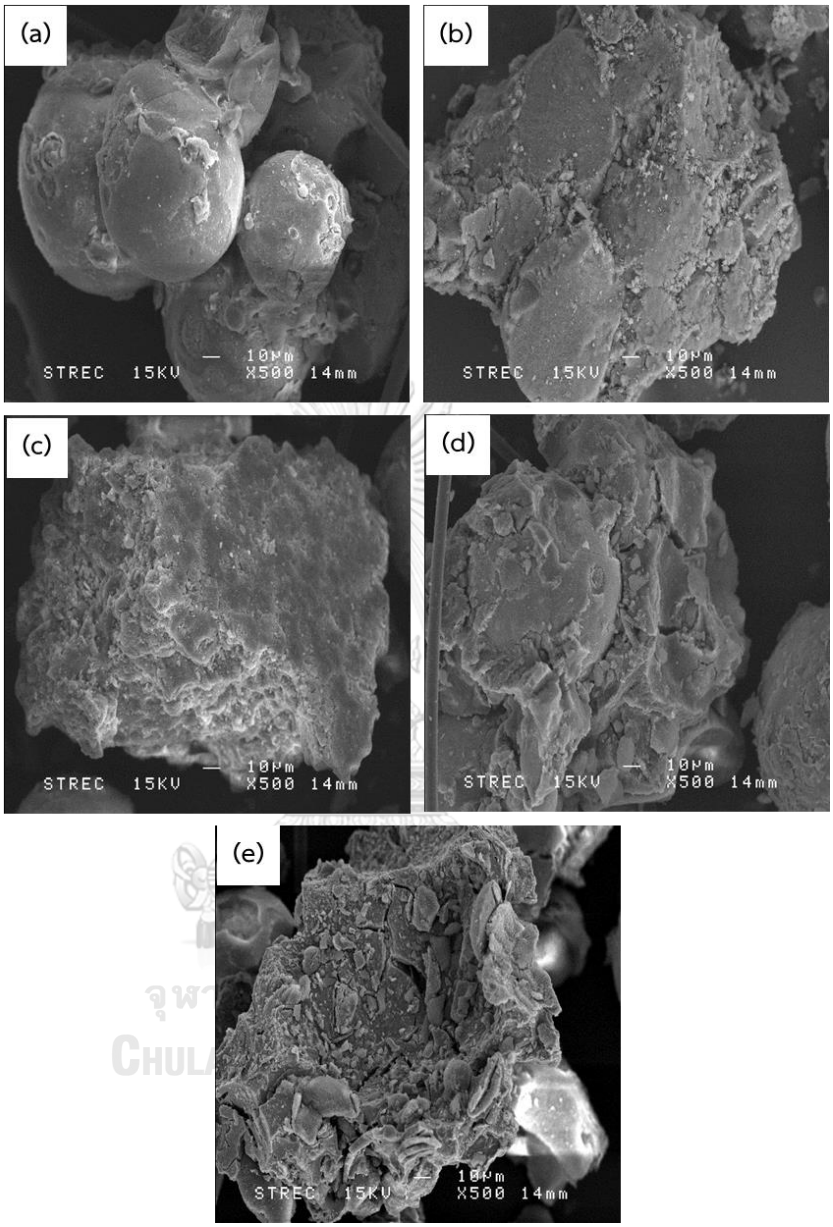

Figure 4.1 SEM micrograph of (a) Imp, (b) 0.05CA, (c) 0.1CA, (d) 0.2CA and (e) 0.3CA

Figure 4.1 shows the SEM micrographs of Imp catalyst and calcined catalysts with different CA:N molar ratios. The Imp catalyst showed a smooth external surface, in Figure 4.1 (a). On the other hand, all calcined catalysts displayed relatively rough

morphology but the 0.3CA catalyst had rougher surface than the other three catalysts. It can be observed that there are many amounts of micropores in the calcined catalysts which had influence on the diffusion of gases during FTS [62].

Energy-diffusive X-ray spectroscopy (EDX) was used to calculate metal contents. The metal contents of Fe, Cu, K and C on Imp catalyst and calcined catalysts are summarized in Table 4.1. The carbon on the surface increased slightly from 3.2 wt% to 6.3 wt% and 10.1 wt% and then finally markedly to 15.7 wt% as the CA:N molar ratios increased from 0.05 to 0.1, 0.2 and 0.3, respectively. Consequently, increasing the CA:N molar ratios led to an increased level of the carbon on catalyst surface, which was originated from the decomposition of CA [81, 82].

4.1.3 Phase structure of the catalysts

4.1.3.1 XRD for calcined catalysts before FTS

จุฬาลงกรณ์มหาวิทยาลัย
CHULALONGKORN UNIVERSITY

To study the dispersion of catalysts, the XRD patterns of Imp catalyst and calcined catalysts with different CA:N molar ratios before FTS are shown in Figure 4.2. The catalysts showed iron phases in hematite phases (Fe_2O_3), magnetite phases (Fe_3O_4) and carbides phases (Fe_xC) [83, 84]. Increasing the CA:N molar ratios caused a further reduction of Fe_2O_3 to Fe_3O_4 and then carburization of iron metal (Fe) to Fe_xC, as followed: $Fe_2O_3 \longrightarrow Fe_3O_4 \longrightarrow Fe \longrightarrow Fe_xC$ [85]. Consequently, the autocombustion completed the conversion of metal compounds to metal oxides and then to metal carbides without a reduction step. During the decomposition of CA, large amounts of

gases such as H_2, CH_4, H_2O, CO, CO_2, NH_3, NO_2 and NO were released. These reducing gases (H_2 and CO) played a key role as the reducing and carburizing agents to produce Fe_xC from metal oxides phases. No XRD peaks were assigned to Cu or K species due to their high dispersion and low concentration.

The mean crystallite sizes of catalysts were calculated by the Scherrer formula and revealed in Table 4.1. The iron crystallite sizes of Imp and 0.05CA were only Fe_2O_3 phases. Increasing the CA:N molar ratios resulted in the enlarged crystallite sizes. This suggested the crystallite sizes were closely corresponded with the CA:N molar ratios.

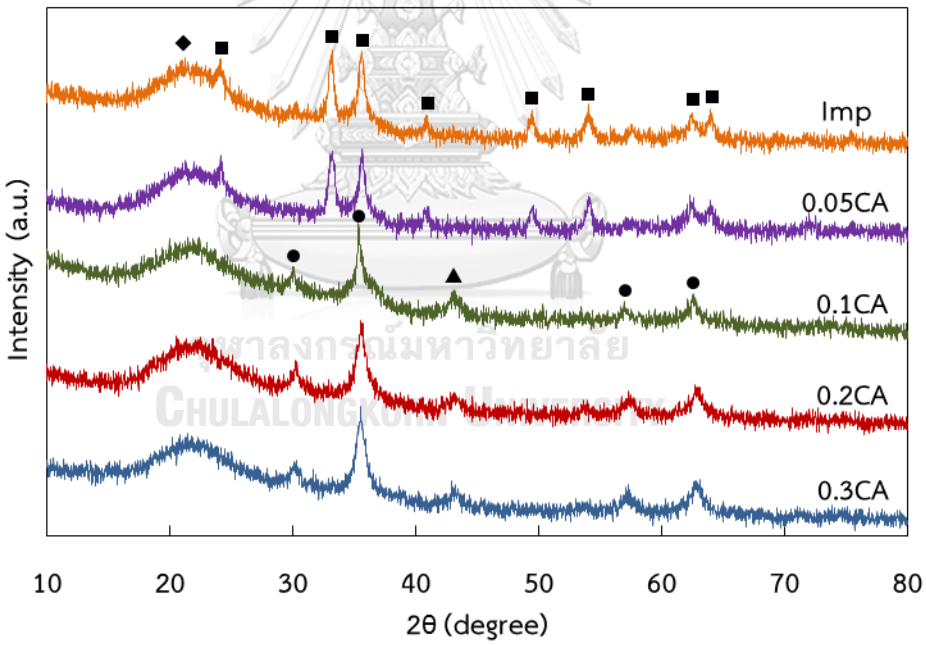

Figure 4.2 XRD patterns of Imp and calcined catalysts with different CA:N molar ratios before FTS; (◆) SiO_2; (■) Fe_2O_3; (●) Fe_3O_4 and (▲) Fe_xC

4.1.3.2 XRD for used catalysts after FTS

Figure 4.3 displayed the XRD patterns of used catalysts after FTS. The XRD patterns of all catalysts showed iron phases as Fe_3O_4 and Fe_xC. Increasing the CA:N molar ratios resulted in a gradually increased intensity of Fe_xC, as observed with the crystallite sizes which were calculated by the Scherrer formula in Table 4.1. Interestingly, there were some differences for calcined and used catalysts, especially the formation of Fe_xC after FTS. However, CO conversion of autocombustion catalysts did not show a significant change since the first hour time on stream as shown in Figure 4.9. Therefore, the phase change had no effect on CO conversion. This may be due to the fact that the existence of CA significantly improved the reduction and carburization of iron oxide phases during catalysts preparation from autocombustion method.

This suggests that carbonaceous material (CA) works as reducing agent during decomposition of nitrate with formation of partially reduced iron species. Similar results have been obtained by Cheng et al. [86], addition of carbonaceous material into precursors led to stabilization of highly dispersed oxide phase and resulted in more reduced active phase after heat treatment in inert atmosphere.

Chulalongkorn University

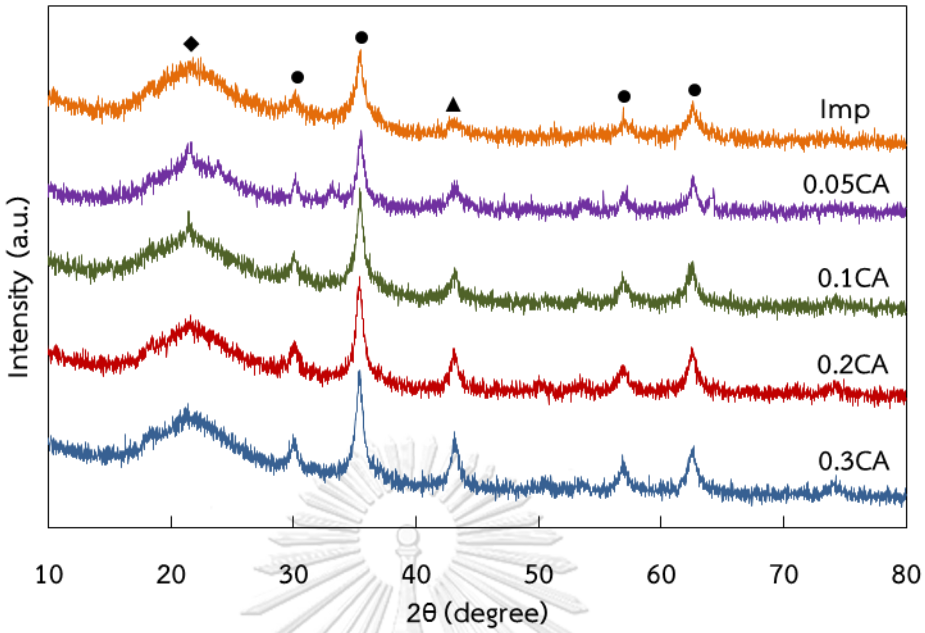

Figure 4.3 XRD patterns of used catalysts after FTS with Imp and different CA:N molar ratios; (◆) SiO_2; (●) Fe_3O_4 and (▲) Fe_xC

4.1.4 Reduction behavior of catalysts

H_2-TPR was evaluated to investigate the reduction behavior of Fe-based/SiO_2 catalysts. TPR profiles of Imp catalyst and calcined catalysts with different CA:N molar ratios are shown in Figure 4.4. From many literatures, it can be explained that the two stages of iron phase change occurred, firstly from Fe_2O_3 to Fe_3O_4 and then to Fe. The two step reduction of Fe_2O_3 to Fe was as follows [87].

$$3Fe_2O_3 + H_2 \longrightarrow 2Fe_3O_4 + H_2O$$

$$Fe_3O_4 + 4H_2 \longrightarrow 3Fe + 4H_2O$$

As mentioned above, two reduction peaks of Imp catalyst were observed. The first at about 200–350 °C was related to the reduction of CuO ⟶ Cu and the reduction of Fe_2O_3 ⟶ Fe_3O_4. The second, a broad reduction peak at 500–800 °C, was associated with reduction of Fe_3O_4 ⟶ Fe [88]. Increasing the CA:N molar ratios decreased gradually the first reduction peaks and then disappeared, whereas the second reduction peak shifted to a lower temperature region. It is worth marking that the existence of CA played a significant role in helping iron phases change and enhancing the reducibility of catalysts.

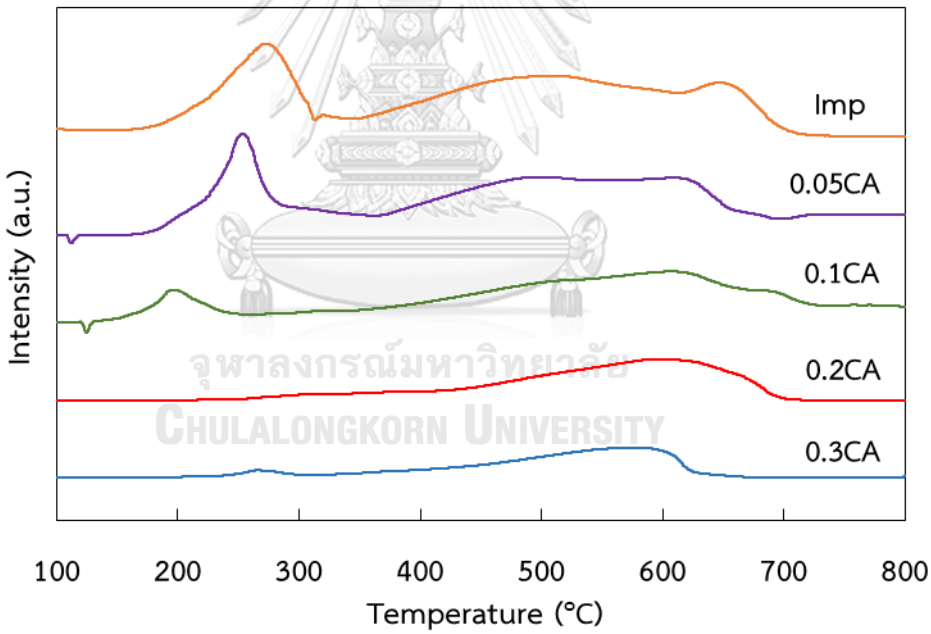

Figure 4.4 H_2-TPR profile of Imp and catalysts with different CA:N molar ratios

4.1.5 Phase structure of the catalysts in the surface region

XPS was applied to investigate the nature of the surface species. Figure 4.5 shows the XPS spectra of Imp catalyst and calcined catalysts with different CA:N molar ratios.

The XPS survey spectrum of Imp catalyst contained Si 2*p*, C 1*s*, O 1*s*, Fe 2*p* and Cu 2*p* elements, in Figure 4.5 (a). While, Figure 4.5 (b–e) shows the XPS spectra of the Fe 2*p* core level for calcined catalysts.

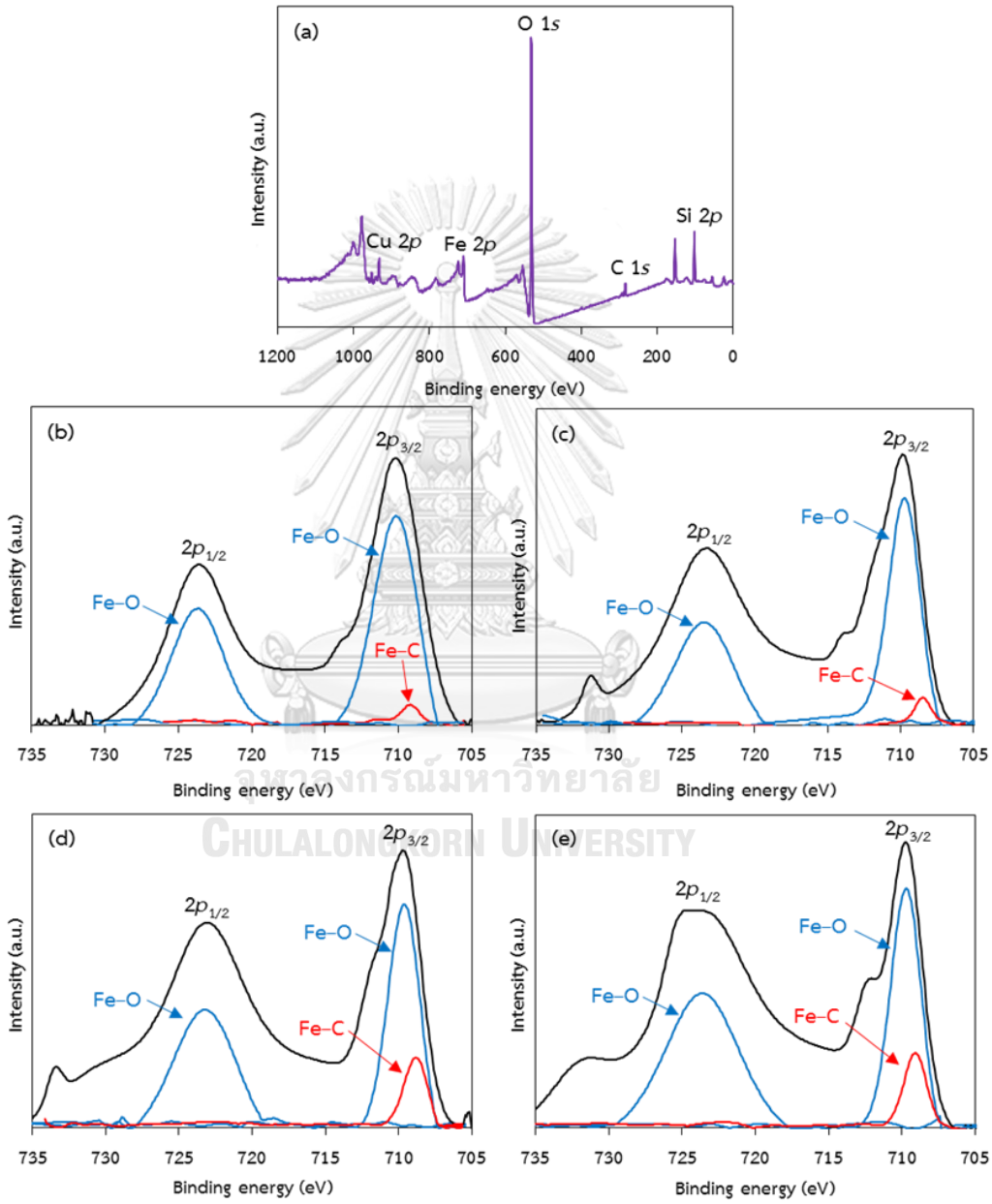

Figure 4.5 XPS spectra of (a) Imp, (b) 0.05CA, (c) 0.1CA, (d) 0.2CA and (e) 0.3CA

Both the Fe $2p_{3/2}$ and Fe $2p_{1/2}$ components of the Fe $2p$ were asymmetric peaks, with corresponding core level binding energy values of about 710–711 and 724–725 eV in Fe_3O_4 species (Fe–O), respectively and that of iron carbides species (Fe–C) was determined at 707–708 eV are exhibited in Figure 4.5 (b–e). This result was closely related to several previous studies [89-91]. Increasing the CA:N molar ratios led to an increased intensity of Fe–C and this was rather high in the 0.2CA and 0.3CA catalysts. It is important to note that Fe_xC was the dominant iron phase which displayed on the surface of Fe-based/SiO_2 catalysts.

4.1.6 TG-DTA analysis of catalysts

4.1.6.1 Combustion process of catalysts

TG-DTA measurement of calcined catalysts and citric acid in N_2 atmosphere was examined to evaluate the autocombustion process, with the results in Figure 4.6. The DTA curves demonstrated one exothermic peak at about 200–400 °C arose from occurrence of a redox reaction, using NO_3^- as the oxidizing agent and CA as the reducing agent [62]. Increasing the CA:N molar ratios enhanced the height of the exothermic peak, indicating that the autocombustion process occurred more severely. At the same time, the TG curves revealed a weight loss which decreased deeply. It is inferred that more CA:N molar ratios led to more large amounts of gases which were released in during the decomposition of CA.

จุฬาลงกรณ์มหาวิทยาลัย
Chulalongkorn University

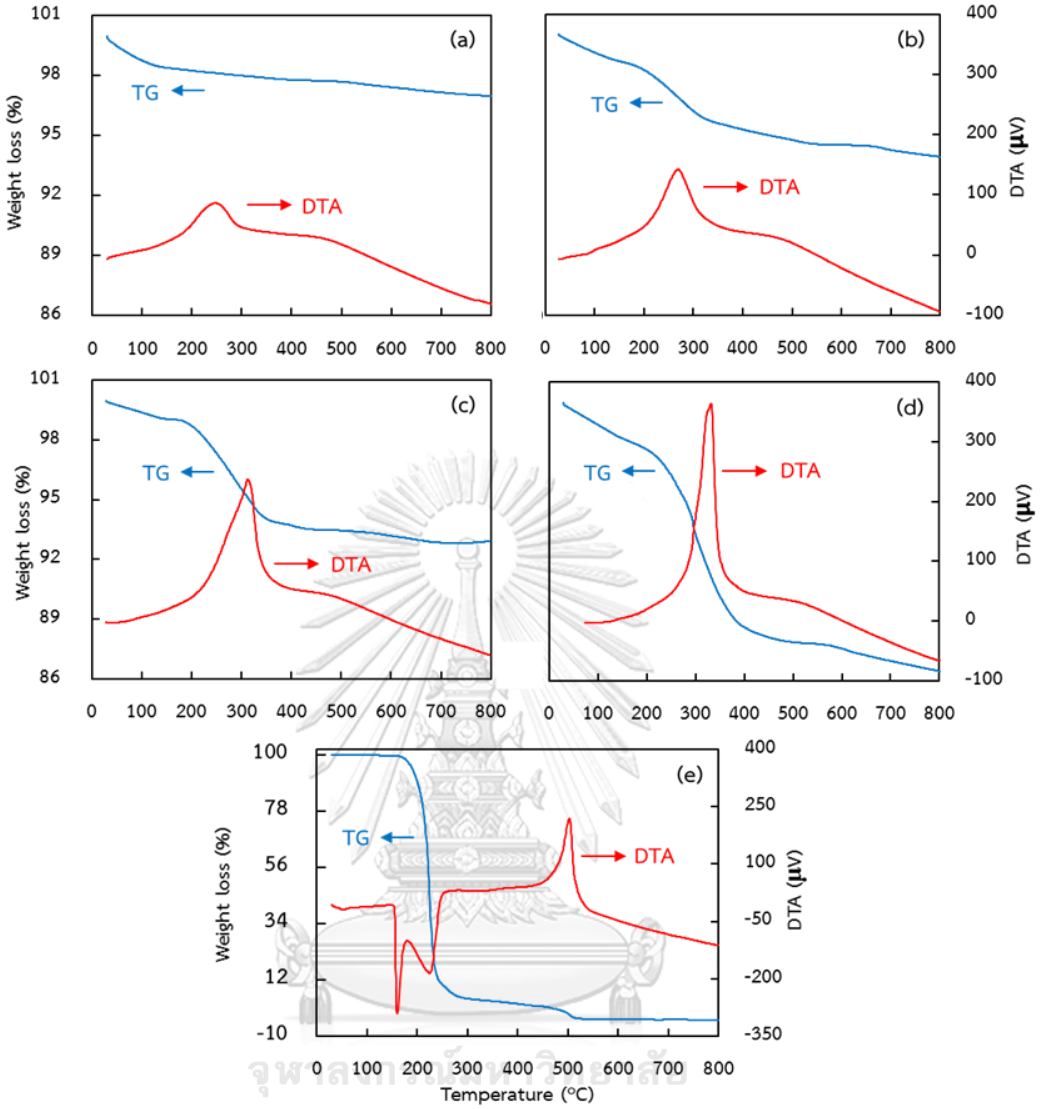

Figure 4.6 TG-DTA curves of calcined catalyst before FTS of (a) 0.05CA, (b) 0.1CA, (c) 0.2CA, (d) 0.3CA and (e) citric acid

Figure 4.6 (e) displays decomposition of pure citric acid that was divided into two endothermic peaks and an exothermic peak. First, the endothermic peak about 100–200 °C provided the melting of the CA, followed by another endothermic peak about 200–300 °C arose from the decomposition of CA. Finally, the exothermic peak about

450–550 °C came from the pyrolysis of the residue organics [62, 63]. Furthermore, in previous several works, the attack on citric acid is possible on four points of the molecule. Firstly, position one on the carboxyl group bound to the tertiary carbon, position two on the methylenic groups, position three on the OH bound to the central carbon and finally, position four on the carboxyl groups bound to the methylenic groups [59].

4.1.6.2 Level of residual carbon on used catalysts

To provide further insight into the residual carbon on used catalysts, they were determined by TG-DTA equipment in air atmosphere. Figure 4.7 shows the TG curves of used catalysts after FTS which was specified to the oxidation of carbon. A weight loss of Imp catalyst was 6.3%. On the other hand, a weight loss of about 4.6%, 5.4%, 8.9% and 11.8% was obtained for the 0.05CA, 0.1CA, 0.2CA and 0.3CA catalysts, respectively. Therefore, increasing the CA: N molar ratios significantly increased the loss of carbon. The TG curve of the 0.3CA catalyst elucidated a much more weight loss than the others, mainly because the residual carbon had arisen from the pyrolysis of the residual organic compounds.

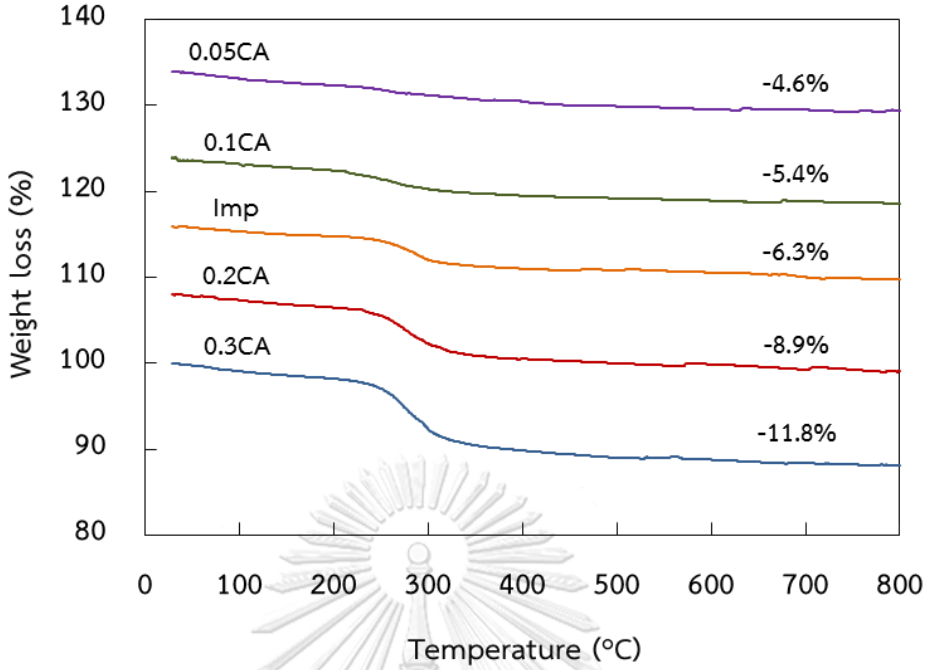

Figure 4.7 TG curves used catalysts after FTS with Imp and different CA:N molar ratios

4.1.7 TEM observation of catalyst

The TEM images of the Imp, 0.05CA, 0.1CA 0.2CA and 0.3CA for the used catalysts after FTS are compared in Figure 4.8. All the TEM images were significantly almost the same [92]. Therefore, the average crystallite sizes Fe_xC phase of the used catalysts was calculated by the SemAfore program. The crystallite sizes Fe_xC of Imp catalyst was 27.5 nm. Furthermore, it was found that crystallite sizes Fe_xC increased initially from 17.9 nm to 21.4 nm and 25.2 nm and then finally markedly to 29.8 nm as the CA:N molar ratios increased from 0.05 to 0.1, 0.2 and 0.3, respectively. Therefore, increasing the CA: N molar ratios made the average crystallite sizes gradually increasing.

จุฬาลงกรณ์มหาวิทยาลัย
CHULALONGKORN UNIVERSITY

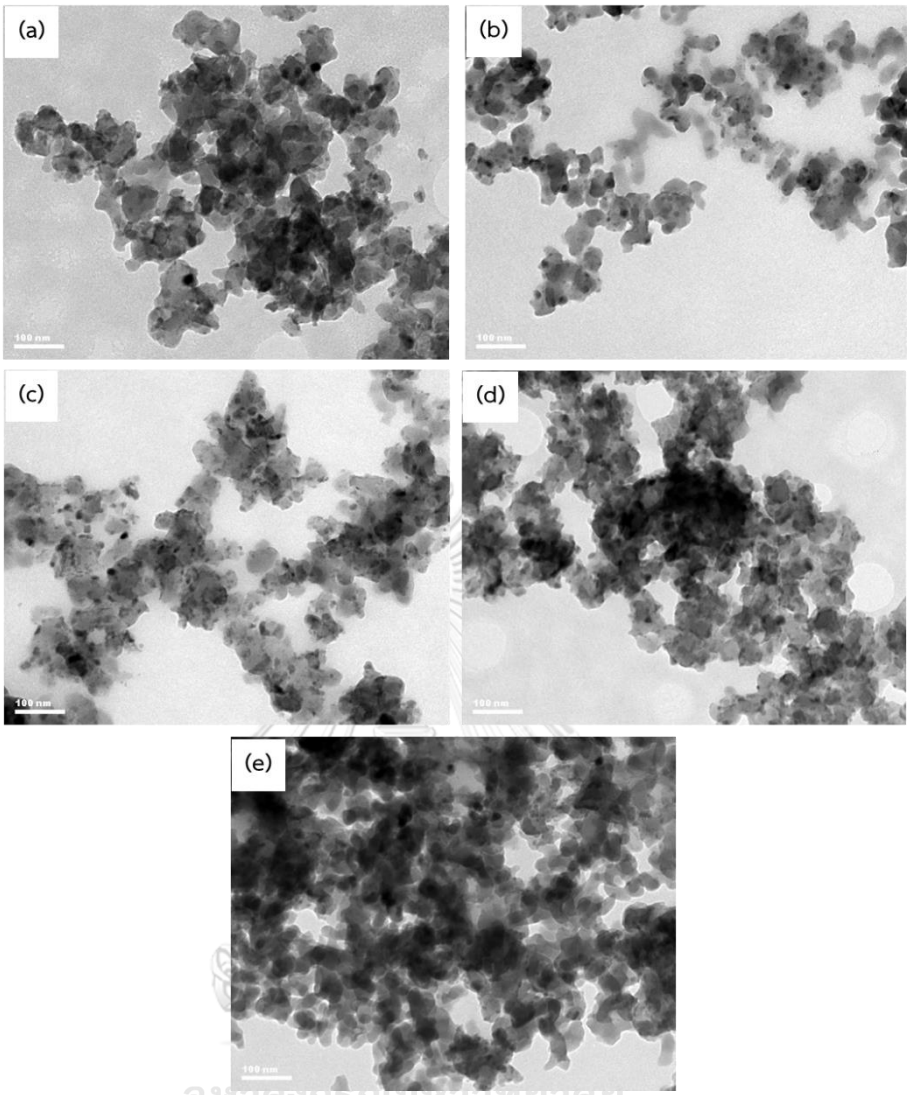

จุฬาลงกรณ์มหาวิทยาลัย
Chulalongkorn University

Figure 4.8 TEM images of used catalysts after FTS (a) Imp, (b) 0.05CA, (c) 0.1CA, (d) 0.2CA and (e) 0.3CA

4.2 FTS activity and selectivity with different CA:N molar ratios

4.2.1 CO conversion

The CO conversion and products selectivity of autocombustion with different CA:N molar ratios and impregnation catalyst are compared in Table 4.2. To ensure the advantage of the autocombustion method, Imp catalyst prepared by the impregnation

method was followed by a reduction step and tested for its FTS activity and selectivity under the same condition as catalysts synthesized by the autocombustion method.

Table 4.2 FTS[a] performance of Imp and calcined catalysts with different CA:N molar ratios

Catalysts	(%) CO conversion	Hydrocarbon Selectivity (%)			
		CO_2	CH_4	C_{2-4}	C_{5+}
0.05CA	67.0	39.5	17.3	28.3	14.9
0.1CA	86.5	37.8	16.8	28.1	17.3
0.2CA	26.6	35.9	11.4	26.5	26.2
0.3CA	19.4	33.2	8.1	23.4	35.3
Imp[b]	71.4	34.4	11.1	23.7	30.8

[a] Condition: 0.5 g catalysts; H_2/CO=1/1; 300 °C; 1.0 MPa; W/F=10 g_{cat}h/mol; [b] Average CO conversion between 4-6 h.

จุฬาลงกรณ์มหาวิทยาลัย
CHULALONGKORN UNIVERSITY

It is interesting that the CO conversion of all catalysts synthesized by autocombustion remained almost unchanged from the initial time to the steady state time on stream. In contrast, the CO conversion of Imp catalyst reached a steady state after about 4 h on stream as exhibited in Figure 4.9. It was deduced that an iron carburization and stability were achieved by surface active carbonaceous species

during the preparation of catalysts were prepared from autocombustion method [93, 94]. Consequently, induction period for conventional Fe-based FTS catalyst of Imp catalyst was not necessary for all catalysts synthesized by autocombustion.

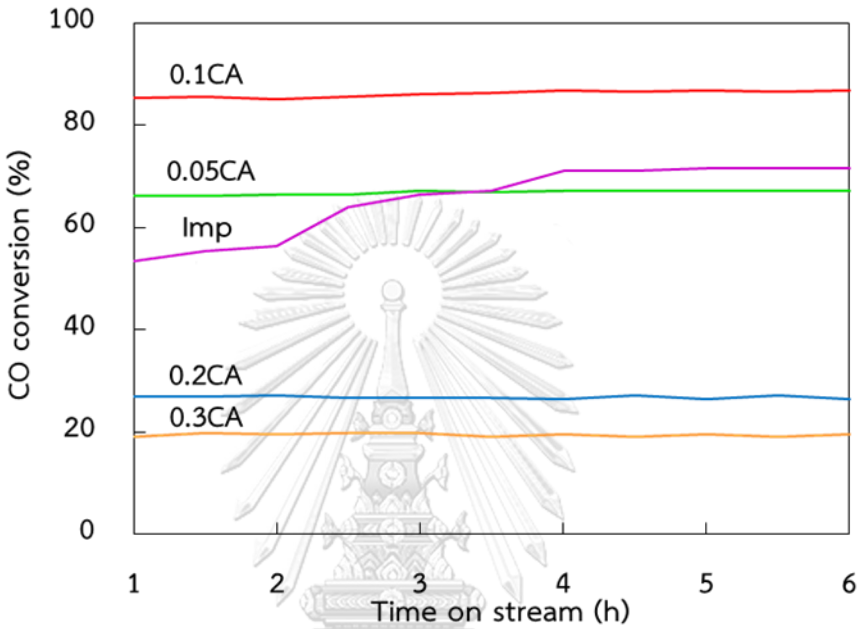

Figure 4.9 CO conversion vs time on stream with different CA:N molar ratios and impregnation method reaction condition: T=300 °C, P=1.0 MPa and W/F=10 g_{cat}h/mol

CHULALONGKORN UNIVERSITY

The 0.1CA catalyst yielded the highest CO conversion, as high as 86.5% which was higher than CO conversion of Imp catalyst (71.4%), as in Table 4.2. It is important that the CO conversion of 0.1CA catalyst (without a reduction step) was 1-fold of that of the Imp catalyst. Increasing the CA:N molar ratios from 0.05 to 0.1 increased the CO conversion to a maximum of 86.5%, they then dramatically decreased with higher CA:N molar ratios, being ranked in the order 0.1CA>0.05CA>0.2CA>0.3CA, as in Table 4.2. Because the excess CA resulted in a higher accumulation of carbon residues on their

surfaces, making the diffusion of syngas more difficult and therefore leading to a lower CO conversion [95]. These results are in accordance with the EDS analysis in Table 4.1.

4.2.2 Products selectivity

The products selectivity of autocombustion with different CA:N molar ratios and impregnation catalyst are compared in Figure 4.10. Fe-based catalysts in FTS commonly had high water gas shift (WGS) reaction ($CO + H_2O \leftrightarrow CO_2 + H_2$) activity. Therefore, the CO_2 selectivity was mainly derived from the WGS reaction [96]. Increasing the CA:N molar ratios significantly decreased the CO_2 selectivity because the WGS reaction was catalyzed by the Fe_3O_4 phase of Fe-based/SiO_2 catalysts, in Figure 4.10. This implied that higher Fe_3O_4 phase could lead to high CO_2 selectivity, and changing Fe_3O_4 to Fe_xC lower CO_2 selectivity [97].

Table 4.2 shows comparison between the 0.05CA and the 0.3CA catalyst, the 0.05CA showed higher CH_4 selectivity than the other due to an influence on the smaller the crystallite size. Increasing the CA:N molar ratios led to a significantly decreased CH_4 selectivity. It is worth marking that the stronger CH_x species which represented carbon intermediates leading to methane, were bonded to the catalyst surface [98].

The olefins appeared predominantly to be the primary products of Fe-based catalysts for FTS. The C_{2-4} selectivity obtained with the 0.05CA and 0.1CA catalysts were significantly higher than the 0.2CA and 0.3CA ones. This marked that paraffin was produced from the secondary hydrogenation of olefins, was inhibited on this catalyst

จุฬาลงกรณ์มหาวิทยาลัย
CHULALONGKORN UNIVERSITY

as less Fe and limited amount of Fe_xC was formed because of the low amount of the CA:N molar ratios [99]. From Figure 4.10, the 0.3CA had the highest C_{5+} selectivity, proving that larger the crystallite size tended to selective heavy hydrocarbons. Increasing the CA:N molar ratios resulted in an increased C_{5+} selectivity. It is suggested that dissociative adsorption of CO which leads to the formation of the $-CH_2-$ fragments required for chain growth [100].

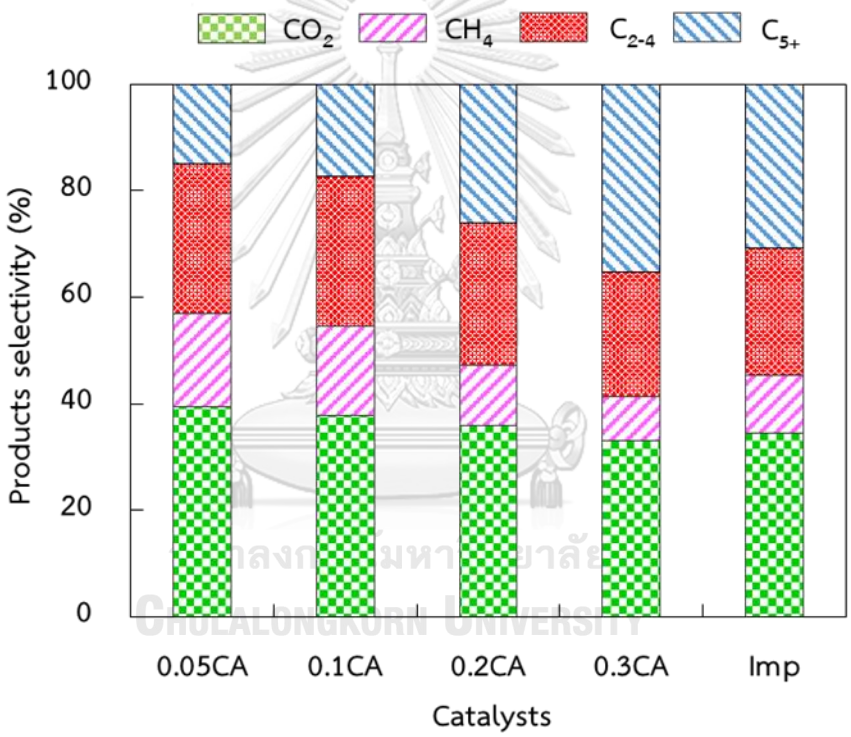

Figure 4.10 Products selectivity with different CA:N molar ratios and impregnation reaction condition: T=300 °C, P=1.0 MPa and W/F=10 $g_{cat}h/mol$

4.3 FTS activity and selectivity with different acid types

Table 4.3 FTS[a] performance of calcined catalysts with different acid types

Catalysts	(%) CO conversion	Hydrocarbon Selectivity (%)			
		CO_2	CH_4	C_{2-4}	C_{5+}
0.1FA	58.0	33.5	13.3	25.0	28.2
0.1OA	24.3	30.6	9.1	19.8	40.5
0.1CA	86.5	37.8	16.8	28.1	17.3

[a] Condition: 0.5 g catalysts; H_2/CO=1/1; 300 °C; 1.0 MPa; W/F=10 g_{cat}h/mol.

To study the influence of acid types, catalysts were prepared using formic acid (FA) or oxalic acid (OA) in place of CA at a FA:N or OA:N molar ratio of 0.1. The FTS performance of calcined catalysts with different acid types are compared in Table 4.3 and Figure 4.11. The CO conversion of catalyst prepared using 0.1CA was higher than that of those prepared using 0.1OA or 0.1FA. The sequence of CO conversion followed the order of 0.1CA>0.1FA>0.1OA. The reason may be more reducing gases being liberated from the CA molecule than from OA or FA molecule [63]. Therefore, these reducing gases (H_2 and CO) played a significant role as reducing and carburizing agents to produce Fe_xC from metal oxides phases. However, the 0.1OA showed the lowest CO_2, CH_4 and C_{2-4} selectivity but it had the highest C_{5+} selectivity.

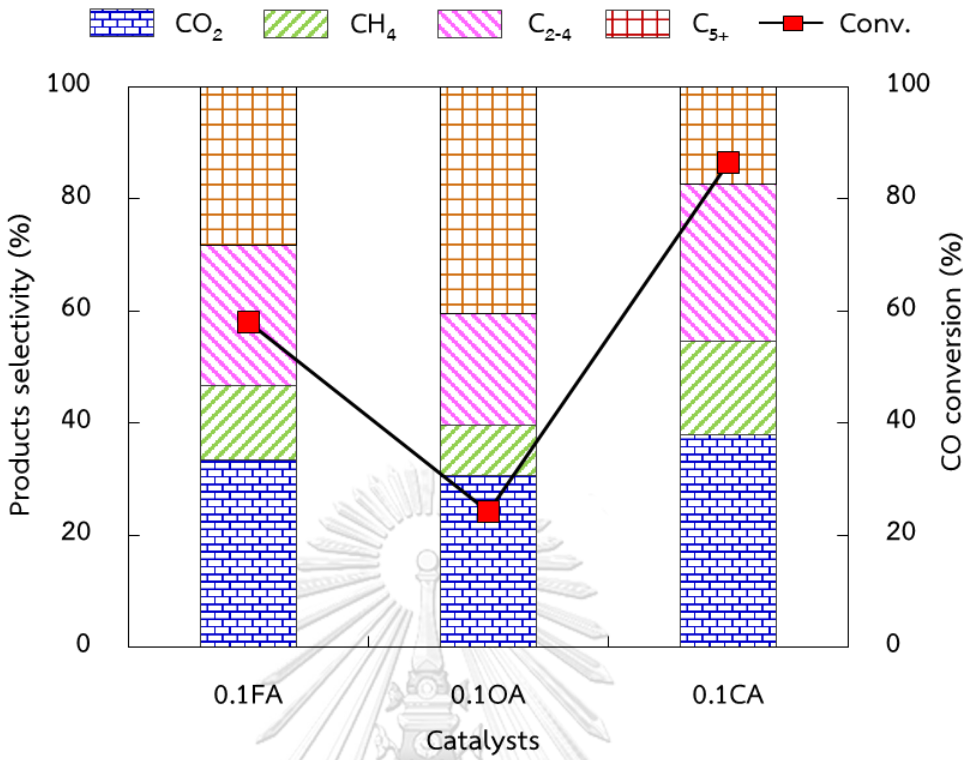

Figure 4.11 Influence of acid types on CO conversion and products selectivity with reaction condition: T=300 °C, P=1.0 MPa and W/F=10 g_{cat}h/mol

4.4 Characterization of catalysts with different SiO_2 supports

จุฬาลงกรณ์มหาวิทยาลัย
CHULALONGKORN UNIVERSITY

4.4.1 Textural characteristic of catalysts

For comparison, the effect of different SiO_2 supports (pore size), the catalysts with the same composition were prepared by using Q-3 and Q-10 (Fuji Silysia Co.Ltd.,) as supports instead of the Q-50 with a CA:N molar ratio of 0.1. The physical properties of SiO_2 and calcined catalysts with different SiO_2 supports are shown in Table 4.4. Due to the formation of small pores, the S_{BET} of the 0.1CA/Q-3 catalyst decreased from 760 m^2/g to 661 m^2/g as well as the S_{BET} of 0.1CA/Q-10 catalyst decreased from 475 m^2/g

to 446 m^2/g. These indicated that the introduced components may be deposited on the entrance of large pores to block the pores. It can be showed that V_p of 0.1CA/Q-3 and 0.1CA/Q-10 catalysts decreased significantly, indicating that the introduced species entered the small pores of Q-3 and Q-10 supports [77].

Table 4.4 Physical properties of SiO_2 and calcined catalysts with different SiO_2 supports

Supports/ catalysts	S_{BET}[a] (m^2/g)	V_p[a] (cm^3/g)	D_p[a] (nm)	d_{XRD}[b] (nm)	
				before[c]	used[d]
Q-3	760	0.35	3.6	-	-
0.1CA/Q-3	661	0.19	3.5	4.8	7.1
Q-10	475	1.53	13.4	-	-
0.1CA/Q-10	446	0.96	8.7	17.7	12.4
Q-50	80	1.10	48.5	-	-
0.1CA/Q-50	92	0.57	20.2	27.5	14.8

[a] Determined by the N_2 adsorption method; [b] Derived from diffraction line in XRD and calculated the crystalline sizes by the Scherrer formula; [c] Fe_2O_3 at 35.5° and Fe_3O_4 at 35.3° for calcined catalysts before FTS; [d] Fe_xC at around 43° for used catalysts after FTS.

จุฬาลงกรณ์มหาวิทยาลัย
CHULALONGKORN UNIVERSITY

The D_p^a of calcined catalysts with different SiO_2 supports are shown in Table 4.4. The Q-3, Q-10 and Q-50, as expected, had the uniformly distributed pore with size of 3.6 nm, 13.4 nm and 48.5 nm, respectively. After autocombustion method with mixed solutions of Fe, Cu, K and citric acid and calcination, the D_p^a of calcined catalysts with different SiO_2 supports decreased significantly [77].

4.4.2 Phase structure of the catalysts

4.4.2.1 XRD for calcined catalysts before FTS

The XRD patterns of calcined catalysts with different SiO_2 supports before FTS are shown in Figure 4.12. The broad peak observed at 2θ range from 20–25° corresponds to amorphous SiO_2. The calcined catalysts exhibited the presence of as iron phases in hematite phases (Fe_2O_3), magnetite phases (Fe_3O_4) and carbides phases (Fe_xC). The width XRD peaks of the Fe_3O_4 was strongly affected by the pore sizes of SiO_2. The XRD patterns were very broad, especially for the 0.1CA/Q-3 catalyst which this indicates a relatively small size catalyst. Increasing the pore sizes results in narrowing XRD peaks and respectively in larger sizes of Fe_3O_4 crystallites, as shown in Table 4.4. Moreover, the crystallite sizes followed the same trend as the pore sizes of SiO_2. Therefore, larger crystallite sizes were located in larger of pore sizes [101].

CHULALONGKORN UNIVERSITY

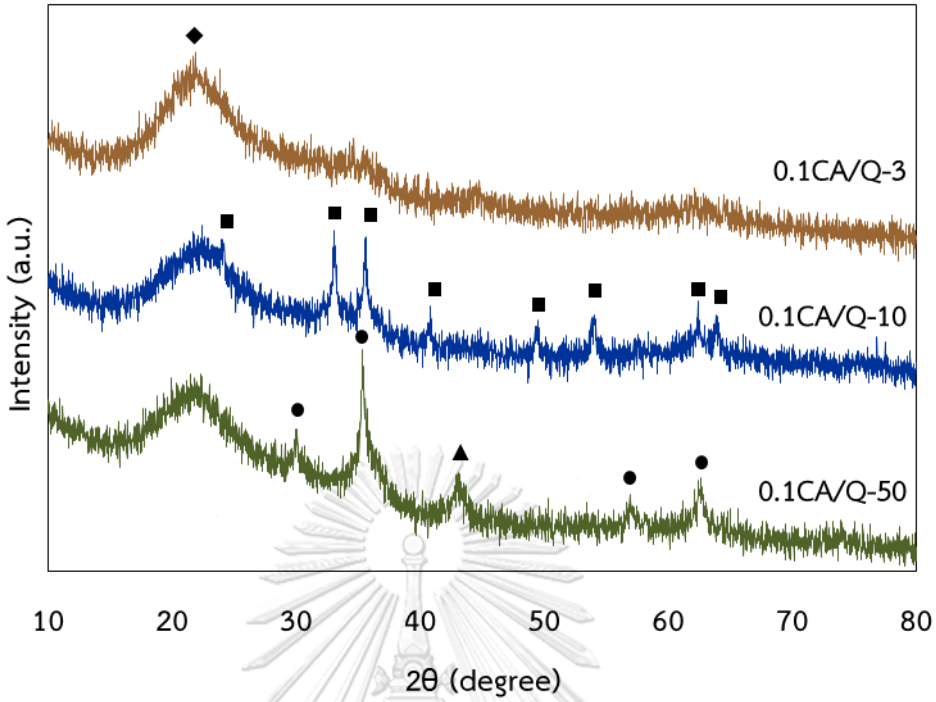

Figure 4.12 XRD patterns of calcined catalysts with different SiO_2 supports before FTS; (◆) SiO_2; (■) Fe_2O_3; (●) Fe_3O_4 and (▲) Fe_xC

4.4.2.2 XRD for used catalysts after FTS

Figure 4.13 displays the XRD patterns of used catalysts after FTS. The XRD patterns of all catalysts showed iron phases as Fe_3O_4 and Fe_xC. Increasing pore sizes led to a gradually increased intensity of Fe_xC, as observed in Table 4.4. After reactions, 0.1CA/Q-50 catalyst contained more Fe_xC than 0.1CA/Q-3 and 0.1CA/Q-10 catalyst. Thus, 0.1CA/Q-50 catalyst exhibited a CO conversion in FTS reaction [102]. These results are in accordance with the CO conversion in Table 4.5.

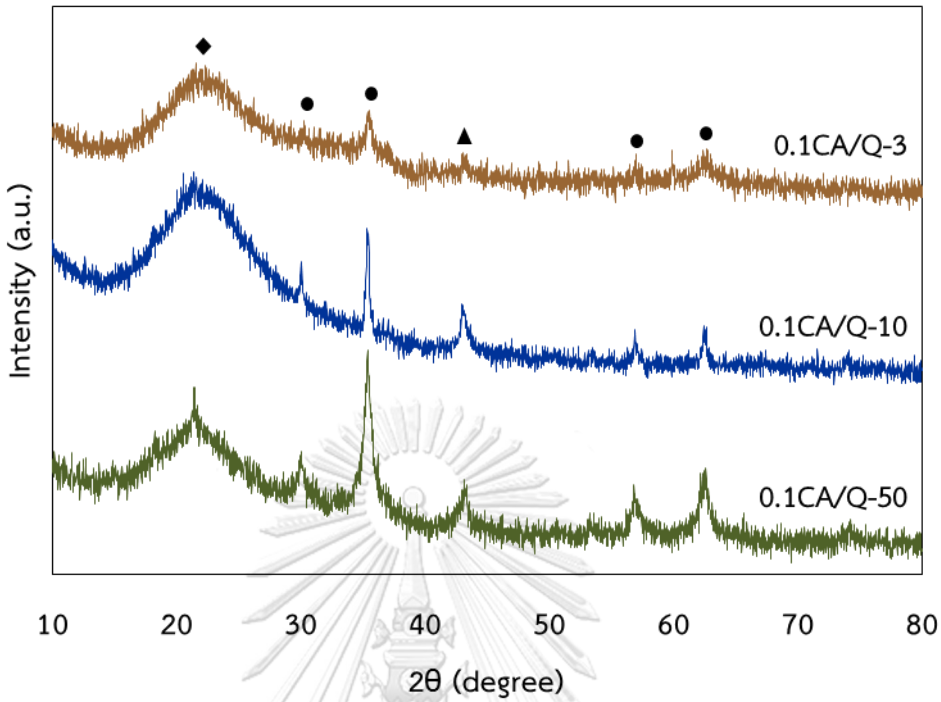

Figure 4.13 XRD patterns of used catalysts with different SiO_2 supports after FTS reaction; (◆) SiO_2; (●) Fe_3O_4 and (▲) Fe_xC

4.4.3 TEM observation of catalyst

The TEM images of the used catalysts after FTS are compared in Figure 4.14. The TEM images showed the effect of SiO_2 supports (pore size) on the dispersion of Fe_xC phase. More dispersed Fe_xC phase were observed in larger pore supports. The average crystallite sizes Fe_xC phase in the used catalysts increased from 9.5 nm, 17.8 nm to 21.4 nm in 0.1CA/Q-3, 0.1CA/Q-10 and 0.1CA/Q-50 catalyst, respectively [103].

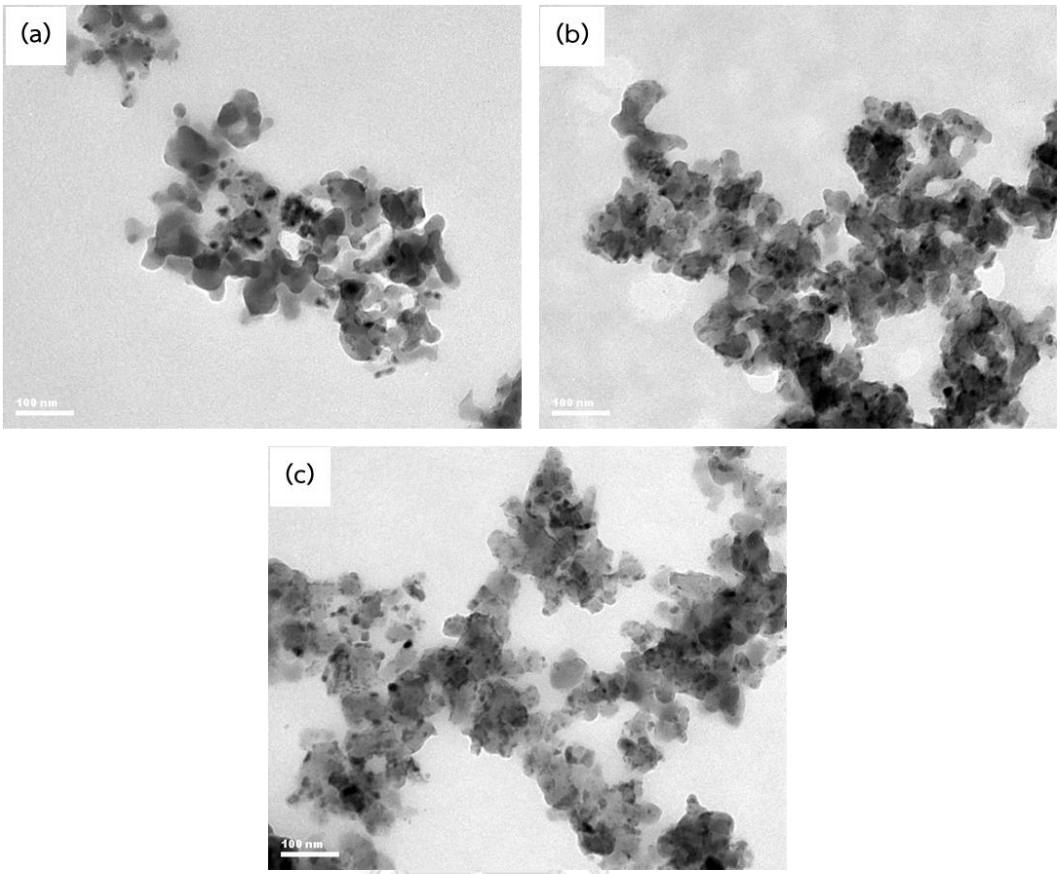

Figure 4.14 TEM images of used catalysts after FTS (a) 0.1CA/Q-3, (b) 0.1CA/Q-10 and (c) 0.1CA/Q-50

จุฬาลงกรณ์มหาวิทยาลัย
CHULALONGKORN UNIVERSITY

4.5 FTS activity and selectivity with different SiO_2 supports

4.5.1 CO conversion

The calcined catalysts with different SiO_2 supports were applied to FTS reaction to investigate the promotional role of pore structure. Table 4.5 shows the CO conversion of autocombustion for calcined catalysts with different SiO_2 supports prepared from Q-3, Q-10 and Q-50 supports. The 0.1CA/Q-3 catalyst with the largest surface area (661 m^2/g) and with average pore size of only 3.5 nm showed the lowest

CO conversion. Comparing the two catalysts, 0.1CA/Q-3 and 0.1CA/Q-50, the latter with only the large pore showed a higher CO conversion although its surface area was much lower, as shown in Table 4.4. It is important to remark that the pore size of catalysts played a more important role rather than surface area on CO conversion [77]. The reaction rate may be mainly controlled by the diffusion of reactants and products. As expected, the CO conversion increases as a function of pore size. The general trend is that much higher CO conversion was observed on larger pore size located in larger pore supports [101]. Several previous work showed that the prepared catalyst exhibited much higher CO conversion in FTS depended on fastened diffusion efficiency and the improved active metal dispersion [104].

Table 4.5 FTS[a] performance of calcined catalysts with different SiO_2 supports

Catalysts	(%) CO conversion	Hydrocarbon Selectivity (%)			
		CO_2	CH_4	C_{2-4}	C_{5+}
0.1CA/Q-3	10.8	28.8	45.7	15.9	9.6
0.1CA/Q-10	33.3	35.7	24.2	25.2	14.9
0.1CA/Q-50	86.5	37.8	16.8	28.1	17.3

[a] Condition: 0.5 g catalysts; H_2/CO=1/1; 300 °C; 1.0 MPa; W/F=10 g_{cat}h/mol.

จุฬาลงกรณ์มหาวิทยาลัย
CHULALONGKORN UNIVERSITY

4.5.2 Products selectivity

The products selectivity of autocombustion for calcined catalysts with different SiO_2 supports prepared from Q-3, Q-10 and Q-50 supports are shown in Table 4.5 and Figure 4.15. The 0.1CA/Q-3 catalyst had the lowest C_{5+} selectivity, proving that the small pore catalyst tended to produce lighter hydrocarbons, while the large pore was preferable for C_{5+} selectivity (Figure 4.15) [77]. On the other hand, the 0.1CA/Q-50 catalyst had the highest C_{5+} selectivity and lowest CH_4 selectivity. This suggested the higher C_{5+} selectivity and lower CH_4 selectivity were observed on larger pore supports, as shown in Table 4.4. Therefore, the products selectivity was significantly affected by the pore size in the supports. Increasing pore size was also beneficial for C_2-C_4 selectivity [101, 103].

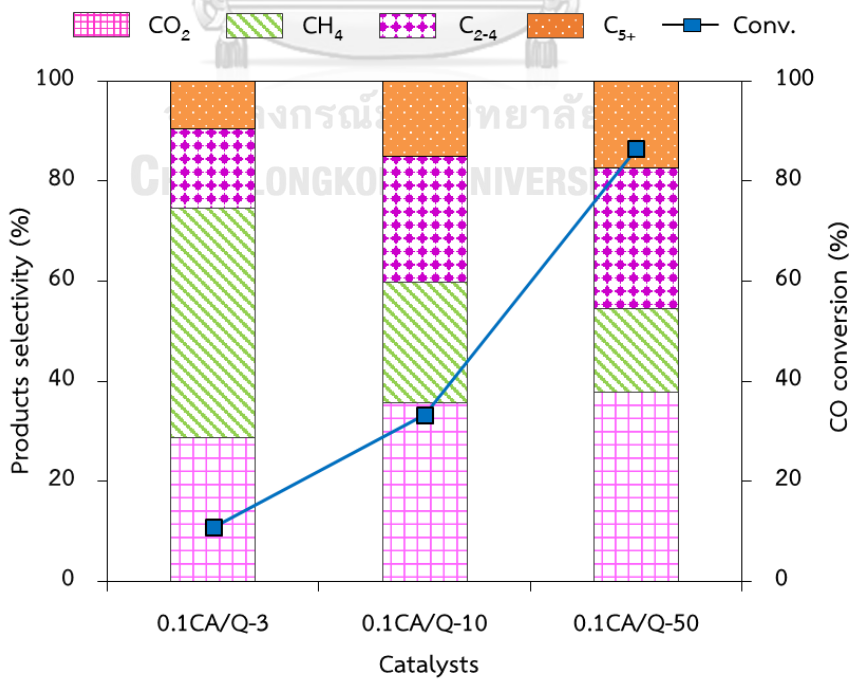

Figure 4.15 Influence of different SiO_2 supports on CO conversion and products selectivity with reaction condition: T=300 °C, P=1.0 MPa and W/F=10 g_{cat}h/mol

จุฬาลงกรณ์มหาวิทยาลัย
CHULALONGKORN UNIVERSITY

CHAPTER V

CONCLUSION AND RECOMMENDATION

5.1 Conclusion

Fe-based catalysts supported on SiO_2, containing Cu, K and CA were successfully prepared by autocombustion method for directly using in a fixed-bed reactor for FTS without a reduction step. CA played a key role in catalyst structure, phase structure, reduction behavior and FTS activity and selectivity which depended on the CA:N molar ratio of Fe-based/SiO_2 catalysts. The existence of CA significantly resulted in the improved the reduction and carburization during catalyst preparation and increased FTS activity without a reduction step. During the decomposition of CA, large amounts of gases such as H_2, CH_4, H_2O, CO, CO_2, NH_3, NO_2 and NO were released. These reducing gases (H_2 and CO) were as acting the reducing and carburizing agents to produce Fe_xC from metal oxide phases. Increasing the CA:N molar ratio up to 0.1 increased CO conversion of catalyst to 86.5%. But it then decreased markedly at higher CA:N molar ratios. Excessive CA resulted in carbon residues coating the catalysts surface and declined FTS activity.

The optimal 0.1CA catalyst achieved the highest CO conversion when compared with other autocombustion catalysts as well as reference catalyst prepared by impregnation method, followed by a reduction step at 300 °C for 10 h in H_2/CO. The

employed acid types in catalyst preparation were significantly influential in FTS activity and selectivity. The catalyst prepared using CA gave a maximum CO conversion when compared with other acid types. The effect of different SiO_2 supports led to higher pore size and CO conversion. Increasing pore size resulted in larger Fe particles. The CO conversion of Fe-based/SiO_2 catalysts by different SiO_2 supports seemed to be attributed to the presence of Fe_xC. The catalyst prepared using Q-50, as a support had a maximum CO conversion when compared with other SiO_2 supports. The autocombustion method approach is another choice to synthesize nanostructured metallic catalysts without a reduction step.

5.2 Suggestion and Recommendation

The characterization of the effect of different acid types catalysts such as formic acid, oxalic acid could be used as reductant in the autocombustion method will be investigated in future work. Many research works suggest that there are remarkable influences from organic acid on the catalytic performance. The different in amount of C, H, and O atoms in organic compound can release different reducing gases during the combustion and the reducibility of the metals. So, the acid types should play an important role in controlling the structures and FTS performance of the catalysts.

Catalyst deactivation process is an important problem in iron-based for Fischer–Tropsch synthesis. There are several causes of catalyst deactivation include poisoning by sulphur and/or nitrogen, oxidation of the active metal, sintering, surface carbon

จุฬาลงกรณ์มหาวิทยาลัย
CHULALONGKORN UNIVERSITY

formation, and surface reconstruction. Catalyst stability test is a significant determination the plot between conversion/rate (decay) versus time on stream (TOS). Both catalyst deactivation and stability test will be examined in future work.

The different loading Fe-based catalysts supported on SiO_2, containing Cu, K and CA were prepared by autocombustion method will be studied in future work.

Studies on the thermodynamics, mechanisms and kinetics of the complexity autocombustion method are a challenging and difficult task with resulting from the great variation of factors such as reductant molar ratios, acid types, specific surface area and porosity of support, type of metal catalysts, types of reactor, diffusion of gaseous reagents or reaction products. The extension on the thermodynamic data calculation from the kinetic data is expected to be the useful data for further applications.

จุฬาลงกรณ์มหาวิทยาลัย
CHULALONGKORN UNIVERSITY

REFERENCES

1. Luque, R., et al., *Design and development of catalysts for Biomass-To-Liquid-Fischer–Tropsch (BTL-FT) processes for biofuels production.* Energy & Environmental Science, 2012. **5**(1): p. 5186-5202.
2. Liu, G., et al., *Nitrogen-rich mesoporous carbon supported iron catalyst with superior activity for Fischer-Tropsch synthesis.* Carbon, 2018.
3. Wang, D., et al., *Iron-based Fischer–Tropsch synthesis of lower olefins: The nature of χ-Fe5C2 catalyst and why and how to introduce promoters.* Journal of energy chemistry, 2016. **25**(6): p. 911-916.
4. Chen, Q., et al., *Design of ultra-active iron-based Fischer-Tropsch synthesis catalysts over spherical mesoporous carbon with developed porosity.* Chemical Engineering Journal, 2018. **334**: p. 714-724.
5. Xu, J.-D., et al., *Effect of sulfur on α-Al2O3-supported iron catalyst for Fischer–Tropsch synthesis.* Applied Catalysis A: General, 2016. **514**: p. 103-113.
6. Huang, J., H. Zhuang, and W. Li, *Synthesis and characterization of nano crystalline BaFe12O19 powders by low temperature combustion.* Materials Research Bulletin, 2003. **38**(1): p. 149-159.
7. Jiang, Y., et al., *Sol–gel autocombustion synthesis of metals and metal alloys.* Angewandte Chemie, 2009. **121**(45): p. 8681-8683.
8. Zhang, Q., J. Kang, and Y. Wang, *Development of novel catalysts for Fischer–Tropsch synthesis: tuning the product selectivity.* ChemCatChem, 2010. **2**(9): p. 1030-1058.
9. Molino, A., S. Chianese, and D. Musmarra, *Biomass gasification technology: The state of the art overview.* Journal of Energy Chemistry, 2016. **25**(1): p. 10-25.
10. James, O.O., et al., *Increasing carbon utilization in Fischer–Tropsch synthesis using H2-deficient or CO2-rich syngas feeds.* Fuel Processing Technology, 2010. **91**(2): p. 136-144.

จุฬาลงกรณ์มหาวิทยาลัย
Chulalongkorn University

11. Kim, K., et al., *Long-term operation of biomass-to-liquid systems coupled to gasification and Fischer–Tropsch processes for biofuel production.* Bioresource technology, 2013. **127**: p. 391-399.

12. Richardson, Y., J. Blin, and A. Julbe, *A short overview on purification and conditioning of syngas produced by biomass gasification: catalytic strategies, process intensification and new concepts.* Progress in Energy and Combustion Science, 2012. **38**(6): p. 765-781.

13. Gorimbo, J., et al., *A long term study of the gas phase of low pressure Fischer-Tropsch products when reducing an iron catalyst with three different reducing gases.* Applied Catalysis A: General, 2017. **534**: p. 1-11.

14. Jun, K.-W., et al., *Catalytic investigation for Fischer–Tropsch synthesis from bio-mass derived syngas.* Applied Catalysis A: General, 2004. **259**(2): p. 221-226.

15. Kim, J., M. Choi, and R. Ryoo, *Effect of mesoporosity against the deactivation of MFI zeolite catalyst during the methanol-to-hydrocarbon conversion process.* Journal of Catalysis, 2010. **269**(1): p. 219-228.

16. Todic, B., et al., *Fischer–Tropsch synthesis product selectivity over an industrial iron-based catalyst: Effect of process conditions.* Catalysis Today, 2016. **261**: p. 28-39.

17. Li, J., et al., *Jet fuel synthesis via Fischer–Tropsch synthesis with varied 1-olefins as additives using Co/ZrO2–SiO2 bimodal catalyst.* Fuel, 2016. **171**: p. 159-166.

18. de Smit, E. and B.M. Weckhuysen, *The renaissance of iron-based Fischer–Tropsch synthesis: on the multifaceted catalyst deactivation behaviour.* Chemical Society Reviews, 2008. **37**(12): p. 2758-2781.

19. Iglesia, E., *Design, synthesis, and use of cobalt-based Fischer-Tropsch synthesis catalysts.* Applied Catalysis A: General, 1997. **161**(1-2): p. 59-78.

20. Chang, J., et al., *Kinetic modeling of Fischer–Tropsch synthesis over Fe–Cu–K–SiO2 catalyst in slurry phase reactor.* Chemical Engineering Science, 2007. **62**(18-20): p. 4983-4991.

จุฬาลงกรณ์มหาวิทยาลัย
CHULALONGKORN UNIVERSITY

21. Xiang, Y. and N. Kruse, *Cobalt–copper based catalysts for higher terminal alcohols synthesis via Fischer–Tropsch reaction.* Journal of energy chemistry, 2016. **25**(6): p. 895-906.

22. Mousavi, S., et al., *Generalized kinetic model for iron and cobalt based Fischer–Tropsch synthesis catalysts: Review and model evaluation.* Applied Catalysis A: General, 2015. **506**: p. 57-66.

23. Bhatelia, T., et al., *Chain length dependent olefin re-adsorption model for Fischer–Tropsch synthesis over Co-Al2O3 catalyst.* Fuel Processing Technology, 2014. **125**: p. 277-289.

24. Sarkari, M., et al., *Catalytic performance of an iron-based catalyst in Fischer–Tropsch synthesis.* Fuel Processing Technology, 2014. **127**: p. 163-170.

25. Okeson, T.J., et al., *On the kinetics and mechanism of Fischer–Tropsch synthesis on a highly active iron catalyst supported on silica-stabilized alumina.* Catalysis Today, 2016. **261**: p. 67-74.

26. Zhang, X., et al., *Product distributions including hydrocarbon and oxygenates of Fischer–Tropsch synthesis over mesoporous MnO2-supported Fe catalyst.* Fuel, 2012. **92**(1): p. 122-129.

27. Arsalanfar, M., et al., *Effect of support and promoter on the catalytic performance and structural properties of the Fe–Co–Mn catalysts for Fischer–Tropsch synthesis.* Journal of Industrial and Engineering Chemistry, 2014. **20**(4): p. 1313-1323.

28. Zhang, Q., W. Deng, and Y. Wang, *Recent advances in understanding the key catalyst factors for Fischer-Tropsch synthesis.* Journal of Energy Chemistry, 2013. **22**(1): p. 27-38.

29. Díaz, J.A., et al., *Carbon nanofibers and nanospheres-supported bimetallic (Co and Fe) catalysts for the Fischer–Tropsch synthesis.* Fuel Processing Technology, 2015. **138**: p. 455-462.

30. Vannice, M.A., *The catalytic synthesis of hydrocarbons from H2CO mixtures over the group VIII metals: I. The specific activities and product distributions of supported metals.* Journal of Catalysis, 1975. **37**(3): p. 449-461.

จุฬาลงกรณ์มหาวิทยาลัย
CHULALONGKORN UNIVERSITY

31. Yu, S., et al., *Synthesis and characterization of iron-based catalyst on mesoporous titania for photo-thermal FT synthesis.* International journal of hydrogen energy, 2015. **40**(1): p. 870-877.

32. Schneider, J., et al., *Performance of supported and unsupported Fe and Co catalysts for the direct synthesis of light alkenes from synthesis gas.* Fuel Processing Technology, 2018. **170**: p. 64-78.

33. Khodakov, A.Y., W. Chu, and P. Fongarland, *Advances in the development of novel cobalt Fischer– Tropsch catalysts for synthesis of long-chain hydrocarbons and clean fuels.* Chemical reviews, 2007. **107**(5): p. 1692-1744.

34. Xu, Y., D. Liu, and X. Liu, *Conversion of syngas toward aromatics over hybrid Fe-based Fischer-Tropsch catalysts and HZSM-5 zeolites.* Applied Catalysis A: General, 2018.

35. Sun, B., et al., *Preparation and Catalysis of Carbon-Supported Iron Catalysts for Fischer–Tropsch Synthesis.* ChemCatChem, 2012. **4**(10): p. 1498-1511.

36. Park, H., et al., *Selective Formation of Hägg Iron Carbide with g-C3N4 as a Sacrificial Support for Highly Active Fischer–Tropsch Synthesis.* ChemCatChem, 2015. **7**(21): p. 3488-3494.

37. Zamaniyan, A., et al., *Effect of mass transfer limitations on catalyst performance during reduction and carburization of iron based Fischer-Tropsch synthesis catalysts.* Journal of Energy chemistry, 2013. **22**(5): p. 795-803.

38. Sedighi, B., M. Feyzi, and M. Joshaghani, *Preparation and characterization of Co–Fe nano catalyst for Fischer–Tropsch synthesis: optimization using response surface methodology.* Journal of the Taiwan Institute of Chemical Engineers, 2015. **50**: p. 108-114.

39. Azizi, H.R., et al., *Fischer–Tropsch synthesis: studies effect of reduction variables on the performance of Fe–Ni–Co catalyst.* Journal of Natural Gas Science and Engineering, 2014. **18**: p. 484-491.

40. Ding, M., et al., *Study on reduction and carburization behaviors of iron phases for iron-based Fischer–Tropsch synthesis catalyst.* Applied energy, 2015. **160**: p. 982-989.

41. Zhao, S., et al., *Morphology control of K2O promoter on Hägg carbide (χ-Fe5C2) under Fischer–Tropsch synthesis condition.* Catalysis Today, 2016. **261**: p. 93-100.

42. Cruz, M.G., et al., *On the structural, textural and morphological features of Fe-based catalysts supported on polystyrene mesoporous carbon for Fischer–Tropsch synthesis.* Applied Catalysis A: General, 2015. **495**: p. 72-83.

43. Guo, L., et al., *Fischer–Tropsch synthesis over iron catalysts with corncob-derived promoters.* Journal of energy chemistry, 2017. **26**(4): p. 632-638.

44. Li, S., et al., *Effects of Zn, Cu, and K promoters on the structure and on the reduction, carburization, and catalytic behavior of iron-based Fischer–Tropsch synthesis catalysts.* Catalysis Letters, 2001. **77**(4): p. 197-205.

45. Duan, X., et al., *Fabrication of K-promoted iron/carbon nanotubes composite catalysts for the Fischer–Tropsch synthesis of lower olefins.* Journal of Energy Chemistry, 2016. **25**(2): p. 311-317.

46. Zhang, X., et al., *Preparation of hierarchically meso-macroporous hematite Fe2O3 using PMMA as imprint template and its reaction performance for Fischer–Tropsch synthesis.* Catalysis Communications, 2011. **13**(1): p. 44-48.

47. Klaigaew, K., et al., *Effect of preparation methods on activation of cobalt catalyst supported on silica fiber for Fischer–Tropsch synthesis.* Chemical Engineering Journal, 2015. **278**: p. 166-173.

48. Braganca, L., et al., *Bimetallic Co-Fe nanocrystals deposited on SBA-15 and HMS mesoporous silicas as catalysts for Fischer–Tropsch synthesis.* Applied Catalysis A: General, 2012. **423**: p. 146-153.

49. Sun, X., et al., *Reversible promotional effect of SiO2 modification to Co/Al2O3 catalyst for Fischer–Tropsch synthesis.* Applied Catalysis A: General, 2010. **377**(1-2): p. 134-139.

จุฬาลงกรณ์มหาวิทยาลัย
CHULALONGKORN UNIVERSITY

50. Cheng, X., H. Yang, and B.J. Tatarchuk, *Microfibrous entrapped hybrid iron-based catalysts for Fischer–Tropsch synthesis.* Catalysis Today, 2016. **273**: p. 62-71.

51. Schulz, H., *Short history and present trends of Fischer–Tropsch synthesis.* Applied Catalysis A: General, 1999. **186**(1): p. 3-12.

52. Glasser, D., et al., *Recent advances in understanding the Fischer–Tropsch synthesis (FTS) reaction.* Current Opinion in Chemical Engineering, 2012. **1**(3): p. 296-302.

53. Moazami, N., et al., *Catalytic performance of cobalt–silica catalyst for Fischer–Tropsch synthesis: Effects of reaction rates on efficiency of liquid synthesis.* Chemical Engineering Science, 2015. **134**: p. 374-384.

54. Xing, C., et al., *Fischer–Tropsch synthesis on impregnated cobalt-based catalysts: New insights into the effect of impregnation solutions and pH value.* Journal of energy chemistry, 2016. **25**(6): p. 994-1000.

55. Jiao, L. and J.R. Regalbuto, *The synthesis of highly dispersed noble and base metals on silica via strong electrostatic adsorption: I. Amorphous silica.* Journal of Catalysis, 2008. **260**(2): p. 329-341.

56. Xing, C., et al., *Hierarchical zeolite Y supported cobalt bifunctional catalyst for facilely tuning the product distribution of Fischer–Tropsch synthesis.* Fuel, 2015. **148**: p. 48-57.

57. Van Dillen, A.J., et al., *Synthesis of supported catalysts by impregnation and drying using aqueous chelated metal complexes.* Journal of Catalysis, 2003. **216**(1-2): p. 257-264.

58. Barbooti, M.M. and D.A. Al-Sammerrai, *Thermal decomposition of citric acid.* Thermochimica acta, 1986. **98**: p. 119-126.

59. Meichtry, J.M., et al., *Heterogeneous photocatalytic degradation of citric acid over TiO2: II. Mechanism of citric acid degradation.* Applied Catalysis B: Environmental, 2011. **102**(3-4): p. 555-562.

จุฬาลงกรณ์มหาวิทยาลัย
Chulalongkorn University

60. Prapaipong, P. and E.L. Shock, *Estimation of standard-state entropies of association for aqueous metal-organic complexes and chelates at 25 C and 1 bar.* Geochimica et Cosmochimica Acta, 2001. **65**(21): p. 3931-3953.

61. Van de Loosdrecht, J., et al., *Preparation and properties of supported cobalt catalysts for Fischer-Tropsch synthesis.* Applied Catalysis A: General, 1997. **150**(2): p. 365-376.

62. Shi, L., et al., *Surface Impregnation Combustion Method to Prepare Nanostructured Metallic Catalysts without Further Reduction: As-Burnt Co/SiO2 Catalysts for Fischer–Tropsch Synthesis.* ACS Catalysis, 2011. **1**(10): p. 1225-1233.

63. Phienluphon, R., et al., *Ruthenium promoted cobalt catalysts prepared by an autocombustion method directly used for Fischer–Tropsch synthesis without further reduction.* Catalysis Science & Technology, 2014. **4**(9): p. 3099-3107.

64. Li, F., et al., *Combustion synthesis of γ-lithium aluminate by using various fuels.* Journal of nuclear materials, 2002. **300**(1): p. 82-88.

65. Chandradass, J., B. Jun, and D.-s. Bae, *Effect of different fuels on the alumina–zirconia nanopowder synthesized by sol–gel autocombustion method.* Journal of Non-Crystalline Solids, 2008. **354**(26): p. 3085-3087.

66. Hua, Z., et al., *Sol–gel autocombustion synthesis of Co–Ni alloy powder.* Materials Chemistry and Physics, 2011. **126**(3): p. 542-545.

67. Chen, W., F. Li, and J. Yu, *Combustion synthesis and characterization of nanocrystalline CeO2-based powders via ethylene glycol–nitrate process.* Materials Letters, 2006. **60**(1): p. 57-62.

68. Marinšek, M., K. Zupan, and J. Maeek, *Ni–YSZ cermet anodes prepared by citrate/nitrate combustion synthesis.* Journal of power sources, 2002. **106**(1-2): p. 178-188.

69. Vajargah, S.H., H.M. Hosseini, and Z. Nemati, *Preparation and characterization of yttrium iron garnet (YIG) nanocrystalline powders by auto-combustion of nitrate-citrate gel.* Journal of Alloys and Compounds, 2007. **430**(1-2): p. 339-343.

จุฬาลงกรณ์มหาวิทยาลัย
CHULALONGKORN UNIVERSITY

70. Peng, T., et al., *Effect of acidity on the glycine–nitrate combustion synthesis of nanocrystalline alumina powder.* Materials research bulletin, 2006. **41**(9): p. 1638-1645.

71. Bahadur, D., S. Rajakumar, and A. Kumar, *Influence of fuel ratios on auto combustion synthesis of barium ferrite nano particles.* Journal of chemical sciences, 2006. **118**(1): p. 15-21.

72. Shi, L., et al., *Studies on surface impregnation combustion method to prepare supported Co/SiO2 catalysts and its application for Fischer–Tropsch synthesis.* Applied Catalysis A: General, 2012. **435**: p. 217-224.

73. Gegova, R., et al., *Combustion gel method for synthesis of nanosized ZnO/TiO2 powders".* J. Chem. Techn. Metall, 2013. **48**(2).

74. Xu, G., et al., *Influence of pH on characteristics of BaFe12O19 powder prepared by sol–gel auto-combustion.* Journal of Magnetism and Magnetic Materials, 2006. **301**(2): p. 383-388.

75. Yue, Z., et al., *Synthesis of nanocrystilline ferrites by sol–gel combustion process: the influence of pH value of solution.* Journal of magnetism and magnetic materials, 2004. **270**(1-2): p. 216-223.

76. Shi, L., et al., *Surface impregnation combustion method to prepare nanostructured metallic catalysts without further reduction: As-burnt Cu–ZnO/SiO2 catalyst for low-temperature methanol synthesis.* Catalysis today, 2012. **185**(1): p. 54-60.

77. Zhang, Y., et al., *A new and direct preparation method of iron-based bimodal catalyst and its application in Fischer–Tropsch synthesis.* Applied Catalysis A: General, 2009. **352**(1-2): p. 277-281.

78. Wang, W., et al., *Fe2O3 nanoparticles encapsulated in TiO2 nanotubes for Fischer–Tropsch synthesis: The confinement effect of nanotubes on the catalytic performance.* Fuel, 2016. **164**: p. 347-351.

79. Liu, R.-J., et al., *Factors influencing the Fischer–Tropsch synthesis performance of iron-based catalyst: Iron oxide dispersion, distribution and reducibility.* Fuel Processing Technology, 2015. **139**: p. 25-32.

จุฬาลงกรณ์มหาวิทยาลัย
CHULALONGKORN UNIVERSITY

80. Rafati, M., L. Wang, and A. Shahbazi, *Effect of silica and alumina promoters on co-precipitated Fe–Cu–K based catalysts for the enhancement of CO 2 utilization during Fischer–Tropsch synthesis.* Journal of CO2 Utilization, 2015. **12**: p. 34-42.

81. Zhang, J., et al., *Selective formation of light olefins from CO2 hydrogenation over Fe–Zn–K catalysts.* Journal of CO2 Utilization, 2015. **12**: p. 95-100.

82. Jin, Y., et al., *Development of dual-membrane coated Fe/SiO2 catalyst for efficient synthesis of isoparaffins directly from syngas.* Journal of Membrane Science, 2015. **475**: p. 22-29.

83. Ding, M., et al., *Effect of reducing agents on microstructure and catalytic performance of precipitated iron-manganese catalyst for Fischer–Tropsch synthesis.* Fuel processing technology, 2011. **92**(12): p. 2353-2359.

84. Phienluphon, R., et al., *Direct fabrication of catalytically active FexC sites by sol-gel autocombustion for preparing Fischer-Tropsch synthesis catalysts without reduction.* Catalysis Science & Technology, 2016. **6**(20): p. 7597-7603.

85. Cheng, K., et al., *Sodium-promoted iron catalysts prepared on different supports for high temperature Fischer–Tropsch synthesis.* Applied Catalysis A: General, 2015. **502**: p. 204-214.

86. Cheng, K., et al., *The role of carbon pre-coating for the synthesis of highly efficient cobalt catalysts for Fischer–Tropsch synthesis.* Journal of Catalysis, 2016. **337**: p. 260-271.

87. Xiong, H., et al., *Effect of Group I alkali metal promoters on Fe/CNT catalysts in Fischer–Tropsch synthesis.* Fuel, 2015. **150**: p. 687-696.

88. Li, C., et al., *Development of high performance graphite-supported iron catalyst for Fischer–Tropsch synthesis.* Applied Catalysis A: General, 2016. **509**: p. 123-129.

89. Al-Dossary, M. and J. Fierro, *Effect of high-temperature pre-reduction in Fischer–Tropsch synthesis on Fe/ZrO2 catalysts.* Applied Catalysis A: General, 2015. **499**: p. 109-117.

จุฬาลงกรณ์มหาวิทยาลัย
CHULALONGKORN UNIVERSITY

90. Cheng, K., et al., *Support effects in high temperature Fischer-Tropsch synthesis on iron catalysts.* Applied Catalysis A: General, 2014. **488**: p. 66-77.

91. Zhang, Y., et al., *MnO2 coated Fe2O3 spindles designed for production of C5+ hydrocarbons in Fischer–Tropsch synthesis.* Fuel, 2016. **177**: p. 197-205.

92. Li, T., et al., *Effect of manganese on the catalytic performance of an iron-manganese bimetallic catalyst for light olefin synthesis.* Journal of Energy Chemistry, 2013. **22**(4): p. 624-632.

93. Yang, J., et al., *Effect of magnesium promoter on iron-based catalyst for Fischer–Tropsch synthesis.* Journal of Molecular Catalysis A: Chemical, 2006. **245**(1-2): p. 26-36.

94. Riedel, T., et al., *Fischer–Tropsch on iron with H 2/CO and H 2/CO 2 as synthesis gases: the episodes of formation of the Fischer–Tropsch regime and construction of the catalyst.* Topics in Catalysis, 2003. **26**(1-4): p. 41-54.

95. Xu, J., et al., *Design, synthesis, and catalytic properties of silica-supported, Pt-promoted iron Fischer–Tropsch catalysts.* Topics in catalysis, 2003. **26**(1-4): p. 55-71.

96. Özkara-Aydınoğlu, Ş., et al., *α-olefin selectivity of Fe–Cu–K catalysts in Fischer–Tropsch synthesis: Effects of catalyst composition and process conditions.* Chemical Engineering Journal, 2012. **181-182**: p. 581-589.

97. Rao, V., et al., *Iron-based catalysts for slurry-phase Fischer-Tropsch process: Technology review.* Fuel processing technology, 1992. **30**(1): p. 83-107.

98. den Breejen, J.P., et al., *On the Origin of the Cobalt Particle Size Effects in Fischer–Tropsch Catalysis.* Journal of the American Chemical Society, 2009. **131**(20): p. 7197-7203.

99. Kumabe, K., et al., *Production of hydrocarbons in Fischer–Tropsch synthesis with Fe-based catalyst: Investigations of primary kerosene yield and carbon mass balance.* Fuel, 2010. **89**(8): p. 2088-2095.

100. Fan, L., K. Yokota, and K. Fujimoto, *Supercritical phase fischer-tropsch synthesis: Catalyst pore-size effect.* AIChE Journal, 1992. **38**(10): p. 1639-1648.

101. Cheng, K., et al., *Pore size effects in high-temperature Fischer–Tropsch synthesis over supported iron catalysts.* Journal of Catalysis, 2015. **328**: p. 139-150.

102. Suo, H., et al., *A comparative study of Fe/SiO2 Fischer–Tropsch synthesis catalysts using tetraethoxysilane and acidic silica sol as silica sources.* Catalysis today, 2012. **183**(1): p. 88-95.

103. Guo, X., et al., *The effect of SiO2 particle size on iron based F–T synthesis catalysts.* Chinese Journal of Chemical Engineering, 2016. **24**(7): p. 937-943.

104. Zhang, Y., et al., *Multi-functional alumina–silica bimodal pore catalyst and its application for Fischer-Tropsch synthesis.* Applied Catalysis A: General, 2005. **292**: p. 252-258.

จุฬาลงกรณ์มหาวิทยาลัย
CHULALONGKORN UNIVERSITY

APPENDIX

จุฬาลงกรณ์มหาวิทยาลัย
Chulalongkorn University

APPENDIX A

CALCULATION FOR CATALYST PREPARATION

1. Calculation for preparation Fe-based/SiO_2 by autocombustion method when Fe: Cu: K molar ratios = 200:30:5 and 20 wt% Fe metal loading on SiO_2

Chemicals	MW (g/mol)
$Fe(NO_3)_3.9H_2O$	403.99
$Cu(NO_3)_2.3H_2O$	241.60
KNO_3	101.10
$C_6H_8O_7$ (citric acid)	192.12
$C_2H_2O_4$ (oxalic acid)	90.03
CH_2O_2 (formic acid)	46.03

จุฬาลงกรณ์มหาวิทยาลัย
CHULALONGKORN UNIVERSITY

1.1 Calculation weight of $Fe(NO_3)_3.9H_2O$

SiO_2 = 80 g and Fe = 20 g, assume of SiO_2 was weighted 5 g, Fe = $\frac{20 \times 5}{80}$ = 1.25 g

When MW of Fe = 55.85 g/mol, MW of Cu = 63.55 g/mol and MW of K = 39.09 g/mol

Fe 55.85 g from $Fe(NO_3)_3.9H_2O$ 403.99 g

Fe 1.25 g therefore; weight of $Fe(NO_3)_3.9H_2O$ $\frac{403.99 \times 1.25}{55.85}$ = 9.043 g

And mol of Fe $\frac{9.04}{403.99}$ = 0.022 mol

1.2 Calculation weight of $Cu(NO_3)_2.3H_2O$

Molar ratio of Fe:Cu:K = 200:30:5

Fe 200 mol Cu 30 mol, Fe 0.022 mol, and mol of Cu $\frac{30 \times 0.022}{200}$ = 0.0034 mol

Therefore; weight of Cu $\frac{0.0034}{63.55}$ = 0.213 g

Cu 63.55 g from $Cu(NO_3)_2.3H_2O$ 241.60 g

Cu 0.213 g therefore; weight of $Cu(NO_3)_2.3H_2O$ $\frac{241.60 \times 0.213}{63.55}$ = 0.811 g

1.3 Calculation weight of For KNO_3

Fe 200 mol K 5 mol, Fe 0.022 mol, and mol of K $\frac{5 \times 0.022}{200}$ = 0.0005 mol

Therefore; weight of K $\frac{0.0005}{39.09}$ = 0.021 g

K 39.09 g from KNO_3 101.10 g

K 0.021 g therefore; weight of KNO_3 $\frac{101.01 \times 0.021}{39.09}$ = 0.057 g

1.4 Calculation weight of citric acid

NO_3^- of Fe 0.022×3 = 0.067, Cu 0.0034×2 = 0.0067 and K 0.0005×1 = 0.00056

And all NO_3^- $0.067 + 0.0067 + 0.00056$ = 0.0074

จุฬาลงกรณ์มหาวิทยาลัย
CHULALONGKORN UNIVERSITY

Citric acid: NO_3^-	Citric acid (mol)	Citric acid (g)
0.05	0.05×0.0074 = 0.004	0.004×192.12 = 0.72
0.1	0.1×0.0074 = 0.007	0.007×192.12 = 1.43
0.2	0.2×0.0074 = 0.015	0.015×192.12 = 2.86
0.3	0.3×0.0074 = 0.022	0.022×192.12 = 4.29

1.5 Calculation weight of oxalic acid and formic acid

At molar ratio = 0.1, for weight of oxalic acid 0.007×90.03 = 0.67 g and for weight of formic acid 0.007×46.03 = 0.34 g

2. Calculation for preparation Fe-based/SiO_2 by impregnation method

For weight of $Fe(NO_3)_3.9H_2O$ = 9.043 g, $Cu(NO_3)_2.3H_2O$ = 0.811 g and KNO_3 = 0.057 g, which similar autocombustion catalysts were also calculated as above.

จุฬาลงกรณ์มหาวิทยาลัย
CHULALONGKORN UNIVERSITY

APPENDIX B

EXPERIMENTAL DATA FOR FISCHER-TROPSCH SYNTHESIS

1. Calculation for CO conversion and hydrocarbon product selectivity

$$CO\ conversion\ (\%) = \frac{\left(\frac{CO}{Ar}\right)_{inlet} - \left(\frac{CO}{Ar}\right)_{outlet}}{\left(\frac{CO}{Ar}\right)_{inlet}} \times 100$$

$$CO_2\ selectivity\ (\%) = \frac{moles\ of\ CO_2\ produced}{moles\ of\ inlet\ CO - moles\ of\ outlet\ CO} \times 100$$

$$CH_4\ selectivity\ (\%) = S_{CH_4}$$

$$= \frac{moles\ of\ CH_4\ produced}{moles\ of\ inlet\ CO - moles\ of\ outlet\ CO - moles\ of\ CO_2\ produced} \times 100$$

$$C_x\ selectivity\ (\%, x = 2 - 11) = S_{C_x}$$

$$= \frac{moles\ of\ C_x\ produced}{moles\ of\ inlet\ CO - moles\ of\ outlet\ CO - moles\ of\ CO_2\ produced} \times 100$$

จุฬาลงกรณ์มหาวิทยาลัย
CHULALONGKORN UNIVERSITY

2. Information of synthesis gas and standard gas

Synthesis gas

Syngas	Composition (%)	TCD (Area)
Ar	3.06	12608
CO	48.5	210819
CO/Ar	15.85	16.721

Standard gas

Standard gas	Composition (%)	TCD (Area)	FID (Area)
CO	5.03	23320	N/A
CH_4	4.96	18954	585436
CO_2	5.12	22478	N/A

จุฬาลงกรณ์มหาวิทยาลัย
CHULALONGKORN UNIVERSITY

3. Information of CO conversion and gas product selectivity

Name = 0.05CA, Flow rate = 19.5 ml/min, T = 300 °C, P = 1.0 MPa and W/F = 10 gh/mol, catalyst weight 0.50 g

Time (h)		1	2	3	4	5
Area	Ar	14275	18654	21204	21548	21512
	CO	80769	104729	116782	118734	118409
	CH_4	4741	9920	13256	13682	13490
	CO_2	27847	65530	102220	112658	113565
CO conversion (%)		66.2	66.4	67.1	67.0	67.1
Flowrate (s/10ml)		83.70	83.55	71.75	79.76	81.08
Gas produced (mol/h)		0.018	0.018	0.021	0.019	0.019
CH_4 produced		0.012	0.026	0.035	0.036	0.035
CO_2 produced		0.063	0.149	0.233	0.257	0.259
CH_4C-mol (mol/g·h)		0.001	0.002	0.003	0.003	0.003
CO_2C-mol (mol/g·h)		0.005	0.011	0.020	0.020	0.020
CO (mol/g·h)		0.032	0.032	0.033	0.033	0.033
CH_4 sel (mol%)		17.4	17.4	17.3	17.4	17.3
CO_2 sel (mol%)		39.7	39.6	39.7	39.5	39.4
C_{5+} sel (mol%)		14.7	14.8	14.9	14.9	14.8

จุฬาลงกรณ์มหาวิทยาลัย
CHULALONGKORN UNIVERSITY

4. Information of CO conversion and gas product selectivity

Name = 0.1CA, Flow rate = 19.5 ml/min, T = 300 °C, P = 1.0 MPa and W/F = 10 gh/mol, catalyst weight 0.50 g

Time (h)		1	2	3	4	5
Area	Ar	22691	22060	22428	23097	23536
	CO	55999	54637	52196	51470	51593
	CH_4	19756	26271	27301	28925	29881
	CO_2	100814	170567	175255	181607	183051
CO conversion (%)		85.2	85.2	86.1	86.7	86.9
Flowrate (s/10ml)		55.900	53.587	53.687	51.407	50.807
Gas produced (mol/h)		0.027	0.029	0.029	0.030	0.003
CH_4 produced		0.052	0.069	0.071	0.076	0.078
CO_2 produced		0.230	0.389	0.399	0.414	0.417
CH_4C-mol (mol/g·h)		0.003	0.004	0.004	0.005	0.005
CO_2C-mol (mol/g·h)		0.013	0.023	0.024	0.026	0.027
CO (mol/g·h)		0.041	0.014	0.042	0.042	0.042
CH_4 sel (mol%)		16.7	16.8	16.8	16.8	16.7
CO_2 sel (mol%)		37.5	37.6	37.9	37.8	37.6
C_{5+} sel (mol%)		17.3	17.2	17.4	17.2	17.2

จุฬาลงกรณ์มหาวิทยาลัย
CHULALONGKORN UNIVERSITY

5. Information of CO conversion and gas product selectivity

Name = 0.2CA, Flow rate = 19.5 ml/min, T = 300 °C, P = 1.0 MPa and W/F = 10 gh/mol, catalyst weight 0.50 g

Time (h)		1	2	3	4	5
Area	Ar	15995	16361	15973	15899	15938
	CO	195651	199464	195891	196011	196256
	CH_4	4029	4350	4448	4508	4540
	CO_2	26033	25292	25239	25138	24686
CO conversion (%)		26.3	27.1	26.7	26.3	26.4
Flowrate (s/10ml)		33.673	33.273	33.287	33.153	33.207
Gas produced (mol/h)		0.046	0.046	0.046	0.046	0.046
CH_4 produced		0.011	0.011	0.012	0.012	0.012
CO_2 produced		0.059	0.058	0.057	0.057	0.056
CH_4C-mol (mol/g·h)		0.001	0.001	0.001	0.001	0.001
CO_2C-mol (mol/g·h)		0.006	0.006	0.006	0.006	0.006
CO (mol/g·h)		0.013	0.013	0.013	0.013	0.013
CH_4 sel (mol%)		11.3	11.4	11.4	11.5	11.4
CO_2 sel (mol%)		36.1	35.9	36.0	35.8	35.8
C_{5+} sel (mol%)		26.2	26.3	26.3	26.2	26.1

จุฬาลงกรณ์มหาวิทยาลัย
CHULALONGKORN UNIVERSITY

6. Information of CO conversion and gas product selectivity

Name = 0.3CA, Flow rate = 19.5 ml/min, T = 300 °C, P = 1.0 MPa and W/F = 10 gh/mol, catalyst weight 0.50 g

Time (h)		1	2	3	4	5
Area	Ar	14324	15006	15284	15795	15609
	CO	193670	201966	204909	212333	209922
	CH_4	1042	1354	1510	1604	1734
	CO_2	10068	13062	14628	15505	16654
CO conversion (%)		19.1	19.5	19.8	19.6	19.6
Flowrate (s/10ml)		42.753	43.047	44.707	45.447	44.400
Gas produced (mol/h)		0.036	0.036	0.034	0.034	0.035
CH_4 produced		0.003	0.004	0.004	0.004	0.005
CO_2 produced		0.023	0.030	0.033	0.035	0.038
CH_4C-mol (mol/g·h)		0.000	0.001	0.001	0.001	0.001
CO_2C-mol (mol/g·h)		0.003	0.004	0.005	0.005	0.005
CO (mol/g·h)		0.009	0.009	0.010	0.001	0.009
CH_4 sel (mol%)		8.0	8.1	8.1	8.1	8.2
CO_2 sel (mol%)		33.2	33.3	33.3	33.2	33.2
C_{5+} sel (mol%)		35.2	35.4	35.3	35.4	35.4

จุฬาลงกรณ์มหาวิทยาลัย
CHULALONGKORN UNIVERSITY

7. Information of CO conversion and gas product selectivity

Name = Imp, Flow rate = 19.5 ml/min, T = 300 °C, P = 1.0 MPa and W/F = 10 gh/mol, catalyst weight 0.50 g

Time (h)		1	2	3	4	5
Area	Ar	20948	21105	20697	20082	20424
	CO	163195	154263	116620	97120	97316
	CH_4	13165	16028	16080	17046	16610
	CO_2	105373	133448	130096	1227786	127616
CO conversion (%)		53.4	56.3	66.3	77.1	71.5
Flowrate (s/10ml)		60.033	55.460	50.013	46.400	49.827
Gas produced (mol/h)		0.026	0.028	0.031	0.033	0.031
CH_4 produced		0.034	0.042	0.042	0.045	0.043
CO_2 produced		0.240	0.304	0.296	0.291	0.291
CH_4C-mol (mol/g·h)		0.002	0.002	0.003	0.003	0.003
CO_2C-mol (mol/g·h)		0.012	0.017	0.018	0.019	0.018
CO (mol/g·h)		0.026	0.027	0.032	0.034	0.035
CH_4 sel (mol%)		10.9	11.0	11.0	11.1	11.3
CO_2 sel (mol%)		34.4	34.3	34.5	34.2	34.5
C_{5+} sel (mol%)		30.6	30.7	30.7	30.6	30.9

จุฬาลงกรณ์มหาวิทยาลัย
CHULALONGKORN UNIVERSITY

8. Information of CO conversion and gas product selectivity

Name = 0.1FA, Flow rate = 19.5 ml/min, T = 300 °C, P = 1.0 MPa and W/F = 10 gh/mol, catalyst weight 0.50 g

Time (h)		1	2	3	4	5
Area	Ar	21361	19806	18398	18240	17612
	CO	152400	140007	130169	127921	123302
	CH_4	13898	11598	10113	9572	9213
	CO_2	147244	119472	102514	92572	86335
CO conversion (%)		57.3	57.7	57.7	58.1	58.1
Flowrate (s/10ml)		42.760	44.713	41.727	42.460	40.820
Gas produced (mol/h)		0.036	0.034	0.037	0.036	0.038
CH_4 produced		0.036	0.030	0.026	0.025	0.024
CO_2 produced		0.335	0.272	0.234	0.211	0.197
CH_4C-mol (mol/g·h)		0.002	0.002	0.002	0.002	0.002
CO_2C-mol (mol/g·h)		0.022	0.017	0.016	0.014	0.014
CO (mol/g·h)		0.028	0.028	0.028	0.028	0.028
CH_4 sel (mol%)		9.0	9.1	9.2	9.1	9.1
CO_2 sel (mol%)		30.4	30.5	30.6	30.7	30.5
C_{5+} sel (mol%)		40.4	40.5	40.5	40.4	40.5

จุฬาลงกรณ์มหาวิทยาลัย
CHULALONGKORN UNIVERSITY

9. Information of CO conversion and gas product selectivity

Name = 0.1OA, Flow rate = 19.5 ml/min, T = 300 °C, P = 1.0 MPa and W/F = 10 gh/mol, catalyst weight 0.50 g

Time (h)		1	2	3	4	5
Area	Ar	14624	14835	14549	14623	14545
	CO	181859	185780	182961	183954	184984
	CH_4	2184	2148	2123	2184	2311
	CO_2	34584	31495	29408	28210	28305
CO conversion (%)		25.6	25.1	24.8	24.8	23.9
Flowrate (s/10ml)		34.300	32.400	31.067	33.433	34.313
Gas produced (mol/h)		0.045	0.047	0.049	0.046	0.045
CH_4 produced		0.006	0.006	0.006	0.006	0.006
CO_2 produced		0.079	0.072	0.067	0.064	0.064
CH_4C-mol (mol/g·h)		0.000	0.000	0.000	0.000	0.000
CO_2C-mol (mol/g·h)		0.006	0.006	0.006	0.005	0.005
CO (mol/g·h)		0.012	0.012	0.012	0.012	0.012
CH_4 sel (mol%)		13.2	13.3	13.3	13.2	13.4
CO_2 sel (mol%)		33.4	33.5	33.5	33.5	33.4
C_{5+} sel (mol%)		28.3	28.4	28.2	28.2	28.1

จุฬาลงกรณ์มหาวิทยาลัย
CHULALONGKORN UNIVERSITY

10. Information of CO conversion and gas product selectivity

Name = 0.1CA/Q-3, Flow rate = 19.5 ml/min, T = 300 °C, P = 1.0 MPa and W/F = 10 gh/mol, catalyst weight 0.50 g

Time (h)		1	2	3	4	5
Area	Ar	12636	12974	13069	13677	17457
	CO	187906	194807	195670	205369	258157
	CH_4	600	558	650	899	946
	CO_2	4902	6262	3974	7646	8004
CO conversion (%)		11.1	10.2	10.5	10.2	11.6
Flowrate (s/10ml)		29.787	31.460	33.520	33.893	34.460
Gas produced (mol/h)		0.052	0.049	0.046	0.045	0.045
CH_4 produced		0.002	0.001	0.002	0.002	0.002
CO_2 produced		0.011	0.014	0.009	0.017	0.018
CH_4C-mol (mol/g·h)		0.000	0.000	0.000	0.000	0.000
CO_2C-mol (mol/g·h)		0.001	0.001	0.001	0.001	0.002
CO (mol/g·h)		0.005	0.005	0.005	0.005	0.006
CH_4 sel (mol%)		45.6	45.7	45.5	45.7	45.7
CO_2 sel (mol%)		28.7	28.8	28.6	28.7	28.7
C_{5+} sel (mol%)		9.5	9.6	9.5	9.6	9.6

จุฬาลงกรณ์มหาวิทยาลัย
CHULALONGKORN UNIVERSITY

11. Information of CO conversion and gas product selectivity

Name = 0.1CA/Q-10, Flow rate = 19.5 ml/min, T = 300 °C, P = 1.0 MPa and W/F = 10 gh/mol, catalyst weight 0.50 g

Time (h)		1	2	3	4	5
Area	Ar	16060	16791	16195	16110	15794
	CO	183254	190359	180382	180413	175141
	CH_4	7179	7243	6985	6694	6451
	CO_2	49495	48760	46175	43371	40718
CO conversion (%)		31.8	32.2	33.4	33.0	33.7
Flowrate (s/10ml)		39.087	39.327	38.000	38.653	38.573
Gas produced (mol/h)		0.039	0.039	0.040	0.040	0.040
CH_4 produced		0.019	0.019	0.018	0.018	0.017
CO_2 produced		0.113	0.111	0.105	0.099	0.093
CH_4C-mol (mol/g·h)		0.001	0.001	0.001	0.001	0.001
CO_2C-mol (mol/g·h)		0.008	0.008	0.008	0.007	0.007
CO (mol/g·h)		0.015	0.016	0.016	0.016	0.016
CH_4 sel (mol%)		24.1	24.2	24.3	24.1	24.2
CO_2 sel (mol%)		35.6	35.7	35.8	35.5	35.7
C_{5+} sel (mol%)		14.7	14.9	14.8	14.9	14.9

จุฬาลงกรณ์มหาวิทยาลัย
CHULALONGKORN UNIVERSITY

APPENDIX C

CALCULATION OF CRYSTALLINE SIZE FROM X-RAY DIFFRACTION (XRD)

The average crystalline size was calculated by:

$$D = \frac{K\lambda}{B\cos\theta}$$

D is the crystalline size (nm)

K is a constant (K = 0.89)

λ is the wavelength of X-ray (CuKα = 0.154 nm)

B is $\Delta(2\theta)$, the width of the peak at half height (radian unit)

For 0.05CA; 2θ at 35.5 degree, B = 0.0056

2θ = 35.5 degree θ = 17.75 degree

$= 17.75 \times \frac{\pi}{180} = 0.3$

B = $0.31 \times \frac{\pi}{180}$ = 0.0054 radian

$$D = \frac{K\lambda}{B\cos\theta}$$

$$D = \frac{(0.89)(0.154)}{(0.0054)\cos(0.31)}$$

= 25.8 nm

จุฬาลงกรณ์มหาวิทยาลัย
CHULALONGKORN UNIVERSITY

VITA

Pol. Sub Lt. Suthasinee Pengnarapat was born on October 8, 1977 in Bangkok, Thailand. She graduated with Bachelor's degree, majoring in Chemistry, Faculty of Science, Chulalongkorn University in 2000 and Master's degree, majoring in Petrochemistry and Polymer Science, Faculty of Science, Chulalongkorn University in 2003. She started working at Police Forensic Science as a scientist and then, she worked as a process engineer at PTT Global Chemical Public Co., Ltd. Presence, she has been a graduate student, majoring in of Petrochemistry, Faculty of Science, Chulalongkorn University since 2013 and finished her study in 2017.

Publication

S. Pengnarapat, P. Ai, P. Reubroycharoen, T. Vitidsant, Y. Yoneyama, N. Tsubaki, Active Fischer-Tropsch synthesis Fe-Cu-K/SiO2 catalysts prepared by autocombustion method without a reduction step, Journal of Energy Chemistry, 2018, 27, 432-438.

Oral Presentation Experience

1) Iron based catalysts supported on silica prepared by autocombustion method for Fischer-Tropsch synthesis without reduction. The 3th International Congress on Advanced Materials Science (AM 2016), 27-30/12/2016, Bangkok, Thailand.

2) Development of high performance Fe/SiO2 catalysts, prepared by autocombustion method without a reduction step, Fischer-Tropsch synthesis. 17th Congress of Asian-Pacific Confederation of Chemical Engineering (APCChE), 23-27/8/2017, Hong Kong.

จุฬาลงกรณ์มหาวิทยาลัย
Chulalongkorn University